In vivo assessment of Amyloid deposition, Neuroinflammation, and Metabolic changes in Neurodegenerations of different origin

ANIL FRANK RAMLACKHANSINGH

Imperial College London

Department of Medicine

Neurodegeneration and Neuroinflammation

PhD Thesis

The work enclosed in this thesis is my own apart from what has been referenced

The copyright of this thesis rests with the author and is made available under a Creative Commons Attribution Non-Commercial No Derivatives licence. Researchers are free to copy, distribute or transmit the thesis on the condition that they attribute it, that they do not use it for commercial purposes and that they do not alter, transform or build upon it. For any reuse or redistribution, researchers must make clear to others the licence terms of this work

Abstract

Summary of Objectives:

Neurodegeneration is an important pathological component hallmark of many neurological illnesses. Effective management demands a greater understanding of the changes taking place at a neuronal level.

In this thesis I have investigated the biochemical changes at the cellular level in four conditions associated with neurodegneration – traumatic brain injury (TBI), prion disease, posterior cortical atrophy (PCA) and Parkinson's disease (PD). Positron Emission Tomography (PET) scanning was my main investigative tool.

Each condition was investigated using up to four different radioactive PET ligands:

1. [11C]-PIB, to measure beta amyloid load and detect other β sheet folded proteins in the brain,
2. [11C]-PK11195, to quantitate microglia activation in the brain,
3. [18F]-FDG, to investigate changes in the pattern of cerebral glucose metabolism, and
4. [11C]-SCH442416, used specifically in PD to investigate changes in striatal adenosine 2A receptor concentrations.

Subjects also underwent MRI scanning. Neuropsychological assessments were conducted on TBI subjects in an attempt to correlate any PET changes with clinical findings.

Summary of Results:

Subjects with chronic TBI demonstrated increased [11C]-PK11195 uptake in subcortical structures including the thalamus and putamen distant from the original focal brain lesion. Processing speed in TBI subjects was positively correlated with thalamic [11C]-PK11195 uptake. [11C]-PIB PET did not show a significant increase in signal compatible with amyloid deposition following TBI. In prion disease there was no increased uptake of [11C]-PIB although prion protein form beta pleated sheets. In PCA there is reduced parieto-occpital [18F]-FDG signal despite the [11C]-PIB pattern of binding being more typical of Alzheimer's Disease. Adenosine 2A receptor availability was significantly raised in the striatum of PD patients with levodopa induced dyskinesias.

These studies suggest that amyloid plaque deposition may not be the driving force of neuronal damage while microglial deactivation may play a leading role in driving disease. My work also suggests there is deregulation of adenosine transmission in dyskinetic PD and that A2A adenosine blockade may have therapeutic potential.

Publications arising from this thesis

1. Inflammation after trauma: microglial activation and traumatic brain injury. Ramlackhansingh AF, Brooks DJ, Greenwood RJ, Bose SK, Turkheimer FE, Kinnunen KM, Gentleman S, Heckemann RA, Gunanayagam K, Gelosa G, Sharp DJ. Ann Neurol. 2011 Sep;70(3):374-83. doi: 10.1002/ana.22455. Epub 2011 Jun 27.

2. Adenosine 2A receptor availability in dyskinetic and nondyskinetic patients with Parkinson disease. Ramlackhansingh AF, Bose SK, Ahmed I, Turkheimer FE, Pavese N, Brooks DJ. Neurology. 2011 May 24;76(21):1811-6.

3. 11C-PiB PET does not detect PrP-amyloid in prion disease patients including variant Creutzfeldt-Jakob disease. Hyare H, Ramlackhansingh A, Gelosa G, Edison P, Rudge P, Brandner S, Brooks DJ, Collinge J, Mead S. J Neurol Neurosurg Psychiatry. 2012 Mar;83(3):340-1.

Contribution and collaboration

The work presented in this thesis was primarily conducted by me. I was involved in study design, recruitment, scanning, analysis and interpretation of the results in the TBI studies. In PCA I was involved in recruitment, scanning, analysis and interpretation of results. In the prion disease study my focus was on study design, scanning, analysis and interpretation of results. And finally I was involved in recruitment, scanning, analysis and interpretation of results in the Levo-dopa induced dyskinesia study.

Table of Contents

Chapter 1 Introduction 12

1.1 Introduction 13

1.2 Positron Emission Tomography 14

1.3 PET radiotracers 17

1.4 PET image analysis 19

1.4.1 Generation of the parametric image 20

1.4.2 Region of interest analysis 22

1.4.3 Voxel based statistical parametric mapping 22

1.5 Dementia as a Syndrome 23

1.5.1 Clinical features and Natural history 24

1.5.2 Pathology 25

1.5.3 Management 30

1.6 Amyloid 32

1.6.1 Amyloids in Neuropathology 33

1.6.2 Physiological role of amyloid precursor protein 33

1.7 Levodopa induced Dyskinesia 38

1.8 Figures 42

1.9 References 49

Chapter 2 Microglial activation after Traumatic Brain Injury 57

2.1 Microglial activation after Traumatic Brain Injury 58

2.2 Introduction 60

2.3 Methods 61

2.3.1 Patients: demographic and clinical details 61

Table of contents

2.3.2 Control groups 62

2.3.3 Neuropsychological Assessment 62

2.3.4 Volumetric and diffusion tensor MRI 64

2.3.5 Diffusion tensor imaging analysis 64

2.3.6 PET image acquisition and analysis 65

2.3.7 Brain segmentation and region of interest definition 66

2.4 Results 68

2.4.1 Cognitive Performance 68

2.4.2 TBI patients show increases in microglial activation remote from damaged areas 68

2.4.3 Microglial activation is not increased around the site of focal brain damage 69

2.4.4 Increased thalamic microglial activation correlates with cognitive impairment 70

2.5 Discussion 70

2.6 Tables 75

2.7 Figures 77

2.8 References 80

Chapter 3 Amyloid plaque deposition after Traumatic Brain Injury 84

3.1 Amyloid plaque deposition after Traumatic Brain Injury 85

3.2 Introduction 87

3.3 Methods 88

3.3.1 PET image acquisition 89

3.3.2 PET image analysis – Standardised Uptake Value 90

3.3.3 Neuropsychological Assessment 92

3.4 Results 92

Table of contents

3.4.1 PET scanning 92

3.4.2 Neuropsychological assessment 92

3.5 Discussion 92

3.6 Tables 96

3.7 Figure 98

3.8 References 99

Chapter 4 Amyloid deposition & metabolic changes in Posterior Cortical Atrophy 105

4.1 Amyloid deposition and metabolic changes in Posterior Cortical Atrophy 106

4.2 Introduction 108

4.3 Methods 109

4.3.1 Posterior Cortical Atrophy subjects 109

4.3.2 Sporadic AD and Healthy Control subjects 110

4.3.3 Neuropsychological assessment 110

4.3.4 MRI image acquisition 111

4.3.5 PET image acquisition 111

4.3.6 Image analysis 112

4.3.7 Statistical Analysis 114

4.3.8 Statistical Parametric Mapping (SPM) 114

4.4 Results 115

4.4.1 Subjects 115

4.4.2 PET analysis 116

4.4.2.1 [11C]-PIB 116

4.4.2.2 [18F]-FDG 117

Table of Contents

4.4.3 MRI 118

4.4.4 Neuropsychological assessment 119

4.5 Discussion 119

4.5.1 [11C]-PIB binding is similar in PCA and sporadic AD 119

4.5.2 [18F]-FDG uptake was significantly reduced posteriorly in PCA subjects 120

4.5.3 Posterior metabolism, significantly lower in PCA than sporadic AD 120

4.6 Conclusion 123

4.7 Tables 124

4.8 Figures 125

4.9 References 129

Chapter 5 [11C]-PIB PET does not detect PrP-amyloid in prion disease patients 132

5.1 [11C]-PIB PET does not detect PrP-amyloid in prion disease patients 133

5.2 Introduction 135

5.3 Methods 135

5.3.1 Subjects 136

5.3.2 MRI image acquisition 136

5.3.3 PET image acquisition 137

5.3.4 PET image analysis 137

5.3.5 Statistical analysis 138

5.4 Results 138

5.5 Discussion 139

5.6 Tables 142

5.7 Figures 144

Table of Contents

5.8 References 145

Chapter 6 Adenosine 2A receptor availability in dyskinetic and non-dyskinetic PD patients 148

6.1 Adenosine 2A receptor availability in dyskinetic and non-dyskinetic PD patients 149

6.2 Introduction 151

6.3 Methods 152

6.3.1 Subjects 152

6.3.2 Clinical assessment 153

6.3.3 PET image acquisition 154

6.3.4 MRI image acquisition 155

6.3.5 PET quantification 155

6.3.6 Statistical analysis 156

6.4 Results 156

6.5 Discussion 157

6.6 Tables 160

6.7 Figures 162

6.8 References 163

Chapter 7 Conclusion 168

7.1 Conclusion 169

List of Tables

2.1 Demographics and clinical data of all traumatic brain injury (TBI) patients 75

2.2 Neuropsychological test results: traumatic brain injury and control patients 76

3.1 Clinical features of all traumatic brain injury (TBI) patients 96

3.2 Sample of Neuropsychological test results: traumatic brain injury and control patients demonstrating impaired planning and executive function 97

4.1 Demographic profile of all subjects investigated 124

4.2 Neuropsychological assessment results in the group of PCA patients 124

5.1 Demographics of subjects and controls 142

5.2 Impulse Response Function 75min [11C]-PIB results for patients and controls 143

6.1 Study population 160

6.2 [11C]-SCH442416 Binding Potential of the three groups investigated 161

List of Figures

1.1 Annihilation event produced with a positron being ejected from the nucleus 42

1.2 Possible coincidence events detected by a full ring PET scanner 43

1.3 Summery of pre-preparation steps of PET analysis 44

1.4 Summery of Statistical Parametric Mapping analysis 45

1.5 Illustration of a typical β strand 46

1.4 A – β fibril formation B – X-ray diffraction pattern of fibrillar amyloid 46

1.5 Schematic view of the membrane spanning and cleavage sites of APP770 47

1.6 Schematic diagram of the indirect pathway of the basal ganglia 48

2.1 Transverse sections thought T1 weighted MRI, in traumatic brain injury patients (n=5) with focal brain lesions 77

2.2 Chronic microglial activation is present following TBI 78

2.3 [11C]-PK11195 binding in the regions of interest investigated 78

2.4 Microglia are not activated around the site of focal brain damage following TBI 79

2.5 Thalamic microglial activation correlates with complex information processing speed 79

3.1 [11C]-PIB Standardised Uptake Values (SUV) in control and TBI subjects 98

3.2 Sample [11C]-PIB parametic images for A – Alzheimer's Disease subject, MMSE<25, B – Control and C – TBI subject 98

4.1 A [18F]-FDG parametric rCMRGlc image on a PCA patient 1 (Pt1). B [11C]-PIB cerebellar ratio image on a PCA patient 3 (Pt3) 125

4.2 SPM results comparing PCA, sporadic AD and HC groups 126

4.3 Graphic representation of [11C]-PIB (A) and [18F]-FDG (B) in sporadic Alzheimer's disease (sporadic AD) and Posterior Cortical Atrophy (PCA) 127

4.4 Profound impairment of visual spatial perception in PCA patients 128

5.1 Abundant presence of prion protein plaques in the occipital cortex of the patient with vCJD (PrD1) 144

5.2 Trace PET images at 75 minutes post injection of [11C]-PIB 144

6.1 Sample PET images of [11C]-SCH442416 binding in the groups investigated 162

Chapter 1

Introduction

1.1 Introduction

The world's population is getting older. Improved treatments for cardiovascular, respiratory and metabolic conditions have meant that people are staying healthier for longer. One can however argue that as people age, neurological health and the maintenance of cognitive ability remains an important part of wellbeing. While a definitive cure for any form of neurodegeneration seems some time off our knowledge of these conditions is continuously expanding.

Effective control of the motor manifestations of conditions like Parkinson's disease (PD) has improved survival by years, even decades. Other conditions like Alzheimer's disease (AD) and prion disease are more resistant to control with the latter thought to be resistant to any form of pharmacotherapy.

Our understanding of cognitive decline in neurodegeneration is still in its infancy and more work needs to be done. In this thesis I will be investigating different forms of neurodegeneration. While the overriding emphasis will be on conditions fitting under the umbrella of AD, I will also be investigating PD. With the latter, I would like to investigate how a condition intimately linked to the dopamine pathway may be affected by failure of other, specifically the adenosine, neurotransmitter systems.

I will be thus focusing on four imaging modalities:

1. β amyloid plaque imaging,
2. Imaging of activated microglial cells,
3. Imaging of cerebral metabolism and
4. Adenosine$_{2A}$ (A2A) receptor imaging specifically in PD.

These investigations will help link amyloid pathology and inflammation to conditions predisposing to dementia and improve our understanding of how cognitive impairment develops and progresses. A range of subjects with varying degrees of impairment will be recruited. The demonstration of amyloid pathology and inflammation in these conditions may support usefulness of novel anti-amyloid and anti-inflammatory treatment strategies in these conditions. My investigations in A2A receptors in PD will help strengthen the increasing evidence of the importance of adenosine in the control of PD.

1.2 Positron Emission Tomography

In this section I will be outlining the physics underlying and usefulness of the imaging technology Positron Emission Tomography (PET).

One of the first medical applications of PET scanning was in the imaging of cerebral tumors in 1951[1]. This was performed by the group at the Massachusetts General Hospital making use of the positron emitter [74As]. They found that patients with tumor recurrence had an "unbalanced" scan with increased counts either towards or away from a pair of detectors. Other positron emitting isotopes were subsequently developed including [11C] ($t_{1/2}$ 20 mins), [15O] ($t_{1/2}$ 2 mins), and [18F] ($t_{1/2}$ 110 mins). These were incorporated into molecules and drugs to form radiotracers with known biological properties.

At the heart of positron emitting radionuclides is a proton rich nucleus[1,2]. It achieves stability by converting a proton into a neuron and releasing the residual positive charge as a positron. This particle has specific well defined properties and has an equivalent in mass to an electron. The result of this decay is the loss of positive charge by the atom. A single electron must then be ejected from the atom to balance its charge. This is achieved by a process

called “internal conversion” where upon the nucleus supplies energy to an orbiting electron to overcome the binding energy hence providing it with enough kinetic energy to leave the atom. The result is the ejection of a positron and an electron from the atom leaving it at least 2 electron masses lighter than the parent atom.

The ejected positron becomes deflected from its original path as it interacts with surrounding nuclei and electrons. This interaction can be one of four types:

1. Inelastic collisions with atomic electrons – this is the most common method of loss of kinetic energy,
2. Elastic scattering with atomic electrons – the positron is deflected but energy and momentum are conserved,
3. Inelastic scattering with a nucleus – the positron is deflected often with the emission of Bremsstrahlung radiation[3] (electromagnetic radiation released when charged particles with large energies, compared to their rest energies, decelerate over a very short distance) and
4. Elastic scattering with a nucleus – the positron is deflected but does not radiate any energy or transfer energy to the nucleus.

With its kinetic energy expended the positron comes to rest within 2-6 mm and then combines with a neighboring electron to form a metastable intermediate species call a positronium. This particle has a mean life span of about 10^{-7} second. This annihilation event is coupled to the release of electromagnetic radiation in the form of two gamma ray photons of 0.511MeV (the rest mass equivalent of each particle). The photons should be released at 180^{o} to one another in order to conserve momentum which is close to zero at the time of

annihilation. See figure 1.1. However, the release of the pair of photons is not exactly 180^{o} to each other due to both the uncertainty principle and also to the non-zero momentum of the positron – electron pair at the time of annihilation. In <1% of instances 3 photons of energy (instead of 2), are released.

Positron annihilation and gamma photon emission thus takes place a finite distance away from the parent atom. For [18F] the positron travels around 2mm before annihilation but with a high energy positron, such as released by [82Rb], this can be as much as 5.9mm[1]. The implication of positron travel prior to annihilation is a reduction in the spatial resolution of a PET scan. The calculation of the point of annihilation also relies heavily on two photons being emitted at 180^{o} to each other. If this angle deviates to some extent the resolution of the PET scan is again adversely affected.

Along with the development of new tracers, scanner technology has also improved from the first one dimensional scanners of the 1950's to the three dimensional scanners used today. Many machines employ a 15 cm long cylinder of detectors containing the crystal bismuth germanate $Bi_4(GeO_4)_3$ (BGO). This crystal scintillates emitting visible light when struck by gamma 511 keV radiation and is coupled to photo-detectors responsible for the detection and amplification of visible light. A photon of energy colliding with the BGO crystal results in the production of visible light which is then collected and amplified. The annihilation of a single positron in most instances results in two oppositely sited photo-detectors being activated within nanoseconds of one another in the field of view of the PET scanner. This annihilation coincidence detection allows the locations of positron emissions to be computed. Random coincidences can also occur if two unrelated photons strike opposing detectors at similar times apparently coming from a single coincidence. See figure 1.2. The random coincidence rate of a PET scanner is proportional to $2tA^2$. In this estimation t is the

coincidence window width or the maximum width of time between two detectors being activated allowing it to be linked to a single coincidence and A is the event rate or activity present at each detector in the scanner field of view. PET data can be collected during the scan to estimate the level of random coincidences and a correction applied to negate their effect. In this thesis the Siemens ECAT 962 scanner was used. It has an axial view of 15.5cm with a maximum resolution of 2.42mm x 2.42mm x 2.092mm. This scanner has been used in previous studies in AD and PD providing a library of control and patient PET scans for comparison.

1.3 PET radiotracers

There has been rapid development of PET tracers over the recent years. For this thesis most of the tracers used had a proven track record, reliable production and availability. In investigating the A2A receptor, I however used a radiotracer whose use in humans and production is less well described. [11C] containing compounds were produced on site by Hammersmith Imanet while [18F] containing compounds were purchased from a local supplier.

In vivo amyloid imaging was performed with [11C]-PIB PET, chemical name {N-methyl ^{11}C-}2-(4'-methylamino-phenyl)-6-hydroxy-benzothiazole[4,5]. This marker is a neutral thioflavin-T analogue with nanomolar affinity for fibrillar beta amyloid. It has been used extensively for imaging amyloid in AD and cognitive impairment[6-8]. As a thioflavin-T derivative, ^{11}C-PIB might also be expected to bind to prion protein amyloid aggregates present in Creutzfeldt-Jakob disease. Its usefulness in this scenario has not been systematically tested.

The identification of activated microglia depends on detection of proteins expressed by these cells as they change from their resting state to becoming phagocytic. The mitochondria of activated microglia express a cholesterol transporter known as the translocator protein (TSPO). The isoquinoline carboxamide ligand [11C] -PK11195, chemical name N-butan-2-yl-1-(2-chlorophenyl)-N-methylisoquinoline-3-carboxamide, selectively binds to TSPO making it a useful marker of activated microglial cells[6,8]. TSPO is, however, also expressed by endothelial cells which also bind [11C]-PK11195. Brain uptake can be contaminated with a vascular signal making analysis of uptake kinetics more complex. In these studies I employed an in-house specialized software, SuperPK, which uses cluster analysis to kinetically separate and correct brain signals for vascular binding. This will be discussed further later on.

[18F]-FDG, chemical name [18F]-2-fluoro-2-deoxyglucose is a glucose analogue where the 2' hydroxyl group (-OH) is replaced by 18F. The half-life of 18F is 109.8mins radioactively degrading to 18O. [18F]-FDG is taken up by metabolically active cells and phosphorylated to become [18F]-FDG-6-phosphate. The latter becomes trapped within these cells as it cannot enter the glycolysis pathways until the 2' hydroxyl group is restored by the decomposition of 18F to 18O and the latter combining with surrounding H atoms. PET studies using [18F]-FDG, in AD demonstrate reduced uptake in the hippocampus and association cerebral cortex[8]. Brain [18F]-FDG PET can thus be used to demonstrate areas of altered cerebral metabolism.

The imaging of the A2A pathway has become possible with the development of [11C]-SCH442,416, chemical name 2-(2-furyl)-7-[3-(4-methoxyphenyl)propyl]-7H-pyrazolo[4,3-e][1,2,4]triazolo[1,5-c]pyrimidin-5-amine. The use of this tracer is not yet widespread and both patient and control scans were performed to enable effective comparisons. To ensure that no assumptions are made spectral

analysis will be performed. With this approach, concurrent blood sampling enabled the contribution of [11C]-SCH442416 metabolites to radioactive counts to be calculated and accounted for.

1.4 PET image analysis

Before the analysis of PET data could take place, certain basic preparation steps were undertaken to make the data meaningful. These are outlined below along with the technique used for individual PET ligand image analysis.

The result of PET scanning is anatomical data of tracer uptake during the entire PET acquisition time period. During analysis these dynamic time frames must be combined or added together to provide meaningful information on tracer distribution during the PET scan. Time frames that provided the highest signal to noise ratio for each particular tracer were chosen. Typically however, early time frames consist of mostly noise and were excluded. The result of this combining procedure was an “add image” that could in fact be used to grossly identify large cerebral structures. The investigations performed in my thesis however required precise anatomical definition of intra-cerebral structures. All subjects thus had structural MRI performed to provide the anatomical data needed for analysis.

MRI’s were performed using either a 1.5 or 3 tesla scanner and the T1 sequence was used as it provided the best soft tissue information. The MRI was first segmented into grey matter, white matter and CSF. For my investigations, grey matter maps were mostly used but when necessary white matter regions were hand drawn. The grey matter map was then registered onto the PET scan to provide the anatomy needed.

Cerebral structures must then be labelled. In house probability atlases (e.g. the three dimensional human brain, Chapter 4, reference 16) generated from anatomical data from a bank of normal control MRI scans was used for this purpose. This standard atlas was then applied onto the MRI providing the anatomical data used to label the PET scan.

The result of this early stage of analysis was an anatomically labelled PET scan. Importantly, during this analysis process the PET data was not modified by any registration or normalisation algorithms that could potentially introduce noise to the genuine PET signal.

1.4.1 Generation of the parametric image

In this thesis I have used different techniques to generate parametric maps based on pre-existing evidence in the published literature and its application to the condition being investigated.

In [11C]-PIB and [11C]-SCH442416 analysis cerebellar RATIO images were created for each individual subject. The basis of this technique is the lack of pathological changes in the cerebellum in many (but not all) neurodegenerative conditions. As a region the cerebellum was thus thought to represent background activity against which the rest of the scan could be compared to. Standardised cerebellar RATIO images were thus thought to be comparable.

This technique can only be used if there is a viable reference region where we can be certain of a lack of tracer binding. In TBI and prion disease, the cerebellum could in fact be involved. In TBI parametric [11C]-PIB images were generated by producing standardised uptake values (SUV). SUV images were normalised against a factor taking into account the subject body surface area and the total amount of radioactivity injected at the start of the PET scan. SUV images can thus be

compared. In prion disease, the availability of plasma radioactivity data meant that spectral analysis could be performed. This technique makes no assumptions on the number of compartments for which tracer distribution takes place and results in the generation of a plasma input function. Using this function, parametric images are generated. Spectral analysis was also used to generate the parametric image for the [18F]-FDG scans. Maps of regional glucose metabolism were generated using a plasma input function reference. This technique will be explained further on.

The generation of the parametric image for [11C]-PK11195 scans was complicated by the widespread distribution of this tracer throughout the brain, the cerebral vasculature and the musculature. Cluster analysis was used in the generation of the parametric image. This technique will be explained further in Chapter 2 but briefly, the reference region was generated by extracting from each scan clusters of voxels thought to represent background activity. Images were then standardised against these clusters to generate the parametric map.

At the end of this stage of analysis the following images were in place:

1. PET parametric image,
2. Registered grey matter map and
3. Registered labelled atlas.

Using this data I then performed two types of analysis:

1. Region of interest (ROI) analysis and
2. Voxel based statistical parametric mapping (SPM) analysis.

1.4.2 Region of interest analysis

In ROI analysis, PET tracer uptake in preselected anatomical regions of the brain were sampled compared statically. The regions chosen were based on previous research and on hypothetical models of disease pathology. ROI analysis can thus inform on where PET tracer uptake differs statically between control and patient groups.

1.4.3 Voxel based statistical parametric mapping

In SPM analysis, patient PET scans were normalised into standardised stereotaxic space. The result of this step was to help standardise all PET images ensuring all voxel anatomically correspond. It could be argued that normalising into standard space introduced significant levels of noise. Attempts to overcome this were made by smoothing the images using an isotropic Gaussian kernel. Smoothing thus helped to allow for inter-individual anatomical variability and helped improve the signal to noise ratio.

Control and patient scans were then grouped together to allow for inter-group comparisons to be made. During comparison voxels clusters of a standard size were compared and a t statistic calculated. These SPM(t) maps were then displayed on standardised glass brains to enable anatomical localisation to take place. The SPM analysis enabled the identification of regions of the brain that might of previously have been missed on ROI analysis and can be considered as an exploratory form of analysis. See figure 1.4.

In this thesis I used SPM analysis specifically in the analysis of Posterior Cortical Atrophy (Chapter 4). During this statistical analysis, mean global normalization was omitted as an option. This identifies the deviation of SUV voxel values from the reference. Changes in the pattern of binding

may actually be obscured by global changes affecting all cortical voxels. This must thus be considered as a limitation to this study.

1.5 Dementia as a Syndrome

Dementia is a clinical syndrome. It is associated with a progressive impairment of multiple cognitive functions, including short term recall, affecting the ability to perform activities of daily living despite the presence of normal consciousness[9]. It can result from many different diseases all typified by the relentless loss of neurons and neuronal connections. The result is increasing difficulty with thinking, attention, and memory accompanied by personality change.

Dementia can be further subdivided into cortical, subcortical or mixed depending on the region of the brain primarily affected. In cortical dementia there is thinning of the relevant cortical grey matter. The most common dementia syndrome worldwide is AD. In AD there is selective thinning of the temporo-parietal cortex. However, neuronal loss is not localised to the cortex but also targets subcortical areas e.g. the hippocampus and amygdala[10,11]. The subcortical dementias affect the subcortical grey matter structures early in the course of the illness. Progressive supranuclear palsy (PSP) and Huntington's disease (HD) are both examples of subcortical dementias.

It must however be remembered that in even in conditions like Parkinson's disease where motor symptoms are most prominent there is cognitive decline with disease progression. AD may also exist in conjunction with cerebrovascular disease with the latter contributing to cognitive decline. These mixed dementias also include conditions like Creutzfeldt-Jakob disease (CJD). Dementia syndromes involve neuronal death. While in vascular dementia the

cerebrovascular system is to blame in many other forms of dementia, the cause this demise has long been linked to interaction between an abnormally aggregated protein, the target neuronal cell and a toxic micro-environment related to microglial activation.

1.5.1 Clinical futures and Natural history

The symptoms of dementia can be categorised by the presence of the five A's – Amnesia, Aphasia, Agnosia, Apraxia and Agitation (changes in Behaviour)[12]. Although the features of cortical and subcortical dementia differ in accordance to their differing pathologies these symptoms tend to all be present but with differing severities.

In sporadic AD, the most common cause of cortical dementia, there is typically a progressive impairment of recall. Typically, recent events are not remembered and there may be difficulty putting names to faces. Difficulty with word finding, narrowing of the vocabulary and difficulty with calculations and arithmetic accompany the amnestic problems. Visuo-spatial awareness may become impaired with the development of apraxia. Progression is chronic taking years for symptoms to fully evolve. Loss of frontal lobe control may result in inappropriate behavior, sexual indiscretion and changes in appetite. Continued deterioration leads to immobility, apathy and mutism. The disease seldom occurs before the age of 45 but the incidence rises exponentially after the age of 65.

Apart from the sporadic form of AD there are also monogenic forms typified by earlier onset of symptoms and rapid progression associated with mutations in the presenilin or amyloid precursor protein genes. There also exists, AD variants such as posterior cortical atrophy (PCA) and progressive apraxia and aphasia where presenting clinical features relate to the anatomical area initially damaged during the disease course. There is much debate on

whether these conditions should actually be considered as different illnesses but pathologically they resemble AD and are thought to represent an atypical form of AD.

Traumatic brain injury (TBI) is a common acquired risk factor for the late development of AD[13]. After TBI there is an early rise in levels of the amyloid precursor protein (APP) and an intense inflammatory response with the mobilization of microglia to the site of injury and active phagocytosis of dead and dying cerebral tissue[14]. Clinically, TBI can be associated with a post concussive syndrome, progressive cognitive decline and late onset seizures after recovery from the initial event. Rather than being a single static event TBI seems to kick start a cascade of events leading to cerebral damage. It provides a unique opportunity to observe this process in action.

The subcortical and mixed forms of dementia vary greatly according to the underlying pathology and clinical features relate to the anatomical region of the brain affected. In CJD, cerebellar and basal ganglia involvement leads to the motor ataxia and myoclonus. These changes are marked by the rapid deposition of mutated prion protein arranged into amorphous plaques thought to be responsible for driving degeneration.

1.5.2 Pathology

The pathological changes in all forms of dementia are linked to the abnormal production and aggregation of proteins. The protein constituents vary according the type of dementia and the stage of the disease. In sporadic AD beta amyloid plaques and hyperphosphylated tau arranged into neurofibrillary tangles (NFT) is a typical finding[11].

Not surprisingly, initial postmortem investigations in AD focused on the severe end of the spectrum. Gross findings revealed a severely atrophied brain with extreme involvement of the hippocampus and enthorhinal cortex. Microscopically, characteristic patterns of protein deposition have been identified as[12,15,16].

1. Extracellular beta-amyloid protein. This forms diffuse and neuritic fibrillar plaques characteristic of AD. These amyloid plaques stain with Congo Red, thioflavine, periodic acid – Schiff (PAS) and silver staining methods. Amorphous plaques, seen particularly in cerebellum, do not stain with thioflavins.

2. Hyperphosphorylated microtubular 'tau' proteins forming intracellular pairs of helical filaments. Filaments form loops, coils and tangled masses within the neuron and are known as neurofibrillary tangles (NFT). NFT production and deposition heralds a cascade of events leading to neuronal death leaving behind ghost tangles.

The progressive accumulation of these proteins within the brain has different time courses and relates differentially to cognitive changes[16,17,18]. In the Braak staging of AD (1991)[19] amyloid deposition starts first in the cingulate, inferior temporal, and frontal cortex in asymptomatic subjects (stage A). This is followed by spread dorsally and posteriorly into association neocortical areas (stage B). The subcortical structures and hippocampus are then targeted (stage C) as clinical features worsen and time passes.

In early disease NFTs are localised to a single layer of the transenthorhinal region (stage I – II). Continued progression involves the entire transentorhinal region and entorhinal cortex (stage III – IV). Involvement of the entire entorhinal cortex then follows. Neocortical involvement follows including the hippocampus (stage V – VI)[20]. Clinical deterioration is perhaps the most important factor however.

The deposition of abnormal protein aggregates is accompanied by widespread microglial activation. In their quiescent form microglia are continuously extending their cillary processes surveying the brain milieu for changes. This resting population of cells forms the resident population of macrophages within the brain. They continuously sample the microenvironment around them. Interactions between the glycoprotein CD200 found on neurons and its corresponding receptor on microglial membranes keeps them in this inactive state[21]. Protein aggregation however results in neuronal dysfunction and death resulting in the release of adenosine triphosphate (ATP) into the microenvironment of the neuron stimulating resting microglia into becoming actively phagocytotic. They change morphologically resembling macrophages clearing dead neurons and proteinaceous fibrillar debris. Activated microglia also release cytokines including IL-1 and TNF-α. These pro-inflammatory agents provoke further cytokine release and stimulate the microglia to release free radicals including nitric oxide (NO). This in turn causes lipid oxidation, membrane damage and DNA disruption. MHC type 2 antigens are expressed by these activated microglia. The mitochondria of activated microglia express the cholesterol translocator protein – TSPO. TSPO is absent on quiescent microglia and so provides a distinctive marker of activated microglia[22]. The continued and uncontrolled activation of microglia may contribute to further neuronal damage and death. Indeed correlations have been found between microglial activation and cognitive impairment in mild cognitive impairment patients[23].

The role of amyloids in dementias is debatable. Further discussions into the role of amyloid will follow but is it friend or foe? When does deposition begin during the course of illness? Is amyloid most toxic in its monomer/oligomer confirmation, as the amorphous form or as a fibrillar plaque? In certain conditions with AD pathology, amyloid plaque distribution can be atypical. For example, in monogenic familial AD, the early distribution of amyloid can differ from sporadic AD.

The pattern of deposition appears to fall into one of three groups[24]:

1. Early involvement of the subcortical grey matter, including the basal ganglia
2. Diffuse involvement of the cerebellum or
3. Earlier involvement of the neocortex in a similar pattern to sporadic AD.

PCA is a progressive neurodegenerative condition characterized by early visuospatial perceptual problems[25]. Amyloid deposition can be widespread and has an unclear relationship with the cognitive deficit. Early features can include Balint's syndrome (simultanagnosia, ocular apraxia and optic ataxia)[26] variably accompanied by the Gerstmann's syndrome, visual agnosia, alexia, agraphia, and transcortical sensory aphasia with the later development of memory impairment and features typically associated with AD. For this reason PCA has long been considered as an atypical presentation of AD with a posterior (occipital) focus of degeneration. This view has been strengthened by postmortem studies showing characteristic features of Alzheimer´s disease with senile plaques and neurofibrillary tangles.

In vivo imaging studies of PCA are limited and have produced conflicting results[27-30]. Short case series and singe subject case reports have mostly shown similar patterns of amyloid plaque deposition in PCA and sporadic AD. This is despite a single study suggesting that amyloid plaque deposition has a greater tendency to focus on the posterior parts of the brain[27]. More consistent however is the demonstration of reduced cerebral metabolism in the posterior regions of the brain. Only one study currently exists in the published literature where both amyloid plaque deposition and cerebral metabolism have been performed on the same PCA subjects[30]. Again no difference in regional plaque deposition binding between

PCA and sporadic AD was identified despite a focal reduction in posterior cerebral metabolism.

After TBI, there is a greater risk of developing AD later in life. The underlying pathophysiology of chronic TBI however remains poorly understood. Patient outcomes are highly variable for reasons that are often unclear. Patients can clinically improve or deteriorate years after TBI and may develop unexpected consequences such as post-traumatic epilepsy or late cognitive decline including Alzheimer's disease[31,32]. On-going inflammation, driven by unknown factors, may play a significant role. In animal models, the initial microglial activation provoked by acute TBI has been shown to persist for at least a year[33,34]. In humans, post-mortem studies have shown microglial activation many years after TBI[35]. At a cellular level one might expect to see accumulation of amyloid plaques alongside sustained microglial activation. This remains to be proven in vivo however and this is one of the questions I wish to address in this thesis. This would be especially useful as similarities between sporadic AD and TBI pathology would suggest that AD management strategies may also being applicable to TBI. However, while amyloid precursor protein production is increased after TBI, the formation of amyloid plaques is infrequent.

The prion diseases make up a collection of illnesses characterized by the rapid onset of dementia associated with other neurological signs and symptoms. The prion protein has being identified as the infectious agent[36,37]. The native protein, cellular prion protein, (PrPc) is a normal membrane-bound glycoprotein anchored either by synaptic vesicles or endosomal vesicular organelles. It is a metalloprotein thought to be involved in copper metabolism. In genetic cases, mutation of this protein results in the creation of PrPsc. Microscopic examination of brain sections, demonstrate PrPsc either in plaque or granular aggregates. These PrPsc plaques may have similar biophysical properties of amyloid

plaques. The neuropathology of the prion diseases is highly variable, but certain sub-types, particularly Gerstmann-Sträussler-Scheinker syndrome and variant CJD are associated with large PrPsc-amyloid plaques.

Unknown however is how PrPsc plaques concentration and distribution changes with disease progression. Despite several promising developments in basic science, there is as yet no treatment for prion disease that slows or halts the underlying disease process. The evaluation of putative therapeutics would benefit considerably from a non-invasive biomarker which directly measures the presence and distribution of abnormal PrPsc in the brain.

1.5.3 Management

As with any chronic incurable condition, the management of dementia has to address the needs and wishes of both patients and carers. Issues of capacity may arise as the condition progresses and should be addressed earlier on during the course of the illness. In the absence of a cure two main symptomatic classes of drugs have been used to improve the quality of life of patients[11,12]:

1. Cholinesterase inhibitors and

2. NMDA antagonists.

Both these agents have been used in the management of AD with moderate success usually improving symptoms evidenced by and improvement by 2-3 points on the Alzheimer's Disease Assessment Scale (ADAS-Cog).

The cholinesterase inhibitors include donepezil, galantamine and rivastigmine. As cholinesterase inhibitors they increase the concentration of acetylcholine at the cholinergic

synapses. Side effects include diarrhea, muscle cramps and fatigue. Their use in the UK is limited to mild to moderate AD. Guidelines for their use, in the UK, have been issued by the National Institute for Clinical Excellence (NICE)[38].

Memantine is a voltage dependent, moderate affinity, non-competitive NMDA receptor antagonist. It blocks the effect of pathologically elevated levels of glutamate by preventing calcium influx into the neuron. It has been used in AD and vascular dementia. It is generally used in more severely affected cases where cholinesterase inhibitors are contra-indicated, not tolerated or ineffective. It may also be used in conjunction with cholinesterase inhibitors.

Public health regulations play an important part in controlling conditions like prion disease where in the non-genetic or spontaneous forms transmission has been linked to contaminated blood products and the use of infected sheep for chicken feed. This has been linked to the outbreak of new variant CJD in the UK in the 1990's.

Dementia management remains a developing field. New immune modulation techniques have been developed to aid in the clearance of amyloid plaques from the brains of patients with AD. The usefulness of these treatments is still to be proven, and side effects such as micro-haemorrhages, vasogenic oedema and an inflammatory response may limit their use[39]. There is also debate on when treatment is best begun. Current guidelines focus on the more severe end of the scale, but it may be that treatment should focus on milder cases in an attempt to preserve the already threatened neuronal population.

The presence of non-physiologically active protein aggregates link all these conditions. An understanding of what is meant by amyloid is however important. I shall now discuss what constituent amyloid and how its presence may play a role in neurotoxicity.

1.6 Amyloid

The role of amyloid in neuro-degeneration is a major focus of my thesis. It is however important to have a clear understanding of what amyloid is and the role it plays in dementia. The term amyloid, strictly speaking, refers to a group of proteins that conform to a certain physical characteristic. They are extracellular deposits of protein fibrils with a characteristic appearance under the electron microscope, have a typical X-ray diffraction pattern and an affinity for Congo red with concomitant green birefringence[40,41]. In reality a much broader definition of amyloid is usually applied referring to any amorphous aggregate of native or recombinant protein. Amyloid aggregates are kinetically stable structures persisting for long periods of time and forming visible plaques within tissue.

Amyloid production begins with the synthesis of linear polypeptide chains of amino acids. In the case of Alzheimer's disease β amyloid-40 or -42 are eventually produced. Native proteins then undergo tertiary level folding in the endoplasmic reticulum to become biologically active. Incorrectly folded proteins are usually not allowed to survive, degraded by a complex cellular response involving lysosmes and proteosomes. However if these systems are overwhelmed, inoperable or inhibited the result is the survival of these incorrectly folded proteins which aggregate to produce insoluble amyloid.

The typical tertiary structure adopted by amyloid proteins is that of β sheeting – extended saw toothed sequences of amino acids with amide bonds almost coplanar and side chains

that alternate above and below the plane of the peptide backbone. These parallel or anti-parallel β sheets are held together by inter-strand hydrogen bonds (see figure 1.5). The β sheet conformation usually helps stabilise protein conformations, acting as a scaffold for protein-protein and protein-DNA interaction and enabling the further folding of proteins into quaternary structures[42,43,44]. Amyloid proteins are however more prone to forming protofilament aggregates. Protofilaments become arranged helically forming the amyloid fibrils identified on electron microscopy. Fibrils are also responsible for the binding Congo red dye and producing typical X ray diffraction (see figure 1.6).

1.6.1 Amyloids in Neuropathology

AD is the most intensely studied of the amyloidoses. The amyloid plaques of AD have been the subject of great study since they were first identified on post-mortem studies of AD patients by Alois Alzheimer and colleagues. Amyloid plaques can be diffuse fibrillar plaques or neuritic plaques which contain fibrils of β-amyloid protein surrounding degenerating nerve fibres. Other molecules making up the amyloid plaque include proteoglycans, α_1-antichymotrypsin and apolipoprotein E[40,45].

It remains unclear whether β amyloid plaques are neurotoxic or protective in AD, taking toxic amyloid oligomers out of circulation. Below I wish to discuss these concepts and ideas further.

1.6.2 Physiological role of amyloid precursor protein

APP is the parent molecule of both sAPPα and β amyloid has varied physiological roles. It is a type 1 integral membrane glycoprotein comprising of large N-terminal extracellular domain

and a single transmembrane domain and a short cytoplasmic tail[41,46]. Within the extracellular domain the protein has a cysteine rich terminus followed by an anion region and then a neurotrophic region. It is processed post translationally with glycosylation and proteolytic cleavage. Ubiquitous throughout the body APP knockout mice revealed reduced body weight grip strength, locomotor activity, synaptic transmission, hypersentivity to seizures and forebrain commissure defects[47].

APP is present as three major isoforms APP770, APP751 and APP695[48]. The APP695 isoform is predominant in the brain and it is this isoform to which we refer in the remainder of this introduction. It is a membrane bound protein found on many intracellular structures including endoplasmic reticulum and the Golgi apparatus but importantly it is also found on synaptic and postsynaptic dendrites of axons.

The precise role of APP has not yet been identified but as a large membrane bound protein it may in fact function as a G protein coupled receptor[46]. Binding of an as yet unidentified ligand, results in the dissociation of APP into a G_{α} subunit, $G_{\beta l}$ subunit and G_{o}. The result is the activation of numerous signalling cascades by these subunits, including adenyl cyclase, phospholipase C and voltage dependent calcium channels.

APP also possess several domains that promote binding to specific substrates e.g. heparin, laminin and collagen[46]. This has led to the suggestion that APP also functions as an important cell adhesion molecule important in the regulation of neuronal growth and synapse formation.

Pathology exhibited by APP knockout mice suggests altered neuronal structure and function. Changes include gliosis, decreased neocortical and hippocampal levels of synaptopysin, reduced dendritic lengths in hippocampal neurones, reduced survival of cultured neurones and impaired long term potentiation are present. APP knockout mice however still seem capable of learning and only slightly underperform the wild type cohort on learned tasks[49]. This effect could however be secondary to an APP compensatory mechanism involving the APP like protein (APLP) type 1 and 2 molecules with the relative deficiency in APP becoming more relevant with age.

Despite being a membrane bound receptor molecule APP is acted on enzymatically by secretases at 3 sites of cleavage α, β and ϒ. See figure 1.7. The α site lies relatively close to the membrane spanning domain between lysine 613 and leucine 614. The result is the formation of a soluble protein 612 amino acid sAPPα. The β site occurs between residues 596 and 597 of APP695. The result is the production of a 595 amino acid long sAPPβ. Interestingly β secretase levels and activity are increased in AD[50]. It must be noted that the production of sAPPα and sAPPβ are mutually exclusive. The remaining membrane bound portion of APP known as the carboxy terminal fragment (CFT) also varies in size according to the secretase responsible for cleavage. Beta secretase produces a C99 while α secretase results in a marginally shorter C83 product. The activity of ϒ secretase then comes into play. This enzyme is responsible for cleaving APP at the carboxyl terminus. The cleavage site is located within the APP transmembrane domain. In the case of C99, the result is the production of the non-membrane bound Aβ1-40 or Aβ1-42 along with fragments spanning Aβ1-39 and Aβ1-43 and the C-terminal fragment. The latter molecule, Aβ1-43, is especially important as it forms the nucleus of the amyloid plaques[45]. C83 component cleavage produces a shorter Aβ like fragment called p3 plus the same C terminal fragments.

The parent protein APP is thus responsible for generating sAPPα, sAPPβ, Aβ1-40, Aβ1-42, p3 and CFT. Such a large group of proteins originating from one source would suggest that they have a physiological role.

Neuronal activation of muscarinic acetyl choline receptor (mACh) in hippocampal, striatal, cortical and cerebellar slices of rats resulted in increased levels of secreted sAPP production[51]. Certainly sAPP acts as a ligand, binding to LDL receptor related protein. LDL binding and regulation is an important part of long term potentiation (LTP) and neuronal function. ApoE, another protein linked to LTP can bind sAPP in serum and may regulate its clearance[52]. sAPPα binds to the class A scavenger receptor highly expressed on brain and systemic macrophages. Its primary role is clearance of modified and oxidised lipoproteins but it can also bind Aβ1-42 microaggregates. sAPP binds to activated kininogen, a protein involved in clotting and angiogenesis also found in the brain. sAPP binding to fibulin-1 activates guanylate cyclase and regulates membrane excitability by regulating calcium homeostasis. sAPP thus has many binding sites and is likely to be the principal APP fragment involved in memory processing[41].

Like other bound proteins, it can be internalised into lysosomes and degraded. sAPP activation of guanyl cyclase seems most interesting as it results in the modulation of a GMP dependent protein kinase responsible for the modulation of K^+ channels that become activated during the hyperpolarisation phase of synaptic depolarisation. sAPP also down regulates NMDA receptor mediated currents and regulates calcium homeostasis[53]. Thus though a multitude of physiological effects sAPP is able to modulate neuronal activity and plasticity.

What of the Aβ fragments produced by Ɣsecretase activity on the C99 CTF produced by β secretase activity? Aβ fragments vary in size from 39 to 43 amino acids. Aβ1-42 aggregates more readily than other molecules and levels are increased in AD. The tendency to aggregate means Aβ is found not just as monomers but also dimers and oligomers. It is only after the formation of oligomers that further aggregation leads to the proto-fibril and fibrils that make up the bulk of the amyloid plaque. See figure 1.6.

Unlike the proven physiological importance of APP and sAPP, the Aβ fragments seem to be actively cleared rather than taking part in any signalling pathways. Receptors allocated to this task include the receptor for advanced glycosylation endproducts (RAGE) and serpin enzyme complex receptor (SEC-R)[54,55]. Aβ may also complete with lipids for binding to ApoE thus interfering with neuronal membrane metabolism and interrupt the functioning of the mACh receptor found on neurones. It is not surprising that Aβ fragments inhibit hippocampal LTP and have a negative effect on memory. These proteins are however physiologically active and appear to regulate neuronal function. Aβ solutions containing the Aβ1-42 component can inhibit LTP in the hippocampus when administered minutes before high frequency stimulation. Solutions free of fibrillar Aβ aggregates also inhibited LTP. Careful removal of monomers and oligomers however fails to prevent LTP inhibition[56]. Attention has thus been put on oligomers. These species seem responsible for the LTP inhibition. This inhibition is not clearly understood but may be secondary to the binding of Aβ to nicotinic receptors on pyramidal cells and GABAergic inhibitory interneurons. Activation of the former facilitates LTP[41].

Brief mention will also be made of tau. Abnormal aggregates of this protein are also found in AD. Tau however is independent of APP and Aβ and not found in amyloid plaques. Tau protein aggregates are intraneuronal and hyperphosphorylated and are arranged into paired

α-helices in AD. Other tauopathies include progressive supranuclear palsy, chronic traumatic encephalopathy and fronto-temporal dementia. Native tau protein is an important neuronal microtubule-associated protein. Its main role is to stabilise the microtuble system key to axonal and dendritic function. Tau microtubules are also found in astrocytes and oligodendrocytes. The phosphorylation of tau is a highly regulated process catalysed by kinases[11,57,58].

Hyperphosphorylation in disease states typically occurs at 30 set points along the tau protein. The result is the aggregation of tau into insoluble helices with the disruption of micotubular system and death of the host cell. It is still debated whether tau aggregation can occur in AD before amyloid plaque deposition has occurred. This question will be of increasing importance if it is eventually proven that amyloid plaques formation is actually a protective mechanism not directly driving neuro-degeneration. It may in fact prove that tau is the provoking protein driving the whole process.

1.7 Levodopa Induced Dyskinesia

Described thus far have been conditions where cognitive impairment is a significant symptom. However it must be remembered that even in conditions like PD, typically considered to be a movement disorder, cognitive decline can occur. In fact a person with PD is 5-6 times more likely to dement that an age matched controls without PD. My focus however will be on the motor aspects of PD. People living with PD at some stage will require treatment with dopaminergic drugs. As the condition progresses and doses increase, they run the risk of developing levodopa induced dyskinesia (LID)[59]. With LID there is the development of abnormal writhing, involuntary movements linked to dopamine administration. LID can be diphasic, related to increasing or decreasing plasma dopamine

levels; peak dose dyskinesia, linked to plateau plasma dopamine levels; or off-period dystonias, related to dystonic akinesia occurring prior to dopamine administration.

The pathophysiology of LID is thought to be linked to a loss in the feedback mechanisms controlling the direct and indirect pathways of the basal ganglia. Components of the complex include the globus pallidus interna (GPi), globus pallidus externa (GPe), substantia nigra pars reticulata (SNpr), substantia nigra pars compacta (SNpc), subthalamic nuclei (STN) and the thalamus. See figure 1.8. Alteration in striatal output to the GPi is a key pathological process occurring in Parkinson's disease and in the development of dyskinesias. Output neurones in the striatum express dopamine D1 and D2 receptors and receive a tonic dopaminergic input from the SNpc. Output neurones that make up the direct pathway express D1 receptors. These neurones transmit GABA, substance P, and dynorphin. Dopaminergic input has an excitatory effect on the direct pathway. Striatal neurones of the direct pathway are inhibitory and project directly onto the GPi/SNpr complex. Output neurones of the indirect pathway express D2 and A2A receptors. Dopaminergic input here is inhibitory. The indirect pathway involves GABA inhibitory projections from the striatum to the GPe, GABA inhibitory projections from the GPe to the STN and finally an excitatory glutamatergic projection from the STN to the GPi/SNpr. Striatopallidal neurones give rise to extensive local collateral axons that arborize with surrounding axons, dendrites and spines. It is here that A2A receptors are expressed[60-62]. These neurones also transmit enkephalin A. In PD there is reduced dopaminergic input from the SNpc. The net result is a reduction in the activity of the direct and increased activity of the indirect pathways resulting in reduced activation of the ventral thalamic nuclei and the motor cortex. Levodopa therapy acts to normalise this situation but can overstimulate the direct pathway when dyskinesias occur.

The pathogenesis of dyskinesias is also linked to A2A availability in the indirect pathway. Here receptors are concentrated along the spinous processes of striato – external pallidal neurones and along the collateral feedback branches. The binding of adenosine to these G protein linked receptors results in a cascade of reactions that can inhibit or stimulate the release of GABA. More clearly defined however, is the antagonistic relationship between D2 receptor activation and A2A activation which is thought to result in a reduction of the D2 receptor mediated inhibition of GABA release. Adenosine binding to A2A can also reduce its affinity for dopamine by the formation of the D2/A2A complex.

The variable influence of A2A activation on GABA release is also linked to the presence of this receptor on the presynaptic striatopallidal membrane and the local collateral feedback neurones. Thus while the initial result of increased A2A stimulation may be inhibitory, an increase in GABA from collateral neurones will counteract this effect with a reduction in GABA release. This precise and delicate balance is disrupted in dyskinetic PD. With increased A2A receptor activation there is a reduction in the ability of dopamine to bind to D2 and variations in the activity of the local collaterals which are normally responsible for ensuring a smooth and tonic inhibition of the thalamus. The inhibition of the GPi/SNpr thus becomes variable. Dyskinesias result when the inhibitory output from the GPi/SNpr to the thalamus is reduced resulting in thalamic over activity and increased motor activity.

The relationship between dyskinesia and A2A receptor availability may be more complex. Elevated (pre-proenkephalin) PPE levels are associated with an increased risk of development of dyskinesia[63]. While a causal relationship between dyskinesia and PPE has not been demonstrated, elevated PPE-A is responsible for keeping the brain in a primed condition for the development of dyskinesia. In MTPT-primate models of PD the pro-

dyskinesia influence of PPE-A can be inhibited by the use of A2A receptor antagonist early on in treatment. Higher A2A levels may act to keep the brain in a primed state.

Increased A2A receptor mRNA expression has been demonstrated in the striatum of 6-OHDA lesioned rats and in MPTP-treated primates, as well as in dyskinetic PD patients chronically treated with levodopa[64]. They would also suggest that A2A blockade could be a useful pharmacological target for non-dopaminergic treatment of Parkinson's disease with dyskinesia. A2A receptor antagonism has been shown to reduce dyskinesia in rodent lesion models of PD and relieves Parkinsonian motor deficits in non-human primate models of PD. For example, the A2A receptor antagonist KW-6002 resulted in improved control of the motor symptoms of PD when used as an adjunct with levodopa but did not reduce accompanying dyskinesias[65]. However, no attempt to reduce levodopa dosage was made in this study. The use of an A2A blocker could potentially allow this and so be of benefit to PD patients. By preventing the priming of the brain, it may also be that early use of an A2A antagonist before the occurrence of dyskinesias would prevent or delay their evolution.

In summary, the influence of the A2A receptor on basal ganglia functioning is complex involving regulation of D2 activity. Through its influence on activity in the indirect pathway the A2A site contributes to the development and maintenance of both parkinsonism and LID and so blockade could provide a non-dopaminergic treatment in Parkinson's disease and possibly LID.

I will now move to the individual studies done in an attempt to address the issues and questions raised in this introduction.

1.8 Figures

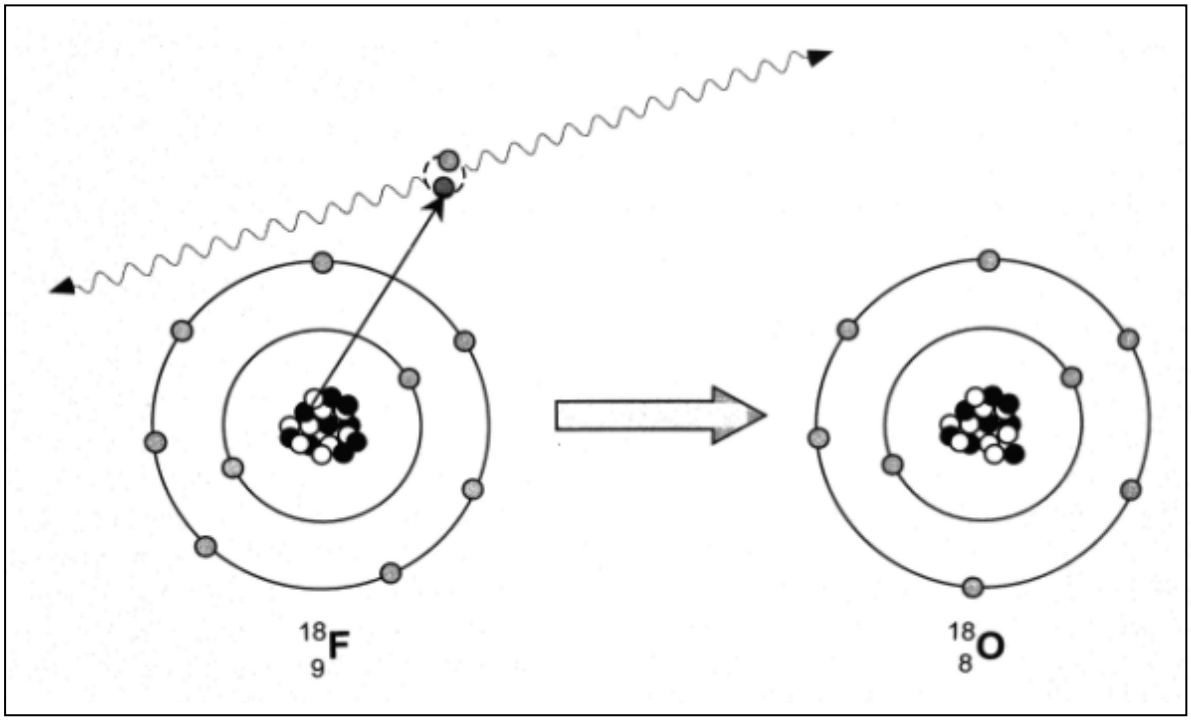


Figure 1.1. Annihilation event produced with a positron being ejected from the nucleus. The positron travels a finite distance and annihilates by combining with an electron releasing two 511keV gamma rays at 180° [2(p.50)].

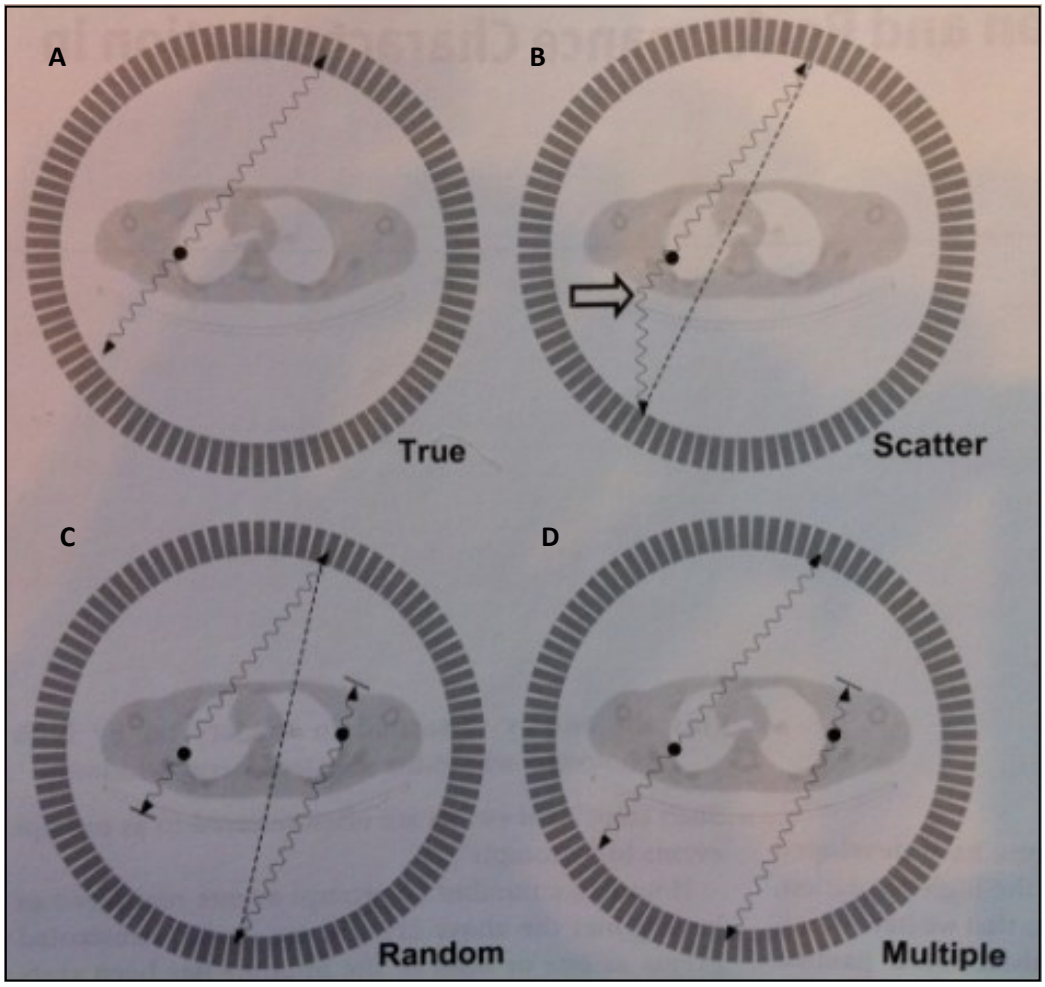


Figure 1.2. Possible coincidence events detected by a full ring PET scanner. The black circle indicates the site of positron annihilation. A – True event, B – Scattered event where electromagnetic radiation ejection does not occur at 180^{o}, C – Random event for which correction can be applied and D – Multiple events resulting in 3 events being counted[2(p.70)].

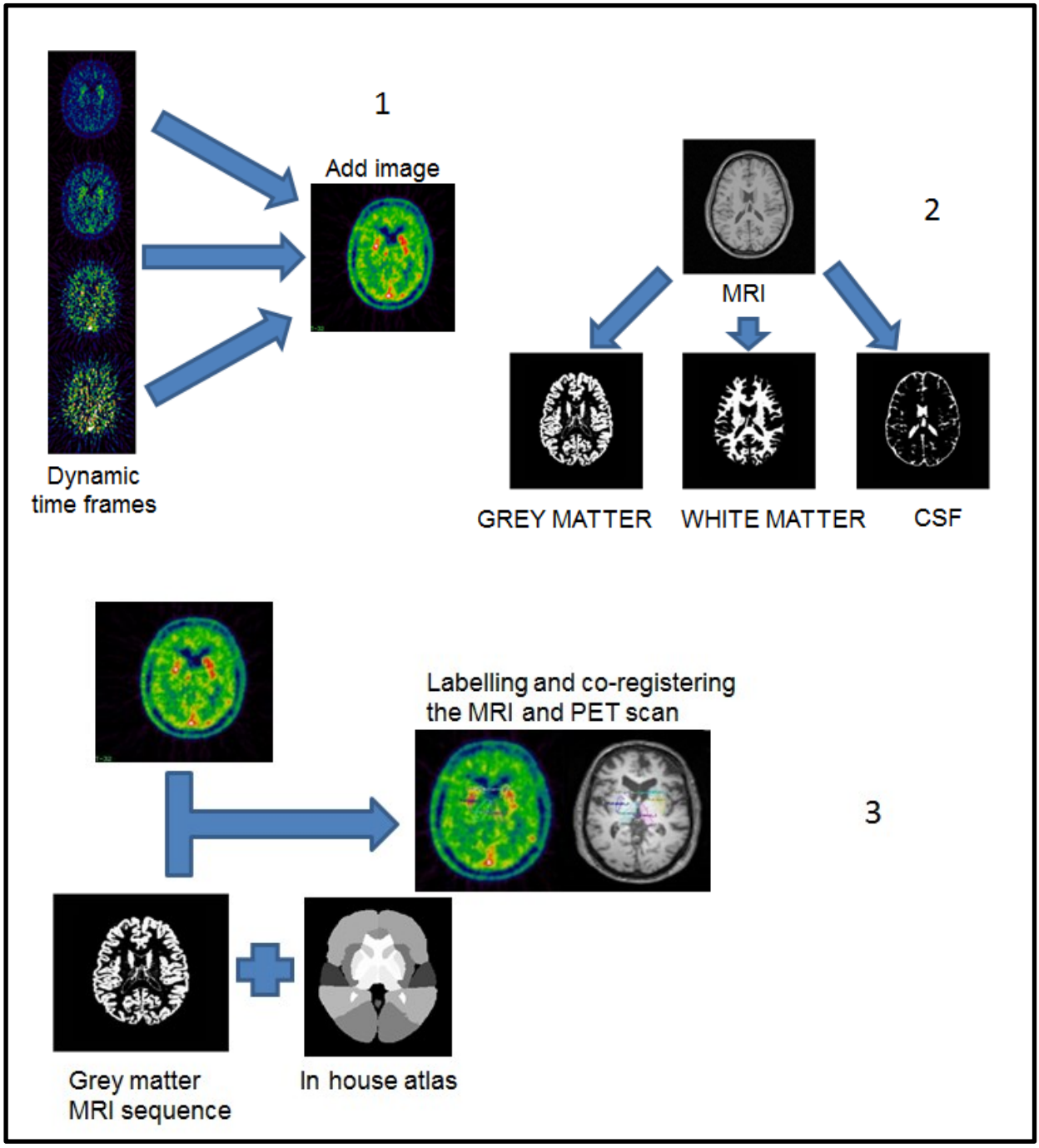


Figure 1.3. Summery for the pre-preparation steps of PET analysis. 1. Creation of the Add Image, 2. Segmentation of the MRI and 3. Creation of the registered and labeled atlas. This atlas can then be used in region of interest analysis.

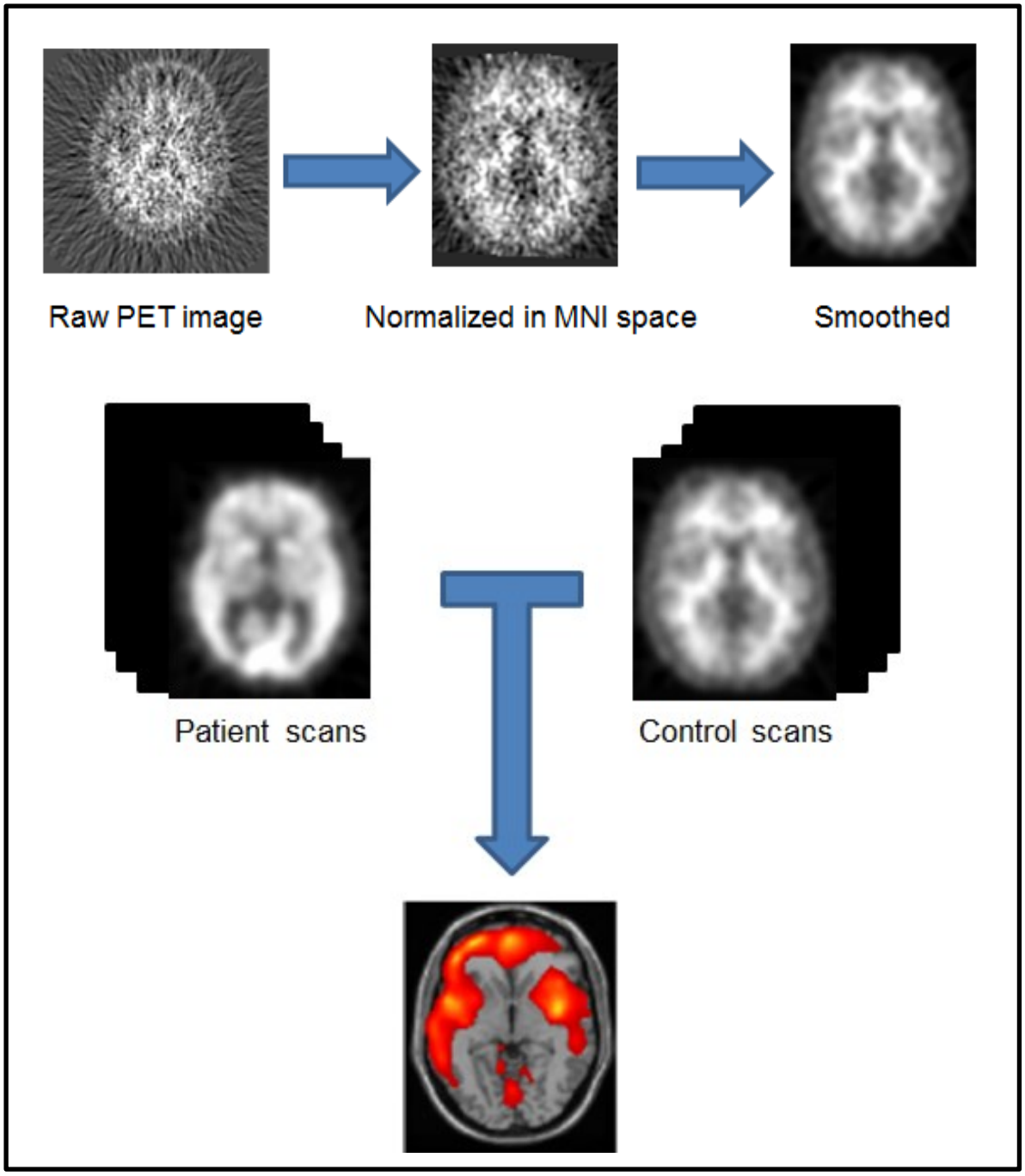


Figure 1.4 Summery of Statistical Parametric Mapping analysis. All subject scans are normalized into standard stereotaxic MNI space and smoothed. Scans are then grouped together and voxel clusters are compared statically.

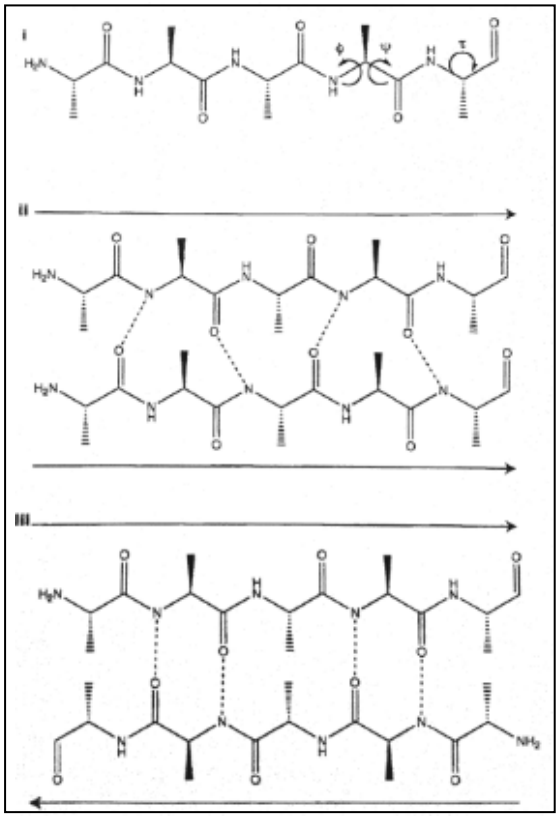


Figure 1.5. i. Illustration of a typical β strand. Strands become arranged by hydrogen bonds (dashed lines) to from ii and iii β sheets. Sheet ii arranged in a parallel strands while sheet iii arranged with anti-parallel strands[36 (p.4)].

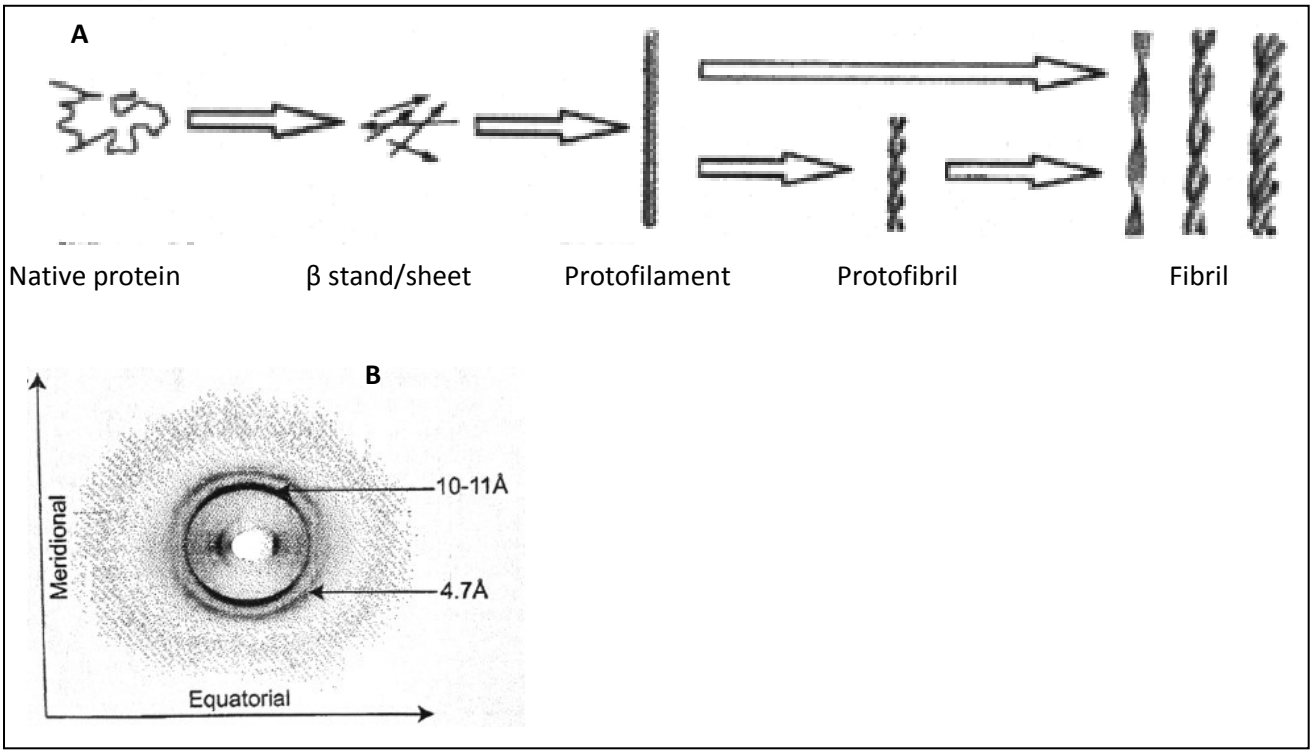


Figure 1.7. A, β fibril formation, native protein arranges into β strands or sheets and then to protofibrils. Protofibrils then become arranged into fibrils binding Congo red. B, X-ray diffraction pattern of fibrillar amyloid. The 4.8Ă meridonal arc measures the distance between β stands while 10-11 Ă is due to spacing between β sheets[38 (p.3,8)].

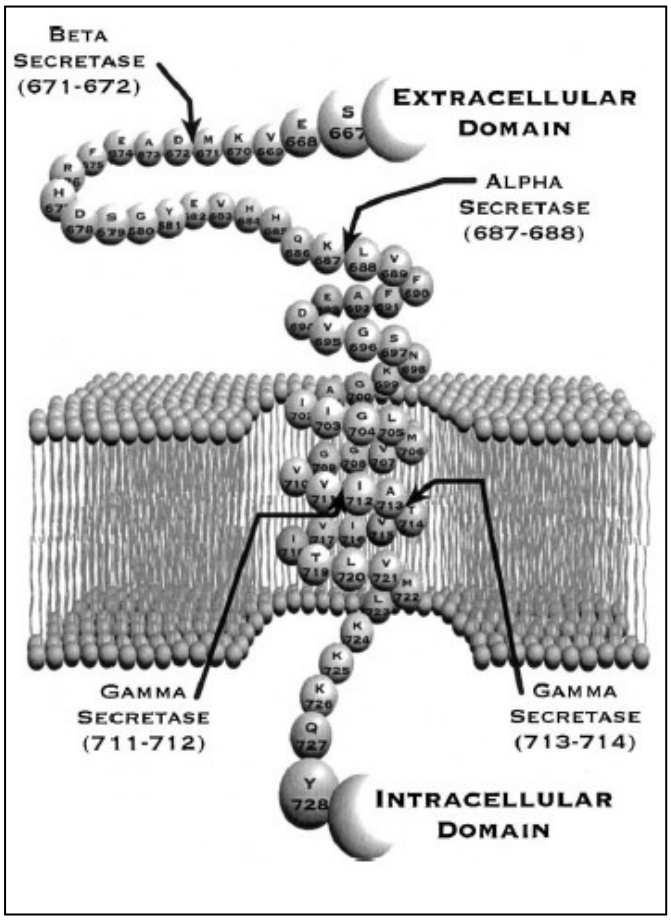


Figure 1.5. Schematic view of the membrane spanning and cleavage sites of APP770. The $A\beta_{1-40}$ fragment and $A\beta_{1-42}$ is generated by β and ϑ cleavage. The p3 fragment, generated by α and ϑ cleavage spans residues 688–711 and 713[37 (p.7)].

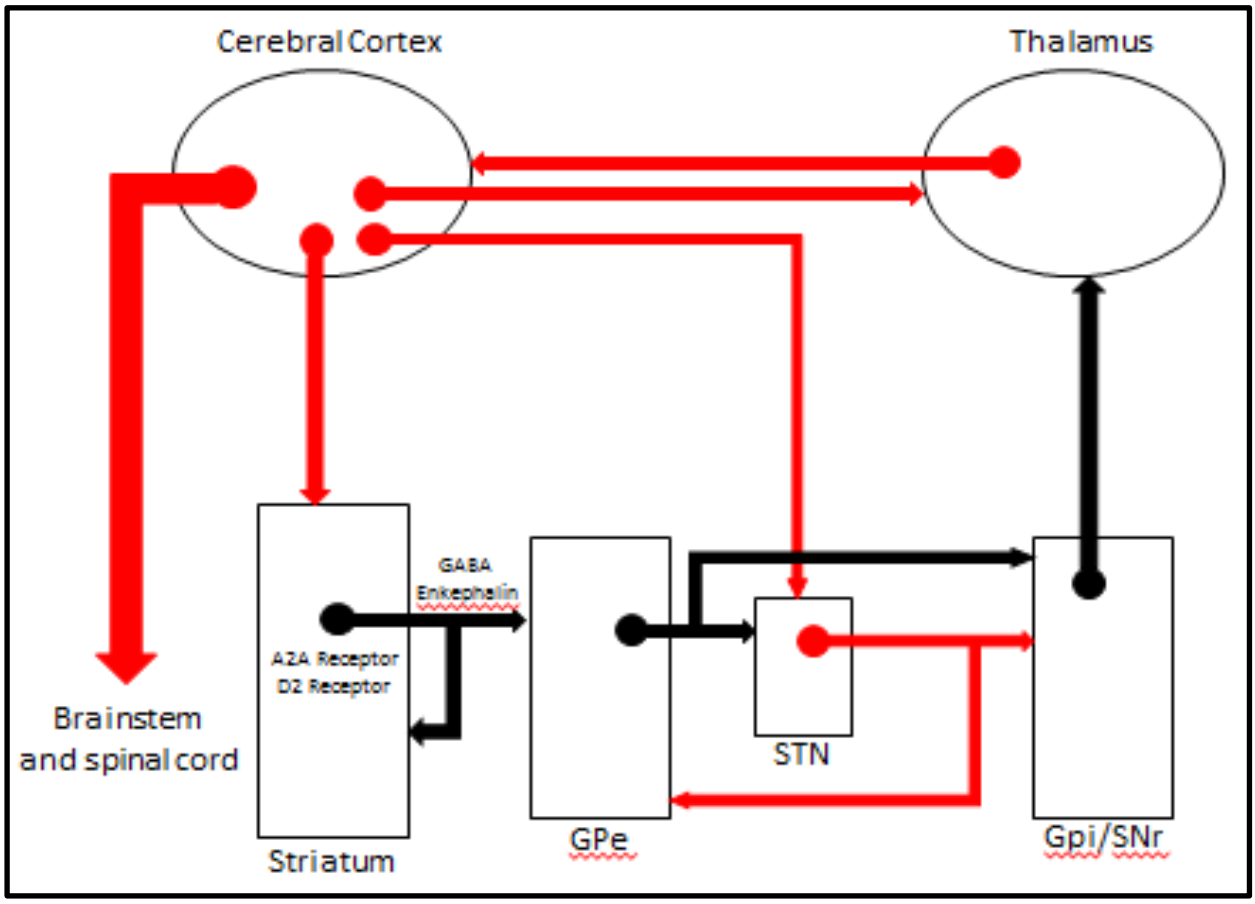


Figure 1.8. Schematic diagram of the indirect pathway of the basal ganglia. Black arrows illustrate inhibitory pathways while red arrows illustrate excitatory pathways. Gpe – globus pallidus externa, STN – subthalamic nuclei, Gpi/SNr – globus pallidus interna/substantia nigra reticulata. Of importance is the presence of a collateral system feeding back on the striatum. A2A receptors are represented along this pathway playing an important role on thalamic and cortical activity.

1.9 References

1. Jones T. Historical Development of Functional In Vivo Studies Using Positron-emitting Tracers. In: Valk PE, Bailey DL, Townsend DW, Maisey MN (eds.)Positron Emission Tomography: Basic Science and Clinical Practice. 3rd ed. London: Springer; 2004. p3-40

2. Bailey DL, Karp JS, Surti S. Physics and Instrumentation in PET. In: Valk PE, Bailey DL, Townsend DW, Maisey MN (eds.)Positron Emission Tomography: Basic Science and Clinical Practice. 3rd ed. London: Springer; 2004. P41-68

3. Wikipedia. *Bremsstrahlung*. http://en.wikipedia.org/wiki/Bremsstrahlung (accessed 10.03.2013).

4. Ikonomovic MD, Klunk WE, Abrahamson EE, Mathis CA, Price JC, Tsopelas ND, et al. Post-mortem correlates of in vivo PiB-PET amyloid imaging in a typical case of Alzheimer's disease. Brain. 2008 Jun;131(Pt 6):1630-45.

5. Mathis CA, Mason NS, Lopresti BJ, Klunk WE. Development of positron emission tomography β-amyloid plaque imaging agents. Semin Nucl Med. 2012 Nov;42(6):423-32.

6. Okello A, Edison P, Archer HA, Turkheimer FE, Kennedy J, Bullock R, et al. Microglial activation and amyloid deposition in mild cognitive impairment: a PET study. Neurology. 2009 Jan 6;72(1):56-62.

7. Cohen AD, Rabinovici GD, Mathis CA, Jagust WJ, Klunk WE, Ikonomovic MD. Using Pittsburgh Compound B for in vivo PET imaging of fibrillar amyloid-beta. Adv Pharmacol. 2012;64:27-81.

8. Herholz K, Carter SF, Jones M. Positron emission tomography imaging in dementia. Br J Radiol. 2007 Dec;80 Spec No 2:S160-7.

9. Scott KR, Barrett AM. Dementia syndromes: evaluation and treatment. Expert Rev Neurother. 2007 Apr;7(4):407-2.

10. Castellani RJ, Rolston RK, Smith MA. Alzheimer disease. Dis Mon. 2010 Sep;56(9):484-546.

11. Rossor M, Collinge J, Fox N, Howard R, Mallucci G, Mummery C, et al. Cognitive Impairment and Dementia. In: Clarke C, Howard R, Rossor M, Shorvon S (eds.)Neurology a Queen Square Textbook. 1st ed. London: Wiley-Blackwell; 2009. p245-89

12. Ropper AH, Brown RH. Dementia and the Amnesic (Korsakoff) Syndrome with Comments on the Neurology of Intelligence and Memory. In: Foltin J, Noguerira I, Edmonson KG, Sheinis LA (eds.)Adams and Victor's Principles of Neurology. 8th ed. New York: McGraw-Hill; 2005. p367-384

13. Breunig JJ, Guillot-Sestier MV, Town T. Brain injury, neuroinflammation and Alzheimer's disease. Front Aging Neurosci. 2013 Jul 11;5:26

14. Owen DR, Howell OW, Tang SP, Wells LA, Bennacef I, Bergstrom M, et al. Two binding sites for [3H]PBR28 in human brain: implications for TSPO PET imaging of neuroinflammation. J Cereb Blood Flow Metab. 2010 Sep;30(9):1608-18.

15. Ikeda K, Haga C, Oyanagi S, Iritani S, Kosaka K. Ultrastructural and immunohistochemical study of degenerate neurite-bearing ghost tangles. J Neurol. 1992 Apr;239(4):191-4.

16. Welzel AT, Walsh DM. Aberrant protein structure and diseases of the brain. Ir J Med Sci. 2011 Mar;180(1):15-22.

17. Braak H, Braak E, Bohl J. Staging of Alzheimer-related cortical destruction. Eur Neurol. 1993;33(6):403-8.

18. Alafuzoff I, Arzberger T, Al-Sarraj S, Bodi I, Bogdanovic N, Braak H, et al. Staging of neurofibrillary pathology in Alzheimer's disease: a study of the BrainNet Europe Consortium. Brain Pathol. 2008 Oct;18(4):484-96.

19. Braak H, Braak E. Demonstration of amyloid deposits and neurofibrillary changes in whole brain sections. Brain Pathol. 1991 Apr;1(3):213-6.

20. Thal DR, Arendt T, Waldmann G, Holzer M, Zedlick D, Rüb U, et al. Progression of neurofibrillary changes and PHF-tau in end-stage Alzheimer's disease is different from plaque and cortical microglial pathology. Neurobiol Aging. 1998 Nov-Dec;19(6):517-25.

21. Gerhard A, Schwarz J, Myers R, Wise R, Banati RB. Evolution of microglial activation in patients after ischemic stroke: a [11C](R)-PK11195 PET study. Neuroimage. 2005 Jan 15;24(2):591-5.

22. Politis M, Su P, Piccini P. Imaging of microglia in patients with neurodegenerative disorders. Front Pharmacol. 2012;3:96.

23. Okello A, Edison P, Archer HA, Turkheimer FE, Kennedy J, Bullock R, et al. Microglial activation and amyloid deposition in mild cognitive impairment: a PET study. Neurology. 2009 Jan 6;72(1):56-62.

24. Knight WD, Okello AA, Ryan NS, Turkheimer FE, Rodríguez Martinez de Llano S, Edison P, et al. Carbon-11-Pittsburgh compound B positron emission tomography imaging of amyloid deposition in presenilin 1 mutation carriers. Brain. 2011 Jan;134(Pt 1):293-300.

25. Crutch SJ, Lehmann M, Schott JM, Rabinovici GD, Rossor MN, Fox NC. Posterior cortical atrophy. Lancet Neurol. 2012 Feb;11(2):170-8.

26. Ropper AH, Brown RH. Neurological Disorders Caused by Lesions in Particular Parts of yj Cerebrum. In: Foltin J, Noguerira I, Edmonson KG, Sheinis LA (eds.)Adams and Victor's Principles of Neurology. 8th ed. New York: McGraw-Hill; 2005. p385-412

27. Formaglio M, Costes N, Seguin J, Tholance Y, Le Bars D, Roullet-Solignac I, Mercier B, Krolak-Salmon P, Vighetto A. In vivo demonstration of amyloid burden in posterior cortical atrophy: a case series with PET and CSF findings. J Neurol. 2011 Oct;258(10):1841-51.

28. de Souza LC, Corlier F, Habert MO, Uspenskaya O, Maroy R, Lamari F, et al. Similar amyloid-β burden in posterior cortical atrophy and Alzheimer's disease. Brain. 2011 Jul;134(Pt7):2036-43

29. Ng SY, Villemagne VL, Masters CL, Rowe CC. Evaluating atypical dementia syndromes using positron emission tomography with carbon 11 labeled Pittsburgh Compound B. Arch Neurol. 2007 Aug;64(8):1140-4.

30. Rosenbloom MH, Alkalay A, Agarwal N, Baker SL, O'Neil JP, Janabi M, et al. Distinct clinical and metabolic deficits in PCA and AD are not related to amyloid distribution. Neurology. 2011 May 24;76(21):1789-96.

31. Ferguson PL, Smith GM, Wannamaker BB, Thurman DJ, Pickelsimer EE, Selassie AW. A population-based study of risk of epilepsy after hospitalization for traumatic brain injury. Epilepsia. 2010 May;51(5):891-8.

32. Kinnunen KM, Greenwood R, Powell JH, Leech R, Hawkins PC, Bonnelle V, et al. White matter damage and cognitive impairment after traumatic brain injury. Brain. 2011 Feb;134(Pt 2):449-63.

33. Nagamoto-Combs K, McNeal DW, Morecraft RJ, Combs CK. Prolonged microgliosis in the rhesus monkey central nervous system after traumatic brain injury. J Neurotrauma. 2007 Nov;24(11):1719-42.

34. Nagamoto-Combs K, Morecraft RJ, Darling WG, Combs CK. Long-term gliosis and molecular changes in the cervical spinal cord of the rhesus monkey after traumatic brain injury. J Neurotrauma. 2010 Mar;27(3):565-85.

35. Gentleman SM, Leclercq PD, Moyes L, Graham DI, Smith C, Griffin WS, et al. Long-term intracerebral inflammatory response after traumatic brain injury. Forensic Sci Int. 2004 Dec 16;146(2-3):97-104.

36. Collinge J. Prion diseases of humans and animals: their causes and molecular basis. Annu Rev Neurosci. 2001;24:519-50.

37. Kepe V, Ghetti B, Farlow MR, Bresjanac M, Miller K, Huang SC, et al. PET of Brain Prion Protein Amyloid in Gerstmann-Straussler-Scheinker Disease. Brain Pathol. 2010 Mar;20(2):419-30.

38. National Institute of Clinical Excellence TA217 Donepezil, galantamine, rivastigmine and memantine for the treatment of Alzheimer's disease Mar 2011.

39. Robert R, Wark KL. Engineered antibody approaches for Alzheimer's disease immunotherapy. Arch Biochem Biophys. 2012 Oct 15;526(2):132-8.

40. Harrison RS, Sharpe PC, Singh Y, Fairlie DP. Amyloid peptides and proteins in review. Rev Physiol Biochem Pharmacol. 2007;159:1-77.

41. Turner PR, O'Connor K, Tate WP, Abraham WC. Roles of amyloid precursor protein and its fragments in regulating neural activity, plasticity and memory. Prog Neurobiol. 2003 May;70(1):1-32.

42. Ferguson N, Berriman J, Petrovich M, Sharpe TD, Finch JT, Fersht AR. Rapid amyloid fiber formation from the fast-folding WW domain FBP28. Proc Natl Acad Sci U S A. 2003 Aug 19;100(17):9814-9.

43. Heise H, Hoyer W, Becker S, Andronesi OC, Riedel D, Baldus M. Molecular-level secondary structure, polymorphism, and dynamics of full-length alpha-synuclein fibrils studied by solid-state NMR. Proc Natl Acad Sci U S A. 2005 Nov 1;102(44):15871-6.

44. Kad NM, Myers SL, Smith DP, Smith DA, Radford SE, Thomson NH. Hierarchical assembly of beta2-microglobulin amyloid in vitro revealed by atomic force microscopy. J Mol Biol. 2003 Jul 18;330(4):785-97.

45. Atwood CS, Martins RN, Smith MA, Perry G. Senile plaque composition and posttranslational modification of amyloid-beta peptide and associated proteins. Peptides. 2002 Jul;23(7):1343-50.

46. Okamoto T, Takeda S, Murayama Y, Ogata E, Nishimoto I. Ligand-dependent G protein coupling function of amyloid transmembrane precursor. J Biol Chem. 1995 Mar 3;270(9):4205-8.

47. Selkoe DJ. Normal and abnormal biology of the beta-amyloid precursor protein. Annu Rev Neurosci. 1994;17:489-517.

48. Tanaka S, Shiojiri S, Takahashi Y, Kitaguchi N, Ito H, Kameyama M, et al. Tissue-specific expression of three types of beta-protein precursor mRNA: enhancement of protease inhibitor-harboring types in Alzheimer's disease brain. Biochem Biophys Res Commun. 1989 Dec 29;165(3):1406-14.

49. Zheng H, Jiang M, Trumbauer ME, Sirinathsinghji DJ, Hopkins R, Smith DW, et al. beta-Amyloid precursor protein-deficient mice show reactive gliosis and decreased locomotor activity. Cell. 1995 May 19;81(4):525-31.

50. Fukumoto H, Cheung BS, Hyman BT, Irizarry MC. Beta-secretase protein and activity are increased in the neocortex in Alzheimer disease. Arch Neurol. 2002 Sep;59(9):1381-9.

51. Farber SA, Nitsch RM, Schulz JG, Wurtman RJ. Regulated secretion of beta-amyloid precursor protein in rat brain. J Neurosci. 1995 Nov;15(11):7442-51.

52. Barger SW, Mattson MP. Isoform-specific modulation by apolipoprotein E of the activities of secreted beta-amyloid precursor protein. J Neurochem. 1997 Jul;69(1):60-7.

53. Kim JH, Choi S, Jung JE, Roh EJ, Kim HJ. Capacitative Ca2+ entry is involved in regulating soluble amyloid precursor protein (sAPPalpha) release mediated by muscarinic acetylcholine receptor activation in neuroblastoma SH-SY5Y cells. J Neurochem. 2006 Apr;97(1):245-54.

54. Yan SD, Chen X, Fu J, Chen M, Zhu H, Roher A, et al. RAGE and amyloid-beta peptide neurotoxicity in Alzheimer's disease. Nature. 1996 Aug 22;382(6593):685-91.

55. Boland K, Behrens M, Choi D, Manias K, Perlmutter DH. The serpin-enzyme complex receptor recognizes soluble, nontoxic amyloid-beta peptide but not aggregated, cytotoxic amyloid-beta peptide. J Biol Chem. 1996 Jul 26;271(30):18032-44.

56. Walsh DM, Klyubin I, Fadeeva JV, Rowan MJ, Selkoe DJ. Amyloid-beta oligomers: their production, toxicity and therapeutic inhibition. Biochem Soc Trans. 2002 Aug;30(4):552-7.

57. Castellani RJ, Rolston RK, Smith MA. Alzheimer disease. Dis Mon. 2010 Sep;56(9):484-546.

58. McKee AC, Cantu RC, Nowinski CJ, Hedley-Whyte ET, Gavett BE, Budson AE, et al. Chronic traumatic encephalopathy in athletes: progressive tauopathy after repetitive head injury. J Neuropathol Exp Neurol. 2009 Jul;68(7):709-35.

59. Ahlskog EA, Muenter MD. Frequency of Levodopa-Related Dyskinesias and Motor Fluctuations as Estimated From the Cumulative Literature. Mov Disord. 2001 May;16(3):448-58.

60. Svenningsson P, Le Moine C, Fisone G, Fredholm BB. Distribution, biochemistry and function of striatal adenosine A2A receptors. Prog Neurobiol. 1999 Nov;59(4):355-96.

61. Jenner P, Mori A, Hauser R, Morelli M, Fredholm BB, Chen JF. Adenosine, adenosine A 2A antagonists, and Parkinson's disease. Parkinsonism Relat Disord. 2009 Jul;15(6):406-13.

62. Svenningsson P, Hall H, Sedvall G, Fredholm BB. Distribution of adenosine receptors in the postmortem human brain: an extended autoradiographic study. Synapse. 1997 Dec;27(4):322-35.

63. Calon F, Birdi S, Rajput AH, Hornykiewicz O, Bédard PJ, Di Paolo T. Increase of preproenkephalin mRNA levels in the putamen of Parkinson disease patients with levodopa-induced dyskinesias. J Neuropathol Exp Neurol. 2002 Feb;61(2):186-96.

64. Zeng BY, Pearce RK, MacKenzie GM, Jenner P. Alterations in preproenkephalin and adenosine-2a receptor mRNA, but not preprotachykinin mRNA correlate with occurrence of dyskinesia in normal monkeys chronically treated with L-DOPA. Eur J Neurosci. 2000 Mar;12(3):1096-104.

65. Lundblad M, Vaudano E, Cenci MA. Cellular and behavioural effects of the adenosine A2a receptor antagonist KW-6002 in a rat model of l-DOPA-induced dyskinesia. J Neurochem. 2003 Mar;84(6):1398-410.

Chapter 2

Microglial activation after Traumatic Brain Injury

2.1 Microglial activation after Traumatic Brain Injury

Investigations into TBI form a major part of this thesis. Previously thought to be a single event it is now apparent that TBI can lead to complications years after initial recovery. Here I will investigate if sustained microglial activation takes place in TBI at least 11 months after the event.

Summary of Objectives

Patient outcomes after TBI is highly variable. The underlying pathophysiology of this is poorly understood, but the inflammatory response is potentially an important factor. Microglia orchestrate many aspects of this response. Their activation can be studied *in vivo* using the PET ligand [11C]-PK11195. Here I investigate whether a persistent inflammatory response is present following chronic TBI, and whether this response relates to structural brain abnormalities and cognitive function.

Ten patients at least 11 months post moderate to severe TBI, underwent [11C]-PK11195 and structural MRI, including diffusion tensor imaging to assess white matter structure. [11C]-PK11195 binding potentials were calculated in and around the site of focal brain damage, and in distant brain regions affected by TBI. Standardised neuropsychological tests were administered.

Summary of results

[11C]-PK11195 binding was significantly raised in the thalami, putamen, occipital cortices, and the posterior limb of the internal capsules after TBI. There was no increase in [11C]-PK11195 binding at the original site of focal brain injury. Higher [11C]-PK11195 binding in

the thalamus was associated with more severe cognitive impairment, although binding was not correlated with either the time since the injury or the amount of structural brain injury.

In conclusion increased microglial activation is present up to seventeen years after TBI. Results suggest that TBI triggers a chronic inflammatory response in sub-cortical regions. This highlights the importance of considering the response to TBI as one that evolves over time and suggests intervention may be possible at times much later than previously thought.

2.2 Introduction

The underlying pathophysiology of TBI remains poorly understood[1]. Patient outcomes are highly variable[2] for reasons that are often unclear. Although TBI is often thought to involve a single event, resulting in a static pathological insult, new clinical effects can emerge many years after the injury. Patients can clinically improve or deteriorate years after TBI[2] and may develop unexpected consequences such as post-traumatic epilepsy[3] or late cognitive decline including AD[4]. In fact TBI is the most common acquired risk factor for AD. These observations suggest the presence of a dynamic element to the underlying pathophysiology of TBI.

An important factor is likely to be the inflammatory response linked to TBI[5,6,7]. The initial insult results in neuronal injury, which can locally disrupt the blood brain barrier. Microglial cells resident in the CNS react to this injury within minutes, becoming chronically activated[8,9]. Once transformed, microglia become indistinguishable from peripheral macrophages, secreting cytokines and acting as antigen presenting cells[10]. In animal models, the initial inflammatory process has been shown to persist for at least a year[5,7,11]. In humans, post-mortem studies have shown microglial activation many years after TBI[12]. Sites of activation often coincide with those of neuronal degeneration, and are seen particularly frequently in regions of axonal abnormality[6,13].

The inflammatory response to brain injury can be studied *in vivo* using the PET ligand [11C]-PK11195[14,15]. [11C]-PK11195 binds to the translocator protein (TSPO), formerly known as the peripheral benzodiazepine receptor, expressed by the mitochondria of activated microglia[16]. Following stroke, microglial activation is observed early at the site of the infarct, as well as in areas such as the thalamus and brainstem that become disconnected from the lesion[14,15]. Here I employ [11C]-PK11195 to study the inflammatory response following TBI. I

selected a group of patients in the chronic phase after TBI to test whether a persistent inflammatory response is present in injuries of varying severity. I then investigated whether microglial activation is related to MRI measures of disease severity including brain atrophy and changes in white matter signal. I also investigated the relationship between microglial activation and cognitive impairment, and tested whether persistent microglial activation is associated with more pronounced cognitive impairment.

2.3 Methods

2.3.1 Patients: demographic and clinical details

Eleven patients with a history of TBI were recruited, and ten included in the analysis (mean age ± st.dev. 43±5.3, range 36–54, and mean time since injury ± st.dev. 6.2±5.3 years, range 0.9-17 years). One subject was excluded from the analysis because a history of alcohol dependency became apparent after scanning. All subjects had attained at least a secondary school level of education. Exclusion criteria were as follows: neurosurgery, except for invasive intracranial pressure monitoring; a history of psychiatric or neurological illness prior to the head injury; a history of previous significant TBI; anti-epileptic medication; pregnancy or breast feeding; current or previous drug or alcohol abuse; contraindication to MRI.

Of the remaining ten TBI subjects, a road traffic accident was responsible for TBI in 6 cases, assaults in 3 cases, and in one case the cause was uncertain. All had suffered moderate to severe traumatic brain injuries based on the Mayo Clinic criteria[17]. To investigate whether persistent microglial activation was present, patients were all recruited in the chronic period after their injury (see table 2.1). Conventional neuroimaging was reviewed by a senior neuroradiologist. Five patients had no abnormalities visible on T1 MRI. The remaining five

had significant focal lesions with damage seen mostly in the frontal (n = 4) or temporal n = 3) lobes (see figure 2.1). Two patients had evidence of microbleeds on gradient echo imaging. Atrophy, contusion, gliosis and siderosis at the injury site were the most common changes described. One patient had undergone a frontoparietal lobectomy following TBI. All patients and control subjects gave written informed consent. The project was approved by Hammersmith and Queen Charlotte's and Chelsea Research ethics committee.

2.3.2 Control groups

Two non-overlapping groups of control subjects were used in this study. Controls were chosen from the adult population and they underwent clinical and neuropsychological assessments to ensure that there were no underlying neurological illnesses. Seven age-matched controls underwent [11C]-11195PK PET scanning and volumetric MRI scanning (mean age 46±4.0, range 42–50). Fifteen age-matched subjects underwent the neuropsychological assessment (mean age 37.3±11.3 range 19-60), and of those ten age-matched control subjects had diffusion tensor imaging (mean age 40±10.9 range 19–60).

2.3.3 Neuropsychological Assessment

The following is a full description of the neuropsychological assessments subjects underwent. Essentially assessments were to include aspects of executive function and planning known to be adversely affected after TBI.

Ten TBI patients (9 males, mean age ± standard deviation: 43.3 ± 5.3 years) and 15 age-matched healthy controls (12 males, 37.3 ± 11.3 years) were compared on neuropsychological functioning. The assessment of the TBI patients was divided into two

one-hour sessions. The average time between the sessions was one week. The healthy volunteers were assessed during a single session of approximately an hour and a half. The battery of tests used was designed to focus on the assessment of executive functions, information processing speed and verbal memory, tapping domains of cognitive function often impaired following TBI. The Verbal Fluency/Letter Fluency (F + A +S) and Color-Word subtests from the Delis-Kaplan Executive Function System (D-KEFS) were administered to assess word generation fluency, complex information processing speed, inhibition and cognitive flexibility. The Trail Making Test (TMT) was used to assess basic perceptual and complex processing speed, attentional capacity, set-maintenance and set-shifting. A computerised two-choice left/right button-press choice-reaction task (CRT) was used as a simple processing speed measure (median reaction time on correct trials). The TMT Form A, as well as the two baseline conditions of the D-KEFS Color-Word interference test, Color Naming and Word Reading also measured simple processing speed. The Digit Span subtest of the Wechsler Memory Scale- Third Edition (WMS-III) assessed initial and working memory. The Logical Memory I and II subtests of the WMS-III were used as a measure of immediate and delayed verbal recall. The People Test (PT) from the Doors and People Test battery was used as a measure of associative learning and recall (immediate recall). In addition, the Wechsler Test of Adult Reading (WTAR) was used to provide an estimate of pre-morbid intellectual functioning. Current verbal and nonverbal reasoning ability were assessed via the Wechsler Abbreviated Scale of Intelligence (WASI) Similarities and Matrix Reasoning subtests. Individual differences in current intellectual ability were taken into account when calculating the group averages for the other indices of cognitive function by comparing the groups on standardised residuals after regressing out intellectual ability.

2.3.4 Volumetric and diffusion tensor MRI

Standard protocols were used for high resolution T1, gradient-echo (T2*) and diffusion tensor imaging (DTI) to assess the extent of focal brain injury and white matter disruption. Fractional anisotropy (FA) and mean diffusivity (MD) were calculated in three regions of interest within the corpus callosum, as well as the anterior and posterior internal capsule. These regions are frequently disrupted by diffuse axonal injury, and were used to provide a representative measure of white matter tract damage after TBI[18,19].

MRI data were obtained using a Philips (Best, The Netherlands) Intera 3.0 Tesla MRI scanner using Nova Dual gradients, a phased array head coil, and sensitivity encoding (SENSE) with an under-sampling factor of 2. The T1 and T2*-weighted images were obtained prior to DTI. For DTI, diffusion-weighted volumes with gradients applied in 16 non-collinear directions were collected in each of the four DTI runs, resulting in a total of 64 directions. The following parameters were used: 73 contiguous slices, slice thickness = 2 mm, field of view (FOV) 224 mm, matrix 128 x 128 (voxel size = 1.75 x 1.75 x 2 mm^3), *b* value = 1000, and four images with no diffusion weighting (*b* = 0 s/mm^2).

2.3.5 Diffusion tensor imaging analysis

Diffusion-weighted images were registered to the *b* = 0 image by affine transformations to minimize distortion due to motion and eddy currents, and then brain-extracted using BET, a part of the FSL image processing toolbox. Fractional anisotropy (FA) and mean diffusivity (MD) maps were generated using the FSL's Diffusion Toolbox. A region of interest approach was taken, focusing on white matter tracts commonly affected by TBI, namely the anterior and posterior limbs of the internal capsule, and the corpus callosum. These regions were hand drawn or manually checked using individual high resolution T1 MRI images, voxel size

1x1x1mm. These regions were hand drawn or manually checked using individual high resolution T1 segmented MRI images (voxel size 1x1x1mm), and the masks then thresholded and binarised. The resultant case specific masks were translated into diffusion space using FSL's Linear Image Registration Tool with nearest neighbour registration and re-thresholded. The mean FA and MD values were then extracted for each ROI.

2.3.6 PET image acquisition and analysis

PET scanning was performed using established protocols at the Cyclotron Building, Hammersmith Hospital, London, UK, with a Siemens ECAT 962 EXACT HR+ scanner. The Siemens ECAT 962 EXACT HR+ scanner has an axial view of 15.5 cm. Prior to scanning, intravenous access was secured in the antecubital fossa of each subject. A 10 minute transmission scan was acquired before the emission study, using a single rotating photon point source of 137Cs, for subsequent attenuation and scatter correction. The resultant dynamic PET consisted of 18 time frames covering all 60 minutes. The PET data, were acquired in 3-dimensional mode. Data were reconstructed using filtered back projection to produce images containing 63 contiguous slices, separated by 2.42mm, of 128x128 pixels 2.092mm square. Reconstruction of emission data was carried out using filtered back projection. The 3D emission data were Fourier-rebinned into 2D data sets to increase the speed of reconstruction. The reconstructed image had a transaxial resolution of 6.5 mm. Thirty seconds after the start of emission scanning a mean dose of 370.9 MBq [11C]-PK11195 was administered intravenously over 10 seconds into the antecubital vein of each subject. This was followed by a 60 minute dynamic emission PET scan acquired as 18 time frames.

The ligand [11C]-PK11195 binds to the translocator protein (TSPO) expressed by activated microglial cells. The widespread expression of this protein after TBI makes it difficult to

select a reference region representing non-specific [11C]-PK11195 uptake. For this reason, I used a supervised clustering procedure for [11C]-PK11195 analysis[20]. Parametric images of [11C]-PK11195 binding potential (BP), reflecting Bmax/Kd, were generated with a simplified tissue reference model (SRTM). No assumptions were made about the distribution of activated microglia in TBI subjects. For each scan, cluster analysis was employed to identify and extract clusters of voxels where [11C]-PK11195 binding is similar to a normal population cortical reference input function. This process is carried out by the automated computational program SUPERPK (Imperial Innovations, Imperial College London) written in Matlab (The Mathworks Inc., Natick MA) [20]. This program compares the time activity curves (TAC) of each pixel with the kinetics of six pre-defined tissue types (normal gray and normal white matter, skull, muscle, gray matter with reactive microglia, endothelial cells rich in the TSPO receptor and smooth muscles) obtained from a database of control subjects and patients. BP's were computed for clusters where tracer retention occurred by comparison with the TAC of the defined reference grey matter cluster. In cluster analysis, these clusters are used as the reference region for creation of the parametric image.

2.3.7 Brain segmentation and region of interest definition

A number of anatomically predefined regions of interests (ROIs) were selected to sample [11C]-PK11195 binding. The MAPER (multi-atlas propagation with enhanced registration) procedure was used to generate anatomical ROIs from the subject's MRI brain image in its native space. The procedure has previously been shown to yield accurate and robust segmentations in normal subjects as well as those with dementia[21,22]. This approach minimised the potential sampling error associated with mis-registration and brain atrophy. The output of automatic segmentation was reviewed visually. Five patients focal brain injury was visible on T1-weighted MRI (see figure 2.1). Where damage fell within an ROI, the ROI was removed from the analysis, as correct anatomical segmentation of the injured region

was not always possible. In five of the ten patients, manual modifications were made to the segmentations before further processing. The volume of the segmented regions was used to investigate whether [11C]-PK11195 binding was associated with brain atrophy following TBI. Regions were chosen to provide a representative sampling of cortical, sub-cortical and white matter structures, and included a number of regions likely to be affected by TBI. The following regions were sampled: the anterior and posterior cingulate cortices, inferior and superior frontal gyri, hippocampi, occipital lobes, cerebellum, caudate, putamen, brain stem and thalamic nuclei, and the corpus callosum, as well as the anterior and posterior limbs of the internal capsule.

In the five patients with focal brain injury (see figure 2.1) I investigated whether [11C]-PK11195 binding was increased within or near the site of this injury. I defined cylinder-shaped ROIs 10 mm long with a 5mm radius in and around the most prominent lesion. One ROI was placed centrally within the lesion. This ROI thus sampled the lesion itself and its borders were not allowed to extend into peri-lesional areas as defined by the T1 weighted MRI. A second ROI was placed within the tissue adjacent to the lesion that returned abnormal T1 signal. Again care was taken to ensure that the ROI borders did not extend into areas of different signal change but rather sampled abnormal peri-lesional tissue. Cylinders were orientated parallel to the long axis of the lesion. A further two ROIs were placed in grey and white matter returning normal MR signal in the same lobe as the lesion sampled. This enabled [11C]-PK11195 binding to be investigated within the lesion, the lesion penumbra, and the normal grey and white matter of the same lobe.

2.4 Results

2.4.1 Cognitive performance

Our TBI patients showed slowed information processing in line with previous reports.[23] Significantly prolonged processing times were seen across a range of cognitive tasks of varying complexity (see table 2.2). In other ways the patients were matched neuropsychologically with controls. One patient could not be fully assessed because of upper limb disability and difficulty communicating verbally.

2.4.2 TBI patients show increases in microglial activation remote from damaged areas

Patient [11C]-PK11195 binding potentials were significantly higher than controls in a number of brain regions distant from any focal damage. Initial analysis showed no significant hemispheric differences in binding potentials (P>0.3 for all paired Student's t-test inter-hemispheric comparisons). Therefore, [11C]-PK11195 binding potentials for paired structures are reported as an average of binding in the two hemispheres where this is appropriate. Using the generalised linear model, ANOVA showed a significant group by region interaction ($F_{(1,13)}$ = 1.09, p=0.033), resulting from higher patient [11C]-PK11195 binding in the thalami (t=4.443, df=15, p<0.001), putamen (t=3.63, df=15, p=0.002), occipital lobes (t=2.75, df=15, p=0.015), and within the posterior limb of the internal capsules (t=2.67, df=15, p=0.017). Non-parametric testing with Mann-Whitney U Tests confirmed these results. Thalamic [11C]-PK11195 binding potentials remained significantly elevated compared to controls after Bonferroni correction for multiple comparisons.

There was no significance between the time interval since head trauma and [11C]-PK11195 binding (P>0.2). The highest [11C]-PK11195 binding was actually observed in the patient whose injury was most remote in time (see figure 2.2). [11C]-PK11195 binding did not

correlate with structural measures of brain injury. In the four regions showing a significantly raised [11C]-PK11195 binding there was no correlation between tracer uptake and the volume of the regions (P>0.2 for all analyses). Additionally, there was no correlation between [11C]-PK11195 binding and the measures of white matter damage provided by DTI. TBI often produces diffuse axonal injury and this can be quantified as loss of white matter anisotropy (directionality of water flow) using DTI[18,24]. As expected, compared to a matched control group, patients showed evidence of white matter disruption. Fractional anisotropy was significantly lower and mean diffusivity higher in all three white matter regions in the patient group, except for FA measured in the anterior limb of the internal capsule. However, there was no significant correlation between [11C]-PK11195 binding and either of these metrics (P>0.2 for all analyses).

2.4.3 Microglial activation is not increased around the sites of focal brain damage

Visual inspection of the TBI patients [11C]-PK11195 images showed no obviously increased uptake in the vicinity of focal lesions evident on MRI (see figure 2.4). To confirm this quantitatively I measured [11C]-PK11195 binding in ROI's placed in and around the most prominent focal lesion in each patient, where lesions were visible on T1–weighted MRI. [11C]-PK11195 binding was similar within the focal lesion and in the penumbral region. In contrast, [11C]-PK11195 uptake in both these regions was significantly lower than in the thalami (lesion t=-20.1, df=4, p<0.005, penumbra t=-25.8, df=4, p<0.005), as well as the normal appearing cortex (lesion t=-3.9, df=-22.4, p<0.005, penumbra t=-4.1, df=4, p=0.015) and white matter (lesion t=-3.9, df=4, p=0.017, penumbra t=-7.1, df=4, p=0.002) of the same hemisphere.

2.4.4 Increased thalamic microglial activation correlates with cognitive impairment

In distant regions showing increased microglial activation following TBI, I next investigated whether levels of cognitive impairment correlated with [11C]-PK11195 binding. Higher thalamic [11C]-PK11195 uptake correlated inversely with the speed of processing complex information, as indexed by reaction times to conflicting items on the Stroop, a test of selective attention (Spearman r=0.828, p=0.006, see figure 2.5). This result remained significant after controlling for current IQ. There was also a correlation between thalamic binding and speed of naming the ink colour in the Stroop, a simpler part of the test, which reached borderline significance (Spearman r=0.650, p=0.058). The other three regions with increased [11C]-PK11195 binding did not show significant correlations with cognitive performance.

2.5 Discussion

TBI is often regarded as a single event causing static pathological damage. Using [11C]-PK11195 PET I have been able to demonstrate *in vivo* that microglial activation persists many years after the initiating insult. This result builds on findings in animal models and in post-mortem human studies, which have also shown that TBI triggers a long-term inflammatory response[5,6,12]. Surprisingly, persistent microglial activation does not involve the original areas of focal brain injury, but rather, is most prominent within sub-cortical structures remote from the site of focal injury, particularly the thalami and putamen. This may reflect the dense connectivity of these structures. TBI often results in diffuse axonal injury that disconnects subcortical structures[25] and microglia have been shown to be persistently activated at such sites helping to remodel connections[5,6,14].

Patients show a highly variable clinical outcome following TBI, for reasons that are poorly understood[2]. Here I have shown that impaired cognitive function after TBI is associated with greater thalamic microglial activation. This suggests that persistent thalamic inflammation, possibly secondary to disconnection, is associated with cognitive outcome. My results emphasize that TBI should be viewed as a condition with a persistent inflammatory component and this may provide a novel target for therapeutic intervention.

These results are consistent with pathological studies on microglial activation following TBI, and other cerebral insults[14,16]. Microglial activation is seen within the first few minutes of focal brain injury [8,9] and, as the inflammatory response develops, activated cells are seen in remote but connected white matter tracts. Two weeks after cortico-spinal tract infarction high [11C]-PK11195 binding is seen at the site of the stroke, accompanied by a lower increase in binding in remote but connected parts of the pyramidal tract[14]. The local and distant sites of inflammation may contain different populations of activated microglial cells showing different patterns of major histocompatibility complex expression[11,26] and distinct time courses for their activation. Follow-up scanning 6 months after the stroke showed that remote microglial activation increases, while binding potentials at the site of the infarct revert to normal values[14]. My work corroborates these findings in TBI. Reduced levels of [11C]-PK11195 binding at the sites of focal lesions demonstrate that microglial activation does not persist in these areas. This may be due to the astrocytic response to TBI enclosing and isolating the damaged area, thereby removing the source of microglial stimulation[27]. Alternatively, microglia may persist at the site of focal lesions but down-regulate expression of TSPO over time.

After TBI, persistent microglial activation was particularly prominent in the thalami and putamen. This may be secondary to widespread white matter damage, due to the presence

of diffuse axonal injury. In animal models of TBI, on-going axonal damage is seen in the striatum and thalamus[28], and activated microglia are present a year after trauma in white matter tracts connected to focal cortical injuries[5,11]. In humans, post-mortem studies show that activated microglia are present in both the thalami and brainstem many years after TBI[6,13]. Within the thalamus, the cells are mainly observed in white matter surrounding separate nuclei. Following motor stroke increased [11C]-PK11195 binding in parts of the pyramidal tract remote from the infarct has been shown to correlate with the extent of white matter damage[14]. As a group patients showed evidence of generalised white matter damage, consistent with the presence of diffuse axonal injury[18,24]. However, the location of increased [11C]-PK11195 binding did not correlate with the white matter structural change detected by DTI, perhaps because the latter is influenced by directionality of water diffusion along fibres rather than the cellular reaction to fibre loss. It must be remembered however that only 3 white matter regions were sampled in this study. It may be that further sampling is necessary to identify areas were DTI makers and [11C]-PK11195 uptake do correlate.

The clinical significance of persistent microglial activation remains uncertain. Microglia play an important role in the immune response, releasing cytokines, acting as antigen presenting cells and clearing debris in the acute phase after brain injury[10]. The initial benefits of debris clearing and synaptic remodelling may be countered by subsequent damaging effects when microglial activation is prolonged and accompanied by excessive and poorly regulated release of cytokines[12]. Activated microglia can be cytotoxic [29] and their persistent activation might predispose to the development of neurodegenerative conditions such as AD in susceptible individuals, or provide the context in which such diseases take a more aggressive course[12,30]. In contrast, recent work suggests that persistent microglial activation in regions remote from focal injury might promote brain repair[5,11,14]. Firstly, in humans, microglial activation in the pyramidal tract remote from a motor stroke was correlated with a positive clinical outcome[14]. In non-human primates, microglia continue to release brain-

derived neurotrophic factor (BDNF) many months after an injury, whilst the production of other cytokines associated with the acute inflammatory reaction is stopped[5]. The release of BDNF is associated with local synaptogenesis, which suggests that activated microglia might play a role in regulating brain repair after TBI[5,11].

My results also reveal a relationship between the amount of microglial activation in the thalamus and cognitive function. Patients with higher [11C]-PK11195 binding within the thalamus showed impaired information processing speed, a common problem after TBI. Cognitive impairment after TBI results in part from the disconnection of distributed brain networks. This is likely to be particularly important for the speed and efficiency with which cognitive functions can be performed. As the thalamus is a key node in most distributed networks, abnormalities within this structure are likely to have a profound influence. TBI is known to produce damage within the thalamic nuclei particularly involved with cognitive functions[6], and observation that microglial activation is localised to the thalamus many years after TBI suggests that an on-going inflammatory response within the structure may be relevant to the cognitive impairment that persists after TBI. Persistent microglial activation in the thalamus may drive adaptive changes in synaptic plasticity, which are most prominent in patients with severe thalamic damage. Alternatively, microglial activation could directly contribute to chronic damage of the thalamus, which impairs its function. A cross-sectional design, such as I employed, does not help to resolve this dilemma. Longitudinal clinical studies using [11C]-PK11195 will be necessary to determine the functional significance of thalamic microglial activation. Of interest as well would be the employment of thalamic maps to help differentiate regional areas of increased uptake within the thalamus itself. This was however beyond the scope of this study.

The observation that microglia are persistently activated emphasizes that TBI should not be viewed as a static insult, but instead as a trigger for a complex cascade of events that includes a persistent inflammatory state. This suggests that the window of opportunity for therapeutic intervention following TBI may be much longer than is usually considered. *In vivo* [11C]-PK11195 imaging provides a biomarker to investigate this inflammatory state, and can be used to study the time course of inflammation after TBI and the effects of interventions aimed at manipulating the inflammatory cascade.

2.6 Tables

Table 2.1. Demographics and clinical data of all traumatic brain injury (TBI) patients

AGE	SEX	HIGHEST LEVEL OF EDUCATION	CAUSE OF TBI	LOWEST GCS RECORDED	POST_ TRAUMATIC AMNESIA (hrs)	CURRENT MEDICATION	INTERVAL SINCE TRAUMA (months)
45	M	Postgraduate	Unknown	4	24	Gabapentin Modafenil Amitriptyline	72
55	M	Postgraduate	Fall	4	UK	nil	36
42	M	School to 18	Pedestrian hit by a car	4	432	nil	72
36	M	Postgraduate	Cycling accident	6	24	nil	24
42	M	School to 16	Motorcycle accident	4	UK	Tropium chloride Folic acid	204
40	M	Graduate degree	Motorcycle accident	4	1008	nil	132
42	F	Postgraduate	Pedestrian hit by a car	3	144	Codine Paracetamol	72
45	M	School to 16	Assault	4	5040	Thiamine	11
49	M	School to 18	Probable assault	4	2	nil	11
38	M	Graduate	Motorcycle accident	6	UK	Citalopram Modafanil Omeprazole	108

UK – unknown

Table 2.2 Neuropsychological test results: traumatic brain injury and control patients.

COGNITIVE DOMAIN	COGNITIVE VARIABLE	TBI Mean±SD [a)]	CONTROL Mean±SD [a)]	TBI vs. CONTROL [b)]
Intellectual ability: Reading	WTAR age-scaled score	107±10.1 (*N*=9)	112±9.8 (*N*=15)	$t = -1.10$ [ns]
Verbal	WASI Similarities	39.4±3.7 (*N*=9)	34.5±6.3 (*N*=15)	$t = 2.45$ *
Non-verbal	WASI Matrix Reasoning	28.1±3.5 (*N*=10)	26.8±5.0 (*N*=15)	$t = 0.71$ [ns]
Executive function: Inhibition	Inhibition – naming (s)	31.8±22.4 (*N*=9)	28.7±17.6 (*N*=15)	$t = 0.23$ [ns]
Cognitive flexibility	Inhibition/switching – naming + reading ÷ 2 (s)	46.7±27.9 (*N*=9)	32.2±10.5 (*N*=14)	$t = 1.39$ [ns]
Word generation fluency	Letter Fluency F+A+S total	40.4±4.8 (*N*=9)	46.0±12.0 (*N*=15)	$t = 0.36$ [ns]
Set-shifting	Alternating-switch cost : TMT Trails B minus A (s)	25.6±17.8 (*N*=10)	23.3±9.8 (*N*=14)	$t = 0.57$ [ns]
Processing time: Visual search	TMT Trail A (s)	31.7±15.0 (*N*=10)	19.7±4.5 (*N*=14)	$t = 2.06$ [ns]
Complex	TMT Trails B (s)	57.3±28.6 (*N*=10)	43.0±12.6 (*N*=14)	$t = 1.16$ [ns]
Naming	Colour Naming (s)	37.9±12.0 (*N*=9)	33.2±.4.0 (*N*=14)	$t = 3.15$ **
Reading	Word Reading (s)	26.3±6.3 (*N*=9)	28.9±6.3 (*N*=15)	$t = -0.53$ [ns]
Complex	Inhibition (s)	69.7±30.7 (*N*=9)	23.3±4.4 (*N*=15)	$t = 4.50$ **
Choice reaction time	CRT median RT (ms)	456±62 (*N*=9)	408±51 (*N*=15)	$t = 2.16$ *
Memory: Immediate/Working	Digit Span forward	10.5±1.5 (*N*=10)	11.5±2.2 (*N*=15)	$t = -1.28$ [ns]
	Digit Span backward	7.2±1.4 (*N*=10)	7.5±2.0 (*N*=15)	$t = -0.66$ [ns]
Logical	WMS-III LM I first recall total	28.4±3.7 (*N*=9)	26.4±9.0 (*N*=15)	$t = 0.02$ [ns]
	WMS-III LM I total	47.1±5.4 (*N*=9)	42.7±13.7 (*N*=15)	$t = 0.17$ [ns]
	WMS-III LM II delayed	31.9±5.1 (*N*=9)	25.6±9.2 (*N*=15)	$t = 0.99$ [ns]
Associative	PT immediate recall total	26.0±5.7 (*N*=10)	26.9±7.1 (*N*=15)	$t = -1.03$ [ns]

Neuropsychological results for TBI patient and age-matched control group. [a)] Following exploratory data analysis control subjects identified as extreme outliers (≥ 3 x interquartile range) were excluded. [b)] Significant group differences shown by *$P \leq 0.05$ and **$P \leq 0.01$; [ns] indicates a not significant result. Group contrasts are made controlling for differences in current intellectual ability. WTAR = Wechsler Test of Adult Reading. WASI = Wechsler Abbreviated Scale of Intelligence; Inhibition, Inhibition/Switching, Letter Fluency, Colour Naming, and Word Reading subtests are from the Delis-Kaplan Executive Function System Color-Word Interference Test; TMT = Trail Making Test; CRT = Choice-Reaction Task; WMS-III = Wechsler Memory Scale- Third Edition; PT = People Test.

2.7 Figures

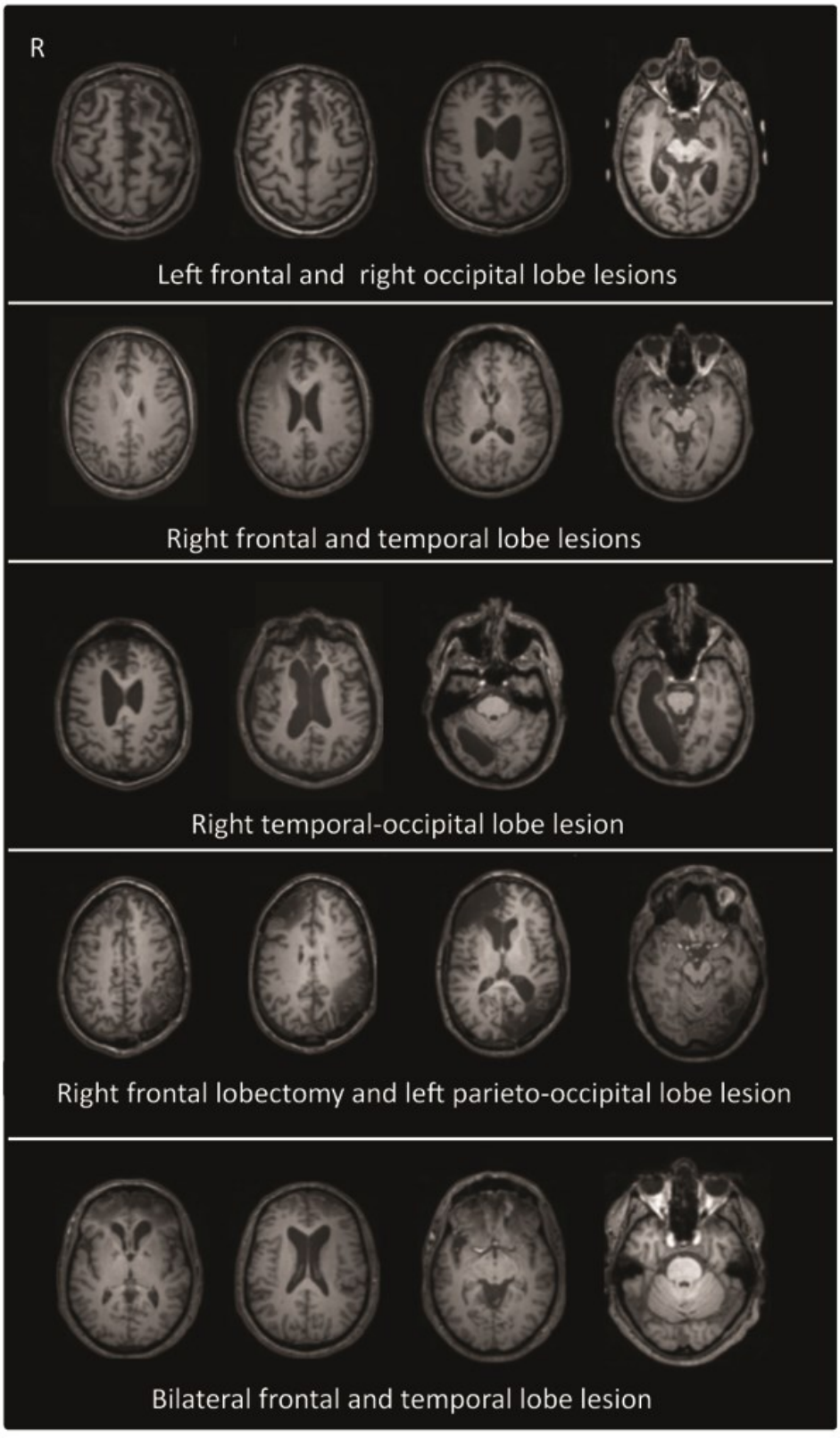


Figure 2.1. Transverse sections through T1 weighted MRI, in traumatic brain injury (TBI) patients (n=5) with focal brain lesions. R=right.

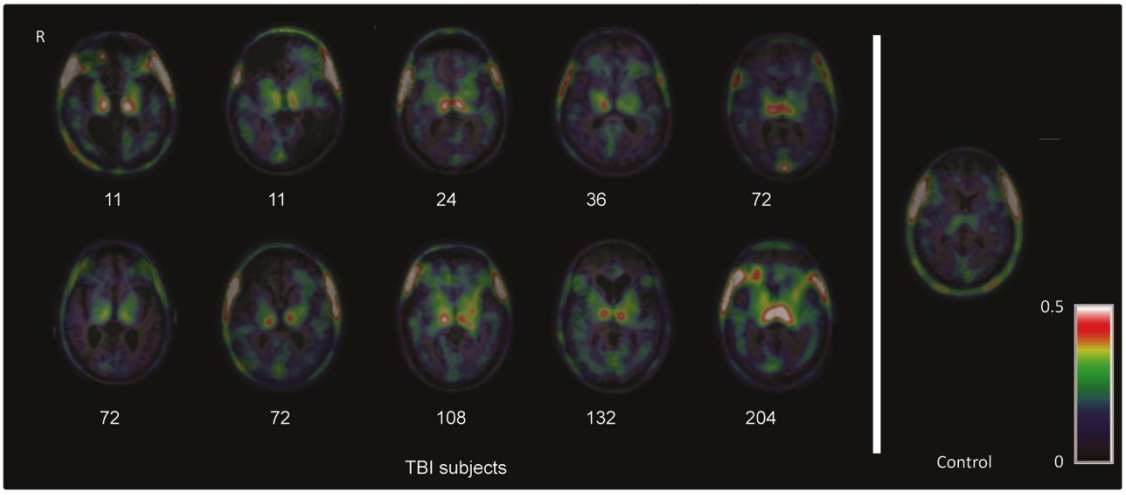


Figure 2.2. Chronic microglial activation is present following TBI. Overlay images of the transverse T1 MRI at the level of the thalamus superimposed with [11C]-PK11195 binding potential images of all traumatic brain injury (TBI) subjects and a representative control subject. Numbers indicate time in months from the time of TBI to PET scanning. Images illustrate the greater binding of [11C]-PK11195 in the thalami of all TBI subjects. R = right.

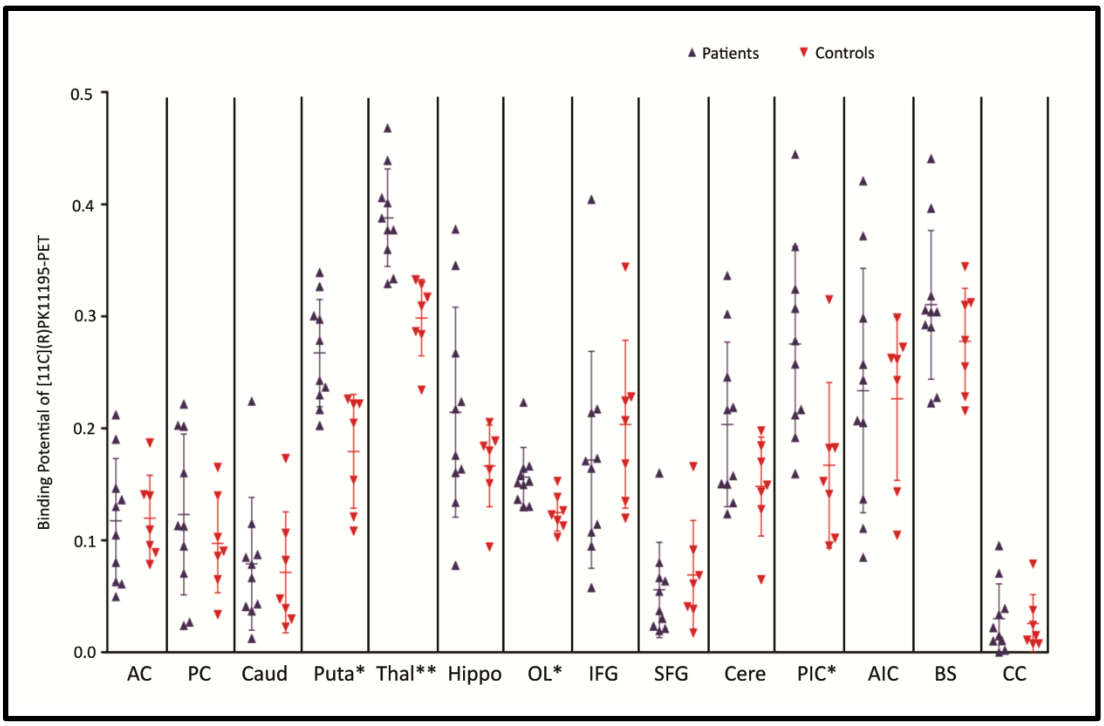


Figure 2.3. [11C]-PK11195 binding in the regions of interests investigated. Error bars, 95% confidence interval. Individual subjects binding potentials are plotted with patients in blue and control subjects in red. AC – anterior cingulate, PC – posterior cingulate, Caud – caudate, Puta – putamen, Thal – thalami, Hippo – hippocampus, OL – occipital lobe, IFG – inferior frontal gyrus, SFG – superior frontal gyrus, Cere – cerebellum, PIC – posterior limb of internal capsule, AIC – anterior limb of internal capsule, BS – brainstem and CC – corpus callosum. *p<0.05 significance, **survives Bonferroni multiple comparison correction.

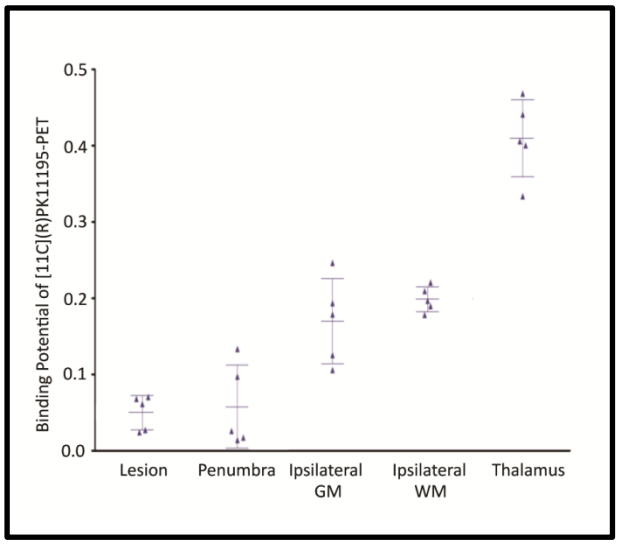


Figure 2.4. Microglia are not chronically activated around the site of focal brain damage following TBI. [11C]-PK11195 binding potentials (BP) in representative regions drawn at the lesion site, in the penumbral region of the lesion, and within normal appearing grey and white matter in the same hemisphere. Thalamic binding values correspond to the mean BP of the right and left thalami. Results demonstrate no abnormal increase in [11C]-PK11195 binding in or around the lesion site. GM = grey matter, WM = white matter.

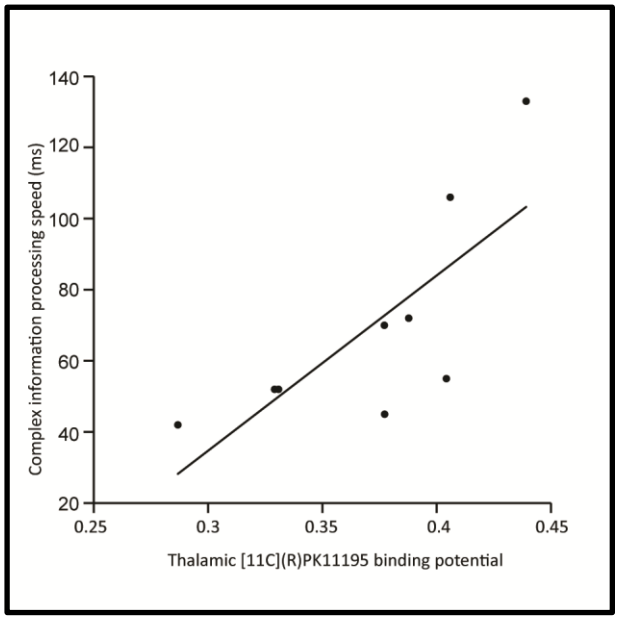


Figure 2.5. Thalamic microglial activation correlates with complex information processing speed. [11C]-PK11195 binding in bilateral thalamic regions plotted against speed of responding to incongruent items on the Color-Word Interference Test Inhibition trial providing a measure of complex information processing speed.

2.8 References

1. Lowenstein DH. Traumatic brain injury: a glimpse of order among the chaos? Ann Neurol 2009;66:A7-A8.

2. Whitnall L, McMillan TM, Murray GD, Teasdale GM. Disability in young people and adults after head injury: 5-7 year follow up of a prospective cohort study. J Neurol Neurosur Ps 2006;77:640-645.

3. Annegers JF, Hauser WA, Coan SP, Rocca WA. A population-based study of seizures after traumatic brain injuries. N Engl J Med 1998;338:20-24.

4. Guo Z, Cupples LA, Kurz A, et al. Head injury and the risk of AD in the MIRAGE study. Neurology 2000;54:1316-1323.

5. Nagamoto-Combs K, McNeal DW, Morecraft RJ, Combs CK. Prolonged microgliosis in the rhesus monkey central nervous system after traumatic brain injury. J Neurotraum 2007;24:1719-1742.

6. Maxwell WL, MacKinnon MA, Smith DH, et al. Thalamic nuclei after human blunt head injury. J Neuropathol Exp Neurol 2006;65:478-488.

7. Smith DH, Chen XH, Pierce JE, et al. Progressive atrophy and neuron death for one year following brain trauma in the rat. J Neurotraum 1997;14:715-727.

8. Koshinaga M, Katayama Y, Fukushima M, et al. Rapid and widespread microglial activation induced by traumatic brain injury in rat brain slices. J Neurotraum 2000;17:185-192.

9. Gehrmann J. Microglia: a sensor to threats in the nervous system? Res Virol 1996;147:79-88.

10. Gehrmann J, Matsumoto Y, Kreutzberg GW. Microglia: intrinsic immuneffector cell of the brain. Brain Res Brain Res Rev 1995;20:269-287.

11. Nagamoto-Combs K, Morecraft RJ, Darling WG, Combs CK. Long-term gliosis and molecular changes in the cervical spinal cord of the rhesus monkey after traumatic brain injury. J Neurotraum 2010;27:565-585.

12. Gentleman SM, Leclercq PD, Moyes L, et al. Long-term intracerebral inflammatory response after traumatic brain injury. Forensic Sci Int 2004;146:97-104.

13. Wilson S, Raghupathi R, Saatman KE, et al. Continued in situ DNA fragmentation of microglia/macrophages in white matter weeks and months after traumatic brain injury. J Neurotrauma 2004;21:239-250.

14. Thiel A, Radlinska BA, Paquette C, et al. The temporal dynamics of poststroke neuroinflammation: a longitudinal diffusion tensor imaging-guided PET study with 11C-PK11195 in acute subcortical stroke. J Nucl Med 2010;51:1404-1412.

15. Gerhard A, Schwarz J, Myers R, et al. Evolution of microglial activation in patients after ischemic stroke: a [11C](R)-PK11195 PET study. NeuroImage 2005;24:591-595.

16. Hashimoto K, Inoue O, Suzuki K, et al. Synthesis and evaluation of 11C-PK 11195 for in vivo study of peripheral-type benzodiazepine receptors using positron emission tomography. Ann Nucl Med 1989;3:63-71.

17. Malec JF, Brown AW, Leibson CL, et al. The mayo classification system for traumatic brain injury severity. J Neurotraum 2007;24:1417-1424.

18. Kinnunen KM, Greenwood R, Powell JH, et al. White matter damage and cognitive impairment after traumatic brain injury. Brain 2011 Feb;134(Pt 2):449-63.

19. Sidaros A, Engberg AW, Sidaros K, et al. Diffusion tensor imaging during recovery from severe traumatic brain injury and relation to clinical outcome: a longitudinal study. Brain 2008;131:559-572.

20. Turkheimer FE, Edison P, Pavese N, et al. Reference and target region modeling of [11C]-(R)-PK11195 brain studies. J Nucl Med 2007;48:158-167.

21. Heckemann RA, Keihaninejad S, Aljabar P, et al. Improving intersubject image registration using tissue-class information benefits robustness and accuracy of multi-atlas based anatomical segmentation. NeuroImage 2010;51:221-227.

22. Heckemann RA, Hajnal JV, Aljabar P, et al. Automatic anatomical brain MRI segmentation combining label propagation and decision fusion. NeuroImage 2006;33:115-126.

23. Stuss DT, Stethem LL, Picton TW, et al. Traumatic brain injury, aging and reaction time. Can J Neurol Sci 1989;16:161-167.

24. Mac Donald CL, Dikranian K, Bayly P, et al. Diffusion tensor imaging reliably detects experimental traumatic axonal injury and indicates approximate time of injury. J Neurosci 2007;27:11869-11876.

25. Povlishock JT, Katz DI. Update of neuropathology and neurological recovery after traumatic brain injury. J Head Trauma Rehab 2005;20:76-94.

26. Morioka T, Kalehua AN, Streit WJ. Characterization of microglial reaction after middle cerebral artery occlusion in rat brain. J Comp Neurol 1993;327:123-132.

27. Myer DJ, Gurkoff GG, Lee SM, et al. Essential protective roles of reactive astrocytes in traumatic brain injury. Brain 2006;129:2761-2772.

28. Pierce JE, Smith DH, Trojanowski JQ, McIntosh TK. Enduring cognitive, neurobehavioral and histopathological changes persist for up to one year following severe experimental brain injury in rats. Neuroscience 1998;87:359-369.

29. Bal-Price A, Brown GC. Inflammatory neurodegeneration mediated by nitric oxide from activated glia-inhibiting neuronal respiration, causing glutamate release and excitotoxicity. J Neurosci 2001;21:6480-6491.

30. Perry VH, Cunningham C, Holmes C. Systemic infections and inflammation affect chronic neurodegeneration. Nat Rev Immunol 2007;7:161-167.

Chapter 3

Amyloid plaque disposition after Traumatic Brain Injury

3.1 Amyloid plaque disposition after Traumatic Brain Injury

Chronic TBI is a hyperinflammatory state. In this chapter eight of the TBI subjects investigated with [11C]-PK11195 form the previous chapter went on to have further PET scanning with [11C]-PIB in an attempt to detect amyloid plaque deposition.

Summary of Objectives

Patients surviving TBI have at least twice the normal risk of developing late onset AD. The underlying pathophysiology of this is poorly understood, but the early deposition of fibrillar amyloid is potentially an important factor. The load of fibrillar amyloid can be determined *in vivo* using the PET ligand [11C]-PIB. In this study I investigate whether fibrillar amyloid can be identified in chronic TBI patients.

Eight patients were studied at least 11 months after moderate to severe TBI. All underwent [11C]-PIB PET and structural MRI (including diffusion tensor imaging). Standardised uptake values (SUV's) of [11C]-PIB were calculated for all TBI subjects as well as 10 normal control subjects previously scanned at the department. The SUV's in anatomically defined regions known to be involved in AD and TBI were investigated and compared. Standardised neuropsychological tests were administered.

Summary of results

There was no significant difference in regional brain SUV's between TBI subjects and normal controls. This was despite differences identified in neuropsychological assessment where the TBI group demonstrated poorer functioning with complex reasoning.

The results demonstrate absence of a significant fibrillar amyloid load in chronic TBI patients. The negative PET findings, however, do not exclude the presence of raised soluble or amorphous forms of amyloid as [11C]-PIB does not label these compounds. These results were evident despite neuropsychological deficits in the TBI group.

These findings should be considered preliminary and the longitudinal investigation of subjects will be necessary to demonstrate eventual amyloid plaque formation. Results suggest, however, that fibrillar amyloid is not directly related to cognitive impairment.

3.2 Introduction

TBI is a major socioeconomic burden and a significant cause of mortality and morbidity in the younger age group[1]. Patient outcome is highly variable and even after an initial good recovery; many survivors still have some degree of residual cognitive impairment. This can worsen over time and there is compelling evidence that survivors of TBI are at a higher risk for the development of AD later on in life [2].

TBI sets off a sequence of events resulting from damage to the blood brain barrier. Within hours there is an intense inflammatory response accompanied by microglia activation and increased expression of the APP and soluble amyloid [3]. TBI should however not be considered a static event and activated microglia have been identified in animals at least a year after the initial event and several years after the initial event in human post mortem studies. I previously reported on sustained microglial activation in the thalami of TBI subjects up to 17 years after their initial event. Accompanying this inflammatory response is an increased β amyloid protein deposition[2]. This has also been reported in 30% of subjects dying within 4 hour to 2.5 years after severe TBI [4]. β amyloid plaque formation and deposition is a pathogonomic marker of AD and is thought to contribute to cortical damage. It is unclear however how amyloid pathology relates to the future development of cognitive impairment in TBI.

It is now possible with PET to identify fibrillar β amyloid plaque deposition *in vivo* using the radioactively labelled tracer Pittsburgh compound B (PIB). This thioflavin analogue binds to a non-physiological site between the planar folds of the β pleated sheets making up the amyloid plaque[5,6]. It has been used in many studies to label and quantify amyloid load in many conditions including AD, mild cognitive impairment (MCI) and healthy elderly controls[7,8]. Two fold higher levels are found in AD, while 60% of MCI show increased uptake.

It should be noted however that up to 50% of healthy elderly controls in their 8th decade have increased [11C]-PIB uptake [9,10].

In this study I make use of [11C]-PIB PET to investigate patients with chronic head injury and hypothesise that these subjects will show cortical β amyloid plaque deposition. A wide range of subjects including those with residual mental and physical disability were included as well as those who had returned to their normal level of premorbid functioning. I hypothesised that amyloid plaque deposition would be higher in chronic TBI subjects with cognitive impairment.

3.3 Methods

Eight subjects were recruited from local head injury clinics in the UK, mean age 44.0±5.2 years. All subjects suffered from a moderate to severe head injury based on the Mayo Criteria at least 11 months before investigation. As before, exclusion criteria were as follows: neurosurgery, except for invasive intracranial pressure monitoring; a history of psychiatric or neurological illness prior to the head injury; a history of previous significant TBI; anti-epileptic medication; pregnancy or breast feeding; current or previous drug or alcohol abuse; contraindication to MRI. Neurosurgery at the time of TBI and the presence of intra-cerebral lesions were not exclusion criteria. Subjects needed to be able to undergo MRI scanning. Significant vascular pathology on T2 MRI was an exclusion criterion. See table 3.1 for the clinical details of the subjects investigated.

Structural neuroimaging was reviewed by a senior neuroradiologist. Three patients had no abnormalities visible on T1 MRI. The remaining five had significant focal lesions with damage seen mostly in the frontal (n = 4) or temporal (n = 3) lobes (see figure 3.1). Two patients had evidence of microbleeds on gradient echo imaging. Atrophy, contusion, gliosis

and siderosis at the injury site were the most common changes described. All patients gave written informed consent. The project was approved by Hammersmith and Queen Charlotte's and Chelsea Research ethics committee.

TBI subject scans were compared to 10 healthy control scans held on a database at Hammersmith Imanet. Controls were from the adult population and had underwent clinical and neuropsychological assessments to ensure that there were no underlying neurological illnesses. The control group formed part of a study on [11C]-PIB uptake in AD and hence were significantly older than the TBI group.

3.3.1 PET image acquisition

All subjects were scanned using a Siemens ECAT 962 EXACT HR+ scanner which has an axial view of 15.5 cm. Prior to scanning, an intravenous cannula was inserted in the antecubital fossa of each subject. A 10 minute transmission scan was acquired before the emission study, using a single rotating photon point source of ^{137}Cs, for subsequent attenuation and scatter correction. The PET data were acquired in 3-dimensional mode. Data were reconstructed using filtered back projection to produce images containing 63 contiguous slices, separated by 2.42mm, of 128x128 pixels 2.092mm square. Reconstruction of emission data was carried out using filtered back projection. The 3D emission data were Fourier-rebinned into 2D data sets to increase the speed of reconstruction. The reconstructed images consisted of sixty-three transaxial image planes were displayed as 2.46-mm slices with a reconstructed axial resolution of 5.4 mm and a transaxial resolution of 5.6 mm.

Following the transmission scan and 30 seconds after the start of the emission scan, all subjects received 367 ±16.4 MBq [11C]-PIB injected IV. This was followed by a 90 minute dynamic emission scan comprising 32 time frames. [11C]-PIB was manufactured by Hammersmith Imanet, GE Healthcare at the Cyclotron Building, Hammersmith Hospital.

All image processing were performed using Analyze (Mayo Clinic, MN) and SPM2 (Wellcome Department of Imaging Neuroscience, University College London, UK) running in MATLAB 5 (R12, Mathworks, Natick, MA).

3.3.2 PET image analysis – Standardised Uptake Value

Time frames corresponding to 10-90 minute (early and late) and 60-90 minute (late) summation images were created for each [11C]-PIB scan. Each subject's MRI was then coregistered to its corresponding PET scan and segmented into grey matter, white matter and cerebrospinal fluid (CSF). An in house atlas was then normalized and convolved with the grey matter segmented image[11]. Individualized cortical grey matter regions were thus defined. The atlas was first applied to the subjects' MRI and visually checked to ensure the regions outlined were structurally correct. Manual alterations were made where appropriate. In the case of the five subjects with focal atrophy, regions which were distorted were again removed from analysis. It is noteworthy that in all case the contralateral region remained intact ensuring that all regions were represented in all subjects for analysis. Checked and modified atlases were then applied to the late [11C]-PIB scans. It should be noted that this late [11C]-PIB PET data was not modified in any way.

For the quantitative analysis of [11C]-PIB scans the cerebellum is normally used as the reference region for non-specific binding. In AD this region is not affected by fibrillar deposits

of amyloid and hence has no specific binding of [11C]-PIB but rather provides a value for background [11C]-PIB uptake[12,13]. TBI however is a heterogeneous condition with widespread areas of focal damage and potential amyloid deposition. As one cannot be certain that TBI would not provoke localised inflammation and amyloid deposition in the cerebellum I chose to calculate standardised uptake values (SUV) to quantitate regional brain [11C]-PIB binding. This factor is calculated according to the subjects' body surface area and the radioactivity injected. The formula below was employed:

SUV (m^2/MBq) = Late Add Image x (body surface area(m^2)/Activity injected (MBq)).

The late summated [11C]-PIB PET image was thus transformed to an SUV image. During this normalization process, region volumes are not changed or warped into standard space.

The use of SUV in creating parametric [11C]-PIB data is less well established than the determination of cerebellar RATIO images. Its use however, enabled meaningful analysis for [11C]-PIB data in this study. Ideally blood data to generate an arterial input function enabling spectral analysis could have been attempted. However SUV ratio parametric images have been shown to be as dependable as spectral analysis using the Logan approach[14]. Arterial blood data was thus thought unnecessary and was not performed in this study.

SUV's were calculated for both TBI and control scans and anatomically defined regions of interest (ROI's) were sampled. SUV's of all ROI's were compared using non-parametric Mann Whitney U test. Significance level was set as P=0.05.

3.3.3 Neuropsychological Assessment

Neuropsychological assessments of the 8TBI patients having [11C]-PIB PET scans were extracted from the original 15 investigated in Chapter 2 and analysed independently. Further neuropsychology was not thought to be necessary specifically for this study.

3.4 Results

3.4.1 PET scanning

For the regions sampled [11C]-PIB retention was not significantly higher in the TBI group compared to the older healthy control group. See figure 3.2. Figure 3.3 gives an example of SUV parametric images for TBI, AD and healthy older control.

3.4.2 Neuropsychological assessment

TBI patients have a characteristic pattern of cognitive impairment. Generally there is information processing speed, memory and executive function. TBI patients showed poorer information processing speeds with higher colour naming and choice reaction times and poorer executive functioning, exemplified by poorer Stroop Inhibition times (see table 3.2). TBI subjects also demonstrated a wider spread of performance within the group with some subjects performing particularly badly. One TBI subject also could not be fully assessed because of limited use of his hands.

3.5 Discussion

In this study we investigated a wide spectrum of chronic TBI subjects. The time range from event to scanning was extensive ranging from 11 months to 17 years, the range of disability

varied from none to speech and movement impaired and over half had structurally abnormal MRI scans. Neuropsychology results demonstrated deficits that are expected in TBI with slowing of complex processing. Despite these factors we were not able to identify any differences in [11C]-PIB uptake compared to an older healthy control group. Within the limitations of this study this would suggest the absence of significantly elevated β amyloid plaque deposition in the TBI group.

On initial consideration this result seems unexpected given the fact that subjects have impaired neuropsychological assessment. These results may however be explained by the specificity and sensitivity of which [11C]-PIB to bind to β pleated amyloid fibrils. It does not label the whole family of compounds that originate from the enzymatic cleavage of APP [5]. Included in this cohort are the soluble APP (sAPP) proteins produced by first cleavage by α or β secretase and the resultant intermediary being acted on by Ɣ secretase[15-18]. Soluble APP is undoubtedly physiologically important in cerebral function binding to an LDL cholesterol receptor, a class A scavenger receptor and fibulin-1 (which is predominantly expressed on neurons in the brain). It has the ability to activate guanylate cyclase, regulate membrane excitability, calcium homeostasis and down regulate NMDA receptor mediated currents[15,19]. Cleavage also produces potentially neurotoxic side products, the most interesting of which are the amyloid β (Aβ) fragments varying in size from 39 – 43 amino acids. Aβ exists as monomers, dimers and higher oligomers[20,21]. These soluble moieties do not bind [11C]-PIB and it is only with further aggregation into protofibrils and then fibrils that thioflavine staining is seen. This process requires both time and the attainment of a certain critical concentration of Aβ suggested by in vitro studies. The result is a “lag” phase during which no aggregation is detected, but after which it proceeds very rapidly [22,23]. It may be that TBI subjects scanned were all still in this lag period with no formal plaque deposition at the time of investigation. Non-fibrillar Aβ arranged oligomers are neurotoxic inhibiting long term potentiation possibly by binding to nicotinic receptors on pyramidal cells and GABAergic

interneurons. Interestingly, in one series, immunohistochemistry confirmed the presence of Aβ42 intra-cerebrally at least one year after severe TBI but only 30% of that group had actual amyloid plaque formation[24].

It should also be recognised that β amyloid and the amyloid group of molecules may in fact not be the main drivers of neuronal damage in TBI. Hyperphosphorylated tau, the main component of toxic neurofibrillary tangles (NFT), must also be considered. On immunohistochemistry, NFT were found in over 30% of TBI subjects under the age of 60. Hyperphosphorylated tau is present 2 – 3 hours after severe brain injury and tau pathology is the major finding in pugilistic encephalopathy [15, 24, 25]. In the acute scenario, the location of tau deposits post TBI seems to be related to the site of injury and is likely to reflect the shearing stresses undergone by damaged axons. A year after TBI the distribution of tau is more widespread and excessive[24]. Investigating the presence and distribution of tau was outside the scope of my study but a hunt for confirmation of its presence would seem to be useful investigation.

Continued thalamic microglial activation has also been demonstrated in this group of patients [26]. The result is the creation of a neuronal microenvironment rich in cytokines and chemokines. At the time of TBI this reaction helps transform and maintain microglial in their activated phagocytic phenotype, actively clearing cellular debris. In the chronic scenario, continued activation maybe responsible indiscriminate neuronal death independent of fibrillar amyloid.

Of the eight TBI subjects investigated, five had structurally abnormal MRI's with significant areas of focal atrophy. Careful consideration thus had to be made about the technique used

in [11C]-PIB analysis. The calculation of SUV's is a well-recognised and frequently used technique in oncology to monitor for tumour recurrence [27-29]. Its use in [11C]-PIB analysis has also been tested and SUV cerebellar-RATIO images have been shown to be reliable[14] but the SUV analysis as performed in this study has not been validated. The lack reference region in this study however should be considered a major limitation. Spectral analysis using an arterial input function may have produced more definitive results. During analysis the PET parametric data were never modified or warped into standard space. This was especially important in areas of focal atrophy where spatial normalisation could result in dilution of the [11C]-PIB signal. Instead the atrophied lobe was masked from the analysis and the signal from the contralateral lobe was compared with controls. It could be argued that these atrophied lobes are in fact the areas where amyloid plaque deposition begins but raised [11C]-PIB signal was not visually evident in these areas. Partial volume correction may however enable more objective analysis but would result in the modification of the raw PET data with the potential for introducing noise into genuine signal. Finally, the control and TBI groups were not equally matched. Control subjects where older and may have had an increased amyloid load[30]. This may explain the tendency for lower binding in patients as compared to control. Comparison with age matched controls may thus produce different result but this question could not currently be addressed. Despite these limitations the results were supported by visual image interpretation, as none of the cases showed an increase of cortical uptake similar to white matter as commonly observed in AD.

In conclusion we have demonstrated a lack of significant [11C]-PIB uptake in chronic TBI patients. We have confirmed that this group of patients do suffer with neuropsychological impairment but β amyloid plaque formation is not likely to be responsible for this. Other neurotoxic molecules should also be considered as driving this. Of these the amyloid oligomers are of particular interest as they may exist for an undetermined period of time before plaque formation occurs.

3.6 Tables

Table 3.1. Clinical features of all traumatic brain injury (TBI) patients

Age	Sex	Highest level of education	Cause of TwhandaerBI	GCS when found	Post-traumatic amnesia (hrs)	Current medications	Scanning interval from time of injury (months)
45	M	Postgraduate	Unknown	4	24	Gabapentin Modafenil Amitriptyline	72
55	M	Postgraduate	Hit plank of wood then fell onto concrete	4	UK	nil	36
42	M	A level	Pedestrian hit by a car	4	432	nil	72
42	M	O level	Motorcycle accident	4	UK	Tropium chloride Folic acid	204
40	M	Graduate degree	Motorcycle accident	4	1008	nil	132
42	F	Postgraduate	Pedestrian hit by a car	3	144	Codine Paracetamol	72
49	M	A level	?assault	4	2	nil	11
38	M	Graduate	Motorcycle accident	6	UK	Citalopram Modafanil Omeprazole	108

UK – unknown

Table 3.2: Sample of Neuropsychological test results: traumatic brain injury and control patients demonstrating impaired planning and executive function. Memory (not shown) was not affected.

COGNITIVE DOMAIN	COGNITIVE VARIABLE	TBI Mean±SD	CONTROL Mean±SD(a)	TBI vs. CONTROL (P value)
Intellectual ability:				
Reading	WTAR age-scaled score	109.4±8.9 (*N*=7)	112±9.8 (*N*=15)	0.435
Verbal	WASI Similarities	39.4±4.2 (*N*=7)	34.5±6.3 (*N*=15)	0.104
Non-verbal	WASI Matrix Reasoning	28.9±2.4 (*N*=8)	26.8±5.0 (*N*=15)	0.359
Executive function				
Inhibition	Inhibition – naming (s)	39.3±13.5 (*N*=7)	28.7±17.6 (*N*=15)	0.006
Cognitive flexibility	Inhibition/switching – naming + reading ÷ 2 (s)	33.6±9.1 (*N*=7)	32.2±10.5 (*N*=14)	0.015
Processing speed:				
Visual search	TMT Trail A (s)	33.6±16.3 (*N*=10)	19.7±4.5 (*N*=14)	0.006
	TMT Trails B (s)		43.0±12.6 (*N*=14)	0.074
	Colour Naming (s)	60.3±30.4 (*N*=10)		0.006
Complex	Word Reading (s)		33.2±.4.0 (*N*=14)	0.812
	Inhibition (s)	39.3±13.5 (*N*=7)	28.9±6.3 (*N*=15)	0.000
Naming	CRT median RT (ms)	27.9±6.3 (*N*=7)	23.3±4.4 (*N*=15)	0.097
		73.6±33.4 (*N*=7)	408±51 (*N*=15)	
Reading		450±65 (*N*=7)		
Complex Choice reaction time				

Neuropsychological results for TBI patient and age-matched control group. (a) Following exploratory data analysis control subjects identified as extreme outliers (≥ 3 x interquartile range) were excluded. WTAR = Wechsler Test of Adult Reading. WASI = Wechsler Abbreviated Scale of Intelligence; Inhibition, Inhibition/Switching, Letter Fluency, Colour Naming, and Word Reading subtests are from the Delis-Kaplan Executive Function System Color-Word Interference Test; TMT = Trail Making Test; CRT = Choice-Reaction Task

3.7 Figures

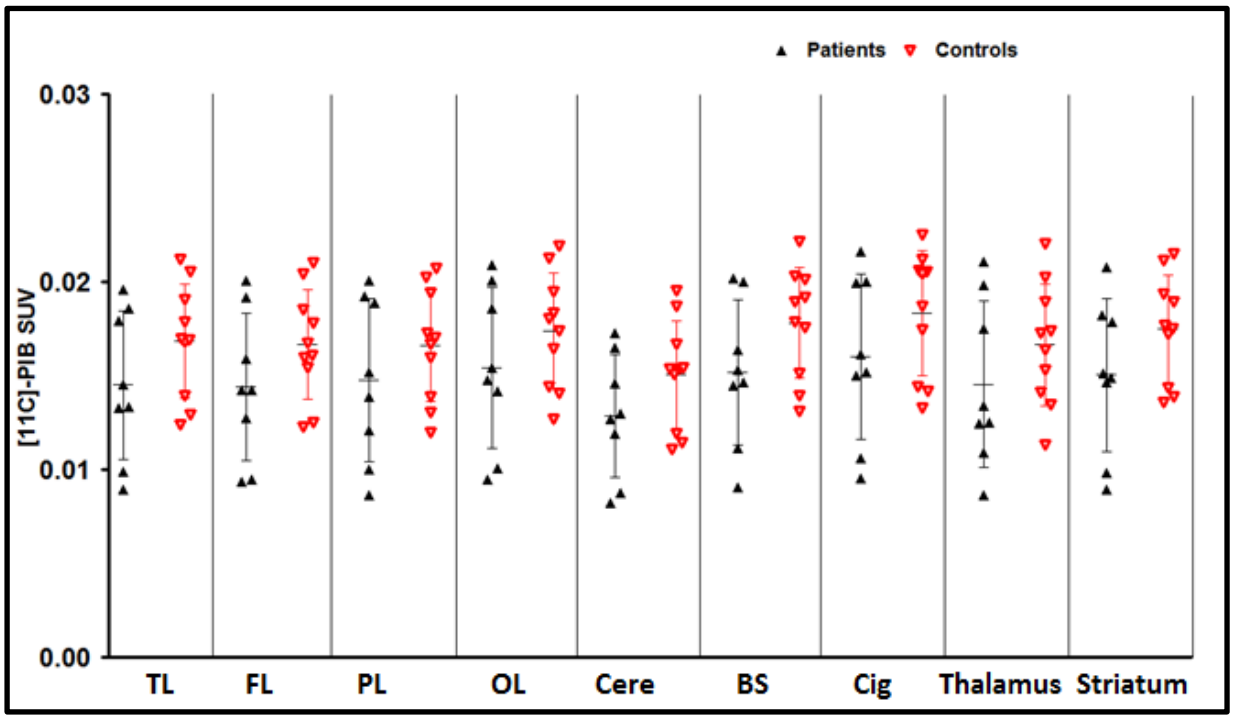


Figure 3.1. [11C]-PIB Standardised Uptake Values (SUV) in control and TBI subjects. Regions sampled include TL=temporal lobe, FL=frontal lobe, PL=parietal lobe, OL=occipital lobe, Cere=cerebellum, BS=brain stem, Cig=cingulate, thalamus and striatum. SUV similar in all regions sampled.

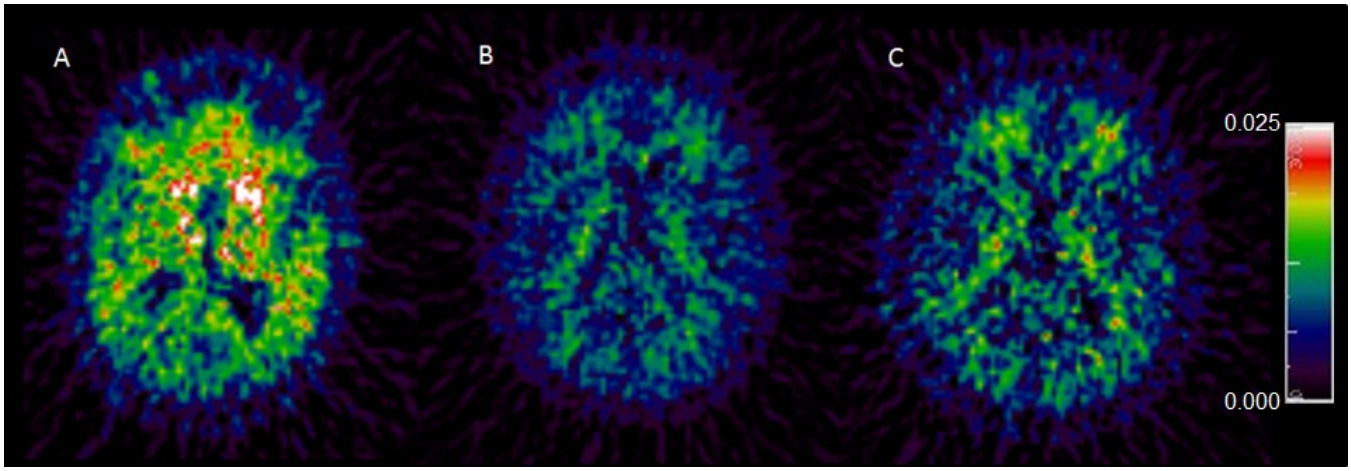


Figure 3.2. Sample [11C]-PIB SUV binding potential parametric images for A – Alzheimers Disease subject, MMSE<25, B – Control and C – TBI subject. [11C]-PIB uptake greater in AD but similar in control and TBI subjects.

3.8 References

1. Maas AI, Stocchetti N, Bullock R. Moderate and severe traumatic brain injury in adults. Lancet Neurol. 2008;7:728-41.

2. Shively S, Scher AI, Perl DP, Diaz-Arrastia R. Dementia Resulting From Traumatic Brain Injury: What Is the Pathology? Arch Neurol. 2012; 9:1-7.

3. Dixon CE, Kochanek PM, Yan HQ, Schiding JK, Griffith RG, Baum E, Marion DW, DeKosky ST.One-year study of spatial memory performance, brain morphology, and cholinergic markers after moderate controlled cortical impact in rats. J Neurotrauma. 1999;16:109-22.

4. GentlemanS.M., Leclercq P.D., Moyes L., Graham D.I., Smith C., Griffin W.S.T., Nicoll J.A.R. Long-term intracerebral inflammatory response after traumatic brain injury. Forensic Science International 2004; 146: 97–104

5. Swahn BM, Wensbo D, Sandell J, Sohn D, Slivo C, Pyring D, Malmström J, Arzel E, Vallin M, Bergh M, Jeppsson F, Johnson AE, Juréus A, Neelissen J, Svensson S. Synthesis and evaluation of 2-pyridylbenzothiazole, 2-pyridylbenzoxazole and 2-pyridylbenzofuran derivatives as 11C-PET imaging agents for beta-amyloid plaques. Bioorg Med Chem Lett. 2010;20:1976-80.

6. Mathis CA, Mason NS, Lopresti BJ, Klunk WE.Development of Positron Emission Tomography β-Amyloid Plaque Imaging Agents. Semin Nucl Med. 2012;42:423-32.

7. Edison P, Brooks DJ, Turkheimer FE, Archer HA, Hinz R. Strategies for the generation of parametric images of [11C]PIB with plasma input functions considering discriminations and reproducibility. Neuroimage. 2009;48:329-38

8. Johnson KA, Fox NC, Sperling RA, Klunk WE. Brain imaging in Alzheimer disease. Cold Spring Harb Perspect Med. 2012;2:a006213

9. Okello A, Koivunen J, Edison P, Archer HA, Turkheimer FE, Någren K, Bullock R, Walker Z, Kennedy A, Fox NC, Rossor MN, Rinne JO, Brooks DJ. Conversion of amyloid positive and negative MCI to AD over 3 years: an 11C-PIB PET study. Neurology. 2009;73:754-60.

10. Okello A, Edison P, Archer HA, Turkheimer FE, Kennedy J, Bullock R, Walker Z, Kennedy A, Fox N, Rossor M, Brooks DJ. Microglial activation and amyloid deposition in mild cognitive impairment: a PET study. Neurology. 2009;72:56-62.

11. Hammers A, Allom R, Koepp MJ, Free SL, Myers R, Lemieux L, Mitchell TN, Brooks DJ, Duncan JS. Three-dimensional maximum probability atlas of the human brain, with particular reference to the temporal lobe. Hum Brain Mapp. 2003;19:224-47.

12. Joachim CL, Morris JH, Selkoe DJ. Diffuse senile plaques occur commonly in the cerebellum in Alzheimer's disease. Am J Pathol. 1989;135:309-19.

13. Yamaguchi H, Hirai S, Morimatsu M, Shoji M, Nakazato Y. Diffuse type of senile plaques in the cerebellum of Alzheimer-type dementia demonstrated by beta protein immunostain. Acta Neuropathol. 1989;77:314-9

14. Yaqub M, Tolboom N, Boellaard R, van Berckel BN, van Tilburg EW, et al. Simplified parametric methods for [11C]PIB studies. Neuroimage. 2008 Aug 1;42(1):76-86.

15. Turner PR, O'Connor K, Tate WP, Abraham WC. Roles of amyloid precursor protein and its fragments in regulating neural activity, plasticity and memory. Prog Neurobiol. 2003;70:1-32

16. Esler W.P., Wolfe M.S. A portrait of Alzheimer secretases—new features and familiar faces. Science. 2001;293:1149–454.

17. Yan R., Bienkowski M.J., Shuck M.E., Miao H., Tory M.C., Pauley A.M., Brashier J.R., Stratman, N.C., Mathews, W.R., Buhl, A.E., Carter, D.B., Tomasselli, A.G., Parodi, L.A., Heinrikson, R.L., Gurney, M.E. 1999. Membrane-anchored aspartyl protease with Alzheimer's disease beta-secretase activity. Nature. 1999; 402: 533–37.

18. Wolfe, M.S., Xia, W., Ostaszewski, B.L., Diehl, T.S., Kimberly, W.T., Selkoe, D.J. Two transmembrane aspartates in presenilin-1 required for presenilin endoproteolysis and gamma-secretase activity. Nature.1999; 398:513–17.

19. Herz, J., Strickland, D.K. LRP: a multifunctional scavenger and signalling receptor. J. Clin. Invest. 2001; 108:779–84.

20. Walsh, D.M., Klyubin, I., Fadeeva, J.V., Cullen, W.K., Anwyl, R., Wolfe, M.S., Rowan, M.J., Selkoe, D.J. Naturally secreted oligomers of amyloid _ protein potently inhibit hippocampal long-term potentiation in vivo. Nature 2002;416:535–39.

21. Walsh, D.M., Klyubin, I., Fadeeva, J.V., Rowan, M.J., Selkoe, D.J. Amyloid-beta oligomers: their production, toxicity and therapeutic inhibition. Biochem. Soc. Trans. 2002;30:552–57.

22. Harper, J.D., Lansbury, P.T., Models of amyloid seeding in Alzheimer's disease and scrapie: mechanistic truths and physiological consequences of the time-dependent solubility of amyloid proteins. Annu. Rev. Biochem. 1997;66:385–407.

23. Jarrett, J.T., Berger, E.P., Lansbury Jr., P.T., The carboxy terminus of the beta amyloid protein is critical for the seeding of amyloid formation: implications for the pathogenesis of Alzheimer's disease. Biochemistry. 1993;32:4693–97.

24. Johnson VE, Stewart W, Smith DH. Widespread Tau and Amyloid-Beta Pathology Many Years After a Single Traumatic Brain Injury in Humans Brain Pathology. 2012;22:142–49

25. McKenzie K. J., McLellan D. R., Gentleman S. M., Maxwell W. L., Gennarelli T. A., Graham D. I. Is β-APP a marker of axonal damage in short-surviving head injury? Acta Neuropathol. 1996; 92: 608–13

26. Ramlackhansingh AF, Brooks DJ, Greenwood RJ, Bose SK, Turkheimer FE, Kinnunen KM, Gentleman S, Heckemann RA, Gunanayagam K, Gelosa G, Sharp DJ. Inflammation after trauma:microglial activation and traumatic brain injury. Ann Neurol. 2011;70:374-83.

27. Shepherd T, Owenius R. Gaussian process models of dynamic PET for functional volume definition in radiation oncology.IEEE Trans Med Imaging. 2012;31:1542-56.

28. Westerterp M, Pruim J, Oyen W, Hoekstra O, Paans A, Visser E, van Lanschot J, Sloof G, Boellaard R. Quantification of FDG PET studies using standardised uptake values in multi-centre trials: effects of image reconstruction, resolution and ROI definition parameters. Eur J Nucl Med Mol Imaging. 2007;34:392-404.

29. Ly J, Garpered S, Höglund P, Jönsson E, Valind S, Edenbrandt L, Wollmer P. Semi-automatic analysis of standard uptake values in serial PET/CT studies in patients with lung cancer and lymphoma. BMC Med Imaging. 2012;12:6.

30. Villemagne VL, Pike KE, Darby D, Maruff P, Savage G, Ng S, et al. Abeta deposits in older non-demented individuals with cognitive decline are indicative of preclinical Alzheimer's disease. Neuropsychologia. 2008;46(6):1688-97.

Chapter 4

Amyloid deposition & metabolic changes in Posterior Cortical Atrophy

4.1. Amyloid deposition and metabolic changes in Posterior Cortical Atrophy

In this Chapter I will be focusing on the atypical form of AD, Posterior Cortical Atrophy. This is a particularly rare form of AD where there is significant posterior cortical involvement. In this Chapter I would like to address the particular question, does the deposition of amyloid match the areas most affected by cortical atrophy and cerebral metabolism?

Summary of Objectives

Atypical presentations of sporadic Alzheimer's disease are rare and can be diagnostically challenging. Posterior Cortical Atrophy (PCA), is such a syndrome, characterized by deficits of visuospatial processing, such as reading, object and facial recognition, as the presenting complaint. *In vivo* investigations into PCA, using PET, have demonstrated reduced cerebral metabolism and fibrillar amyoid deposition. However these studies have not been extensive and results have been inconsistent. Here we make use of the PET tracers [11C]-PIB and [18F]-FDG to investigate changes in amyloid deposition and cerebral metabolism in PCA.

Eight patients with PCA, 12 patients with sporadic AD and 13 healthy controls (HC) were investigated. We evaluated brain amyloid load with [11C]-PIB PET and glucose metabolism with [18F]-FDG. All patients had a neuropsychological assessment (with 5 undergoing extensive neuropsychological testing) and MRI. Cerebellar RATIO images of [11C]-PIB uptake were generated and anatomical regions of interest (ROI's) sampled. Parametric maps of absolute cerebral glucose metabolism were generated with spectral analysis using an arterial input function for [18F]-FDG studies. Pre-defined ROI's were sampled and voxel based analyses were performed with both [11C]-PIB and [18F]-FDG scans comparing PCA, normal HC and sporadic AD group findings.

Summary of Results

Cortical [11C]-PIB binding in the PCA group was raised in the frontal, parietal, temporal and occipital cortex compared with HC ($P < 0.05$). There was no difference in levels of [11C]-PIB retention between the sporadic AD and PCA groups in all cortical areas. Cortical [18F]-FDG retention in the PCA group was deceased in the frontal, parietal, temporal and occipital cortex compared with HC ($P < 0.05$). [18F]-FDG retention was significantly lower in the temporal and occipital cortex in the PCA group compared to sporadic AD. All PCA patients showed parietal cortical atrophy on MRI.

Our findings support the concept of PCA being a subgroup of sporadic AD with both conditions having similar patterns of [11C]-PIB uptake. However the metabolic consequences of this deposition differ, with reduced [18F]-FDG uptake targeting the occipital and temporal cortices of the PCA group.

4.2 Introduction

PCA is a rare progressive neurodegenerative condition characterized by early visuospatial deficits. Early features include the Balint's syndrome consisting of simultanagnosia (the inability to perceive the visual field as a whole), ocular apraxia (difficulty in fixating the eyes) and optic ataxia (an inability to locate objects using vision). Later in the disease process the Gertsmann's syndrome consisting of visual agnosia, alexia, agraphia, and transcortical sensory aphasia develops[1] invariably followed by memory impairment and features typically associated with sporadic AD. For this reason PCA has been considered to be a focal presentation of sporadic AD with early involvement of the visuo-spatial network. This view has been strengthened by post-mortem studies demonstrating characteristic features of Alzheimer´s disease with senile plaques and neurofibrillary tangles in PCA[1]. Neurofibrillary tangles densities were however lower in PCA subjects compared to sporadic AD.

[11C]-PIB PET is a marker of fibrillar amyloid arranged into β pleated sheets[2]. AD patients show twofold increases in mean [11C]-PIB binding in cortical areas[3]. As discussed in section 1.3, [18F]-Fluoro-2-deoxy-D-glucose ([18F]-FDG) is a PET tracer taken up by metabolically active neurones. As a glucose analogue it becomes phosphorylated but becomes trapped within metabolically active cells. Its retention is thus a marker of hexokinase activity reflecting cerebral glucose metabolism[4]. In sporadic AD, characteristic reductions in [18F]-FDG uptake, were found in neocortical association areas including the posterior cingulate, precuneus, temporoparietal and frontal multimodal association regions; the primary visual cortex, sensorimotor cortex, basal ganglia and cerebellum were relatively spared[5].

Studies utilizing these tracers in PCA are however limited and have produced conflicting results. Short case series and single subject case reports have mostly shown a similar pattern of [11C]-PIB retention in PCA and sporadic AD. It has been suggested however that

this uptake has a greater tendency to focus on the posterior parts of the brain[6]. More consistent however is the demonstration of reduced [18F]-FDG retention in the posterior regions of the brain suggesting occipital lobe hypometabolism[7,8,9,10]. Only one study currently exists in the published literature where both [11C]-PIB and [18F]-FDG scans have been performed on PCA subjects[8]. Again the discordance between [11C]-PIB uptake and hypometabolism was highlighted.

In this study I hypothesised that fibrillar amyloid deposition would be independent of the metabolic changes seen in PCA. I have performed both [11C]-PIB and [18F]-FDG scans on PCA subjects along with neuropsychological assessment and structural MRI scanning.

4.3 Methods

4.3.1 Posterior Cortical Atrophy subjects

Eight PCA subjects were recruited from outpatient memory clinics of UK hospitals. Patients were assessed by at least two Neurologists. PCA was defined clinically according to criteria set out by Tang-Wai DF 2004[1]. The presence of signs and symptoms suggestive of dementia with Lewy bodies (DLB) – early visual hallucinations, extrapyramidal features and cognitive fluctuations, sporadic AD – early memory impairment or the presence of ophthalmological disease were exclusion criteria. Subjects with significant cerebrovascular pathology based on MRI rating scales were also excluded[11]. See table 4.1 for a clinical summery of all PCA subjects.

4.3.2 Sporadic AD and Healthy Control subjects

Twelve sporadic AD patients fulfilled the diagnosis of probable AD according to the criteria of the National Institute of Neurological and Communication Disorders, Alzheimer's Disease and Related Disorders Association (NINCDS-ADRDA)[12]. These subjects were recruited as part of an earlier study on [11C]-PIB uptake and [18F]-FDG retention in sporadic AD[3]. Thirteen HC were also recruited as part of this earlier study. They underwent clinical and neuropsychological assessments to ensure that there were no underlying neurological illnesses. Not all sporadic AD and HC subjects had both [18F]-FDG and [11C]-PIB scans, meaning 8 subjects were recruited into each scan group. See table 4.2 for a summary of the clinical details of all cohorts.

4.3.3 Neuropsychological assessment

During the study period, 5 of the 8 PCA subjects completed Neuropsychological assessments. This was performed by a psychologist at Charing-Cross Hospital, London, UK. They underwent a battery of neuropsychological tests that included; Mini Mental State Examination[13], test of attention (digit span), episodic memory (story recall), visual perception (fragmented letters), construction (block design), verbal reasoning (similarities), reading (WTAR)[14], visual naming (GNT)[15] and Rey figure.

Neuropsychological profile for all of the HC and AD patients, were also obtained and have been described previously[3].

4.3.4 MRI image acquisition

All subjects underwent volumetric T1 and T2-weighted MRI for the identification of any underlying structural lesions and for the subjective quantification of cerebro-vascular disease. All scans were reviewed by a consultant neuro-radiologist. Volumetric T1 weighted images were also coregistered to PET images for the generation of subject specific atlases. All PCA subjects were scanned using a 3T Philips scanner while sporadic AD and HC subjects were scanned using a 1.5T GE scanner.

4.3.5 PET image acquisition

All subjects were scanned using a Siemens ECAT 962 EXACT HR+ scanner which has an axial view of 15.5 cm. Prior to scanning, intravenous access was secured in the antecubital fossa of each subject. A 10 minute transmission scan was acquired before the emission study, using a single rotating photon point source of 137Cs, for subsequent attenuation and scatter correction. The PET data were acquired in 3-dimensional mode. Data were reconstructed using filtered back projection to produce images containing 63 contiguous slices, separated by 2.42mm, of 128x128 pixels 2.092mm square. Reconstruction of emission data was carried out using filtered back projection. The 3D emission data were Fourier-rebinned into 2D data sets to increase the speed of reconstruction. The reconstructed images consisted of sixty-three transaxial image planes were displayed as 2.46-mm slices with a reconstructed axial resolution of 5.4 mm and a transaxial resolution of 5.6 mm.

[11C]-PIB scans

Following the transmission scan and 30 seconds after the start of the emission scan, all subjects received 371.9±31.1MBq [11C]-PIB injected IV. This was followed by a 90 minute

dynamic emission scan consisting of 32 different time frames. [11C]-PIB was manufactured by Hammersmith Imanet, GE Healthcare at the Cyclotron Building, Hammersmith Hospital.

[18F]-FDG scans

To ensure standardized [18F]-FDG uptake, subjects were asked to fast for 4 hours before scanning. An arterial line was inserted into the radial artery at the level of the wrist to enable arterial blood sampling to be performed during the emission scan. This enabled spectral analysis to be preformed. At the start of the scan a bolus injection of 188.7±6.9MBq of [18F]-FDG was injected 30 seconds after the start of the emission scan. A 60-minute dynamic emission scan was then acquired using predefined protocol consisting of 28 time frames. Continuous online sampling was performed for 15 minutes and then discrete blood samples were taken at baseline, 5, 10, 15, 20, 30, 40, 50, and 60 minutes. A hematocrit was estimated from the baseline blood sample and plasma glucose levels were measured on selected samples.

4.3.6 Image analysis

All image processing were performed using Analyze (Mayo Clinic, MN) and SPM2 (Wellcome Department of Imaging Neuroscience, University College London, UK) running in MATLAB 5 (R12, Mathworks, Natick, MA). In this study two forms of PET data analysis were undertaken. Firstly region of interest analysis was done and followed secondly by exploratory statistical parametric mapping analysis. Reference should be made to section 1.4 for flow diagrams outlining these methods.

[11C]-PIB PET – Region of Interest

Time frames corresponding to 10-90 minute (early and late) and 60-90 minute (late) summation images were created for each [11C]-PIB scan. Each subject MRI was then coregistered to its corresponding early PET scan and segmented into grey matter, white matter and cerebrospinal fluid (CSF). An in house atlas[16] was then normalized and convolved with the grey matter segment. Individualized cortical grey matter regions were thus defined and applied onto its corresponding late [11C]-PIB scan. The late (60 – 90 minute) scan reference region RATIO approach was used because it provides a robust measure of total: nonspecific PIB relative volumes of distribution in target brain regions without the need for arterial sampling. The cerebellum was chosen as a reference region in the analysis as it has been found to contain only amorphous amyloid plaques that are not detected with thioflavin or Congo red. Cerebellar [11C]-PIB uptake is thus thought to represent baseline, background retention and radioactivity. Using Analyze software, cerebellar [11C]-PIB activity was sampled and the late summation images were normalised to the mean cerebellar cortical uptake value over this 60-90 minute period, generating the late target:cerebellar RATIO image. Cortical RATIO values for frontal, temporal, parietal, occipital lobes and the whole brain were sampled.

[18F]-FDG – Region of Interest

Parametric maps of absolute regional cerebral glucose retention (rCMRGlc) were generated with spectral analysis using an arterial input function as previously described[3]. PET time frames 24 to 28 were summated and the corresponding subject MRI coregistered to the resultant PET add image. White matter has only low metabolism and so only grey matter MRI map was considered for analysis. Grey matter maps were generated by first normalizing the in house atlas to the coregistered whole MRI and followed by multiplication with the grey

matter MRI segment. Cortical frontal, temporal, parietal, occipital lobes and the whole brain were sampled.

4.3.7 Statistical Analysis

Statistical analyses were performed using SPSS for Windows version 16 (SPSS, Chicago, IL). Between groups regional differences were analysed using Mann-Whitney U nonparametric test statistical level set at $p < 0.05$.

4.3.8 Statistical Parametric Mapping (SPM)

Between group comparisons of PET scans were done. We used SPM to interrogate groups of scans. PET images of each group (PCA, AD and HC) were compared statistically producing a map of voxel clusters of significantly increased or decreased tracer uptake.

Using SPM2 [11C]-PIB target:cerebellar ratio images and parametric rCMRGlc images were normalized to the Montreal Neurological Institute (MNI) template provided with SPM2. Normalized scans, were then spatially smoothed using a 10 x 10 x 10 mm (full-width at half maximum) isotropic Gaussian kernel. This spatial filter attempts to accommodate for inter-subject anatomic variability and improves signal to noise for statistical analysis.

SPM comparisons were then performed using appropriately weighted contrasts to localize significant increases or decreases in mean voxel uptake values in patients. The contrasts were used to derive Z scores on a voxel basis using the general linear model[17].

Comparisons between HC, sporadic AD and PCA groups with [11C]-PIB target:cerebellar RATIO images and parametric rCMRGlc uptake were performed using a threshold of $p < 0.001$ with a cluster extent threshold of 50 voxels per cluster.

Global binding potential normalization was omitted allowing a pattern of tracer uptake to be revealed. Any resulting cluster with a corrected p value (cluster level) of <0.05 was considered significant. Voxels showing significant results were overlaid onto the T1 MRI template image provided by SPM.

Ethical approval for this study was obtained from the Ethics Committees of Hammersmith and Queen Charlotte's Hospitals, while permission to administer radiotracers was obtained from the Administration of Radioactive Substances Advisory Committee (ARSAC) UK. Informed written consent was obtained from all participating subjects.

4.4 Results

4.4.1 Subjects

A total of 8 PCA subjects were recruited into the study. All completed MRI, [11C]-PIB and [18F]-FDG PET scans while complete neuropsychological assessments were completed in 5 subjects. Twelve sporadic AD subjects were investigated. MRI scanning and neuropsychology was completed on all 12, 9 completed [11C]-PIB scans and 8 completed [18F]-FDG scans. Thirteen HC were investigated. Again, all completed neuropsychology and MRI scanning but 9 completed [11C]-PIB scans and 8 completed [18F]-FDG scans.

All cohorts were however similarly matched for age and for the PCA and sporadic AD groups disease duration and years of education.

4.4.2 PET analysis

4.4.2.1 [11C]-PIB

ROI analysis of [11C]-PIB data

Cortical [11C]-PIB binding was significantly higher in the frontal, parietal, temporal and occipital cortex in both the sporadic AD and PCA groups compared with HC ($P < 0.01$). Higher uptake was also seen in the anterior and posterior cingulate and in the subcortical regions thalamus and striatum ($P<0.01$). The PCA [11C]-PIB binding pattern was similar to Alzheimer disease in all cortical and subcortical regions compared with sporadic AD patients. Interestingly [11C]-PIB binding in the occipital cortex was similar between the PCA and sporadic AD group ($P = 0.114$).

SPM analysis of [11C]-PIB data

Four comparisons were undertaken: sporadic AD>HC, PCA>HC, PCA<sporadic AD and sporadic AD<PCA.

Sporadic AD>HC and PCA>HC

In both comparisons it was expected that there would be increased [11C]-PIB retention in dementia groups. Of interest the pattern retention was similar in both sporadic AD and PCA. Affected areas included the cortical frontal, temporal, parietal lobes and the anterior and posterior cingulate. In both sporadic AD and PCA groups the occipital lobes were largely

unaffected when compared to HC group.

PCA<sporadic AD and sporadic AD<PCA

The posterior cerebral dysfunction typical in PCA subjects would suggest a higher tendency to involve the posterior parts of the brain. Despite this [11C]-PIB Z scores were greater in sporadic AD than PCA. No significant voxel clusters were identified when [11C]-PIB uptake was compared between PCA and sporadic AD groups.

4.4.2.2 [18F]-FDG

ROI analysis of [18F]-FDG retention

Cortical [18F]-FDG retention was reduced in the frontal, parietal and temporal lobes and in the posterior cingulate in sporadic AD groups compared with HC ($P < 0.05$). Decreases in [18F]-FDG uptake were also widespread in the PCA group when compared to HC. In the cortex of the temporal, parietal and occipital lobes changes were highly significant (P=0.001) while retention in the frontal cortex and thalamus was also significantly decreased (P=0.012 and P=0.005 respectfully).

These differences in [18F]-FDG retention, were further demonstrated by comparing the PCA group with sporadic AD. Here the temporal and occipital lobe retention were relatively lower in the PCA group (P=0.027 and P=0.036 respectively).

SPM analysis of [18F]-FDG

Four comparisons were again undertaken: sporadic AD<HC, PCA<HC, PCA<sporadic AD

and sporadic AD<PCA.

Sporadic AD<HC and PCA<HC

Significant voxel clusters of decreased cortical [18F]-FDG retention were seen in the posterior parietal lobe and the temporal lobe when sporadic AD was compared to HC. A similar pattern of hypometabolism as compared to [11C]-PIB was expected but not found when PCA was compared to HC.

PCA<sporadic AD and sporadic AD<PCA

Areas of relatively decreased [18F]-FDG retention were identified in the cortical posterior parietal and occipital lobes for the comparison PCA<sporadic AD. Of interest, the right hemisphere appeared to be involved to a greater extent than the left. No significant voxel clusters were identified for the comparison sporadic AD<PCA.

Figures 4.1, 4.2 and 4.3 summarises these results.

4.4.3 MRI

All PCA patients showed regional posterior cerebral cortical atrophy. Sporadic AD subjects demonstrated the typical distribution of atrophy involving the cortices of all lobes. Control MRI's were normal.

4.4.4 Neuropsychological assessment

Neuropsychological assessment on 5 PCA patients is summarised on table 4.2. As expected in PCA subjects, tasks involving visual input were severely affected with the relative preservation of episodic and working memory, figure 4.4.

4.5 Discussion

4.5.1 [11C]-PIB binding is similar in PCA and sporadic AD.

PCA is a rare progressive neurodegenerative disorder characterized by neurofibrillary tangle and amyloid plaque deposition. Results support the view that PCA is an AD variant as no differences were identified in regional amyloid deposition when compared to sporadic AD. *In vivo* amyloid deposition thus appears to be similar in PCA and sporadic AD, a finding also demonstrated in a recent series of 15 PCA patients imaged with PIB[8]. These results are also supported by PM studies demonstrating an AD pattern of amyloid plaques deposition in PCA[1]. This pattern of amyloid deposition is however by no means a consistent finding. Smaller studies, consisting mostly of case reports, have demonstrated and increased posterior parietal or occipital lobe PIB uptake. These studies were, however, weakly powered.

The presence of marked posterior parietal and occipital atrophy, however, may have influenced the quantitation of PET results. The apparent lack of occipital PIB binding might be related to the extent of posterior cerebral atrophy found in PCA subjects. During the analysis process the normalization of images onto standardised brains can also result in the warping of subject scans in areas of focal atrophy. The result can be a further dilution of the PIB signal with the production of spurious results. We have however attempted to minimise this complication by not modifying raw PET data during ROI analysis. Rather individualized

subject atlases were created by normalizing the standard atlas onto the subjects MRI scan. Regions were thus defined in a reliable manner.

4.5.2 [18]-FDG uptake was significantly reduced posteriorly in PCA subjects.

Defects in metabolism were expected to be seen in both PCA and sporadic AD. On ROI analysis sporadic AD had reduced metabolism in all cortical regions except for the occipital lobe. The sparing of this can be expected with the late involvement of visual deficits in sporadic AD.

PCA subjects had an overall lower binding of [18]-FDG compared to sporadic AD subjects, although this difference was not significant. This likely reflects the greater clinical severity of PCA with its occurrence in a younger age group and a more aggressive progression that sporadic AD. Hypometabolism affected all cortical regions in the PCA group. The involvement of the occipital lobe can be expected given the early visual impairment described by subjects. Of interest however is the demonstration of hypometabolism in the thalamus of PCA subjects. The involvement of the subcortical regions has not been previously described in PCA and may represent the more rapid progression of the disease process in the cohort we have examined.

4.5.3 Posterior metabolism, significantly lower in PCA than sporadic AD.

Given the clinical features, it is not surprising to identify posterior hypometabolism in PCA. However the discordance between amyloid fibrillar deposition (as identified by [11C]-PIB uptake) and reduced FDG uptake is of interest. It would suggest that fibrial amyloid may not directly be related to neuronal damage and demise. Attempts in sporadic AD and MCI have

also been made to link cognitive impairment and PIB uptake. There however does not appear to be a direct link between these two factors.

Therein lies the possibility that other neurotoxins are at play in sporadic AD and PCA. Possibilities include the hyperphosphorylated tau proteins and amyloid precursor protein monomer and oligomers. Tau proteins are responsible for the neurofibrillar tangles seem in sporadic AD. Their deposition supersedes plaque amyloid along with amyloid oligomers correlates to cognitive decline[18]. Postmortum staining in PCA and sporadic AD shows similar distribution of tau in these cases but longitudinal studies are lacking[1]. The amyloid oligermers are a collection of soluble proteins found in the CSF of sporadic AD subjects. They have neurotoxic properties and are thought to be equilibrium with fibrillar amyloid. After an uncertain "lag" period there is aggregation of amyloid oligomers to from proto-fibrils and filaments. Unstained by PIB, their presence has yet not been demonstrated in PCA, but given the presence of fibrillar amyloid in would seem likely that they play as important a role as in sporadic AD.

The data suggests a similar pathological process taking place in both sporadic AD and PCA. Despite this the visual disturbance experienced by PCA subjects would suggest greater susceptibility of this system to the toxic cerebral environment proposed to be present with Alzheimer's pathology. In sporadic AD a metabolically demanding default mode network is thought to be affected early in the course of AD. The result is cortical dysfunction affecting the posterior parietal areas impairing temporo-parietal systems responsible for memory retrieval. In subjects with PCA, it may be that the parieto-occipital or temporo-occipital networks are more prone to damage and are hence affected early on before the dysfunction of the default system is seen. The results demonstrate impairment of the visual system clinically manifested by Balint's syndrome and prosopagnosia.

This study does have limitations. All PCA scans showed posterior cortical atrophy. I however, did not apply an atrophy correction. This can potentially be identified as major short coming but the usefulness of atrophy correction is however a matter of debate. The presence of atrophy results in a partial volume effect where radioactive uptake appears falsely reduced[19]. It relates to the low resolution of PET imaging where are point source of radioactivity appears in the image as a 3D Gaussian distribution. This blurring effect is the partial-volume effect (PVE) or alternatively called intensity diffusion. PVE biases measurements, e.g. reducing apparent uptake levels in areas of high-uptake and increases apparent uptake levels in areas of low-uptake. Techniques have been used to correct for this blurring mathematically but findings suggest that correct for this effect only becomes necessary at for lesions smaller that FWHM x 3 and at low radioactivity[20].

For [11C]-PIB, the expansion of the posterior regions may artificially boost the signal producing erroneous results. This approach may have resulted in findings reported in other studies were [11C]-PIB uptake was higher in PCA than AD. The opposite would be true for [18F]-FDG. The atrophy may have resulted in the significant reductions in occipital FDG uptake described in PCA compared to AD. The boost in signal that results from the application of atrophy correction may result in the loss of these signal changes. The convolution of images can introduce a significant level of noise into images. A recent study comparing AD to PCA also utilized atophy correction but this did not produce any changes to results[8].

Another limitation of this study can however be considered to be the sample size. The inclusion of 8 subjects prevented potentially useful correlations between clinical features and PET finding to be done effectively. An increase in the sample size would also strengthen the power of the study. However, maintaining strict inclusion / exclusion criteria allowed me to be

confident that the subjects included suffered from PCA and conditions with a similar phenotype.

4.6 Conclusion

This study supports PCA as a variant of AD with a similar pattern of amyloid deposition. The difference in symptomology may however be explained by the greater reduction posteriorly of cerebral metabolism in PCA. The cause of this selective targeting of this part of the brain remains unclear but the responsible neurotoxin is also likely to play a role in sporadic AD. There is increasing evidence pointing towards hyperphosphorylated tau and non-fibrillar, soluble amyloid and the development of in-vivo biomarkers for these compounds may prove invaluable in investigating neuro-degeneration.

4.7 Tables

Table 4.1. Demographic profile of all subjects investigated. PCA=Posterior Cortical Atrophy; AD= Alzheimer's Disease; HC= Healthy Controls; MMSE=Mini-Mental State Examination; SD=standard deviation; PIB=Pittsburgh compound B, M = male, F = female.

	PCA total	**AD total**	**Healthy Controls**
Total No	8	12	13
Sex	3M / 5F	7M/ 5F	9M/4F
Age (yrs ± SD)	60.0 ± 3.9	63.5 ± 6.5	64.8 ± 6.6
MMSE (mean ± SD)	19.2 ± 7.2	19.6 ± 4.08	29.6 ± 0.8

Table 4.2. Neuropsychological assessment results in the group of PCA patients.- =Not Impaired, ~=Borderline, + = Mildly Impaired, ++ = Moderately Impaired, +++ = Severely impaired

	MMSE	Visual Naming (GNT)	Reading (WTAR)	Verbal Reasoning (Similarities)	Construction (Block Design)	Visual Perception (Frag. Letters)	Episodic memory (Log Mem-Del)	Working Memory (Digit Span)
Pt1	13	+++	+++	-	+++	+++	~	~
Pt2	14	+++	+++	-	++	+++	+++	~
Pt3	27	-	+++	-	++	+++	-	-
Pt4	27	+++	+++	-	++	+++	-	-
Pt5	15	+++	+++	-	++	+++	~-	++

4.8 Figures

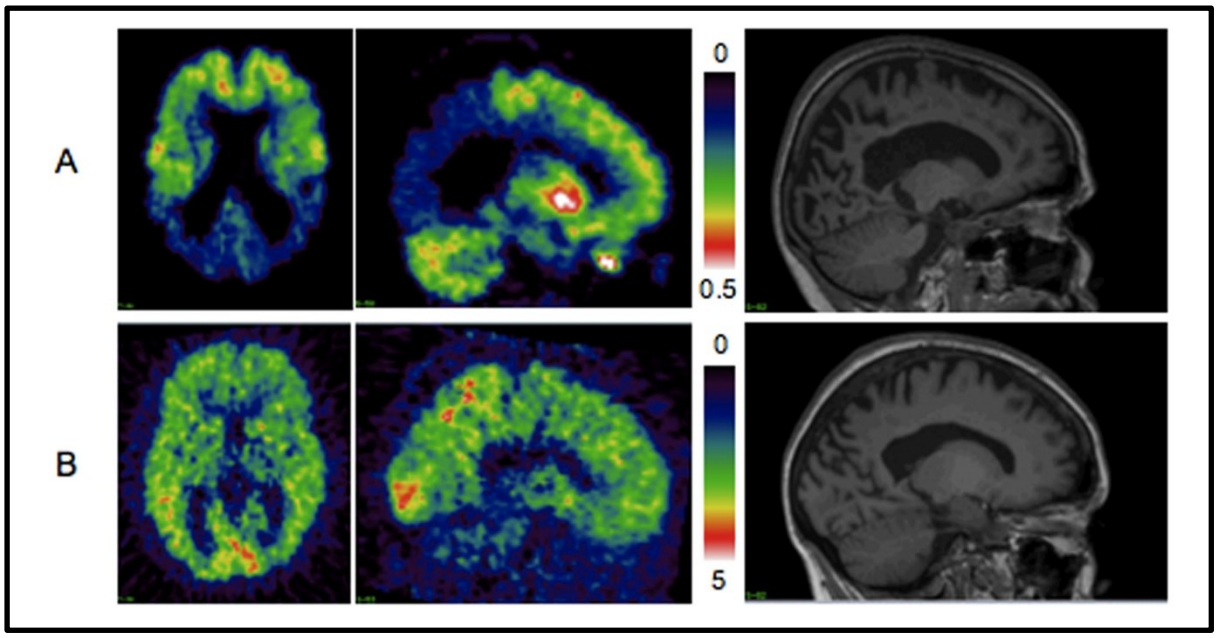


Figure 4.1. A – [18F]-FDG parametric rCMRGlc image on a PCA patient 1 (Pt1), transverse and sagital views (left and middle), showed intense posterior hypometabolism, in occipital and temporo-parietal areas. B – [11C]-PIB-cerebellum ratio image on a PCA patient 3 (Pt3), transverse and sagital views (left and middle), showed posterior deposits, principally parietal and occipital areas. Both patients showed regional parietal cortical atrophy; more marked in case A (top right) than B (bottom right).

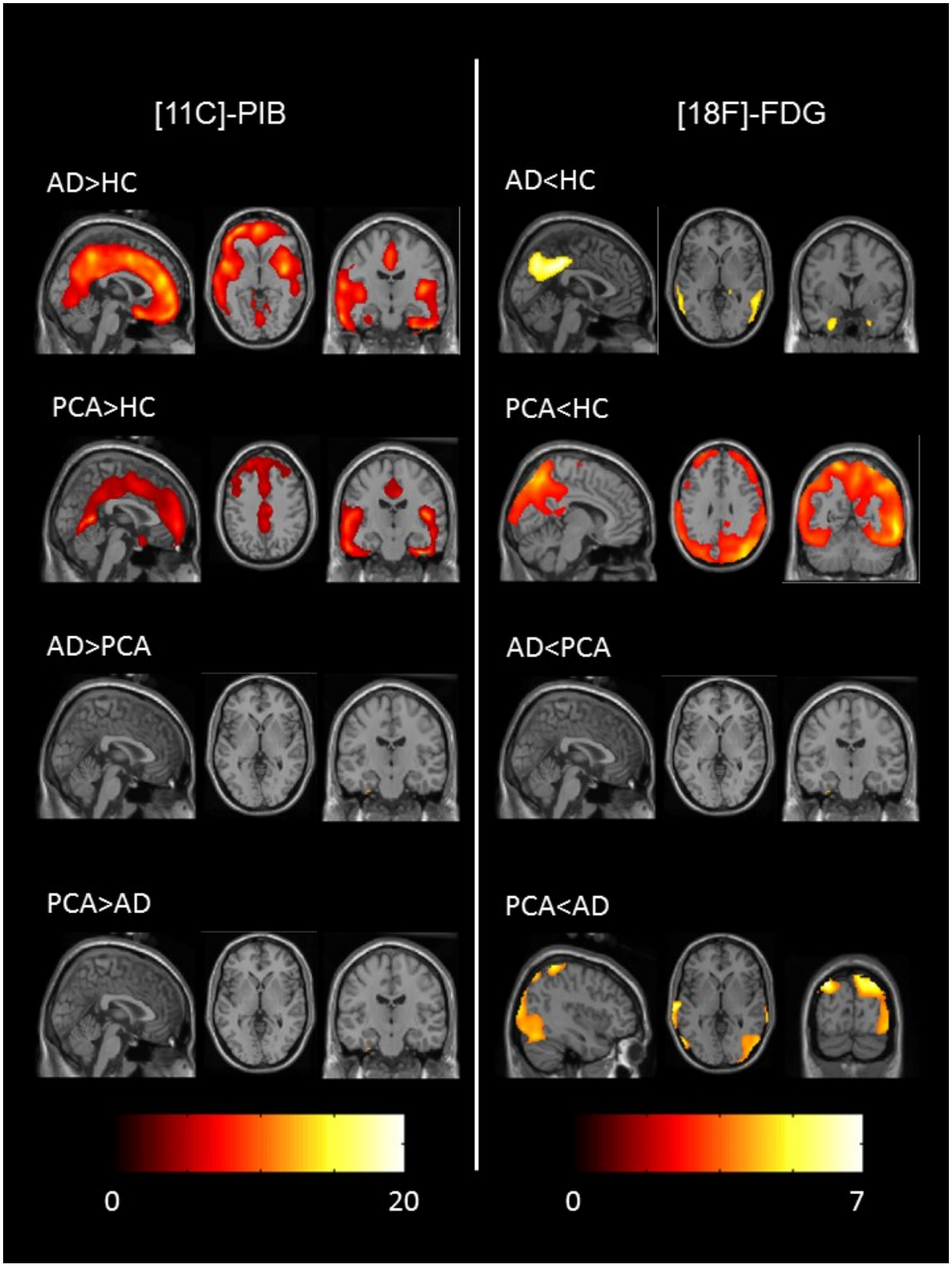


Figure 4.2. SPM t score results comparing PCA, sporadic AD and HC groups. [11]C-PIB results were similar in the PCA and sporadic AD groups. However a clear posterior tendency exists in [18]F-FDG in the PCA group when compared to both HC and sporadic AD.

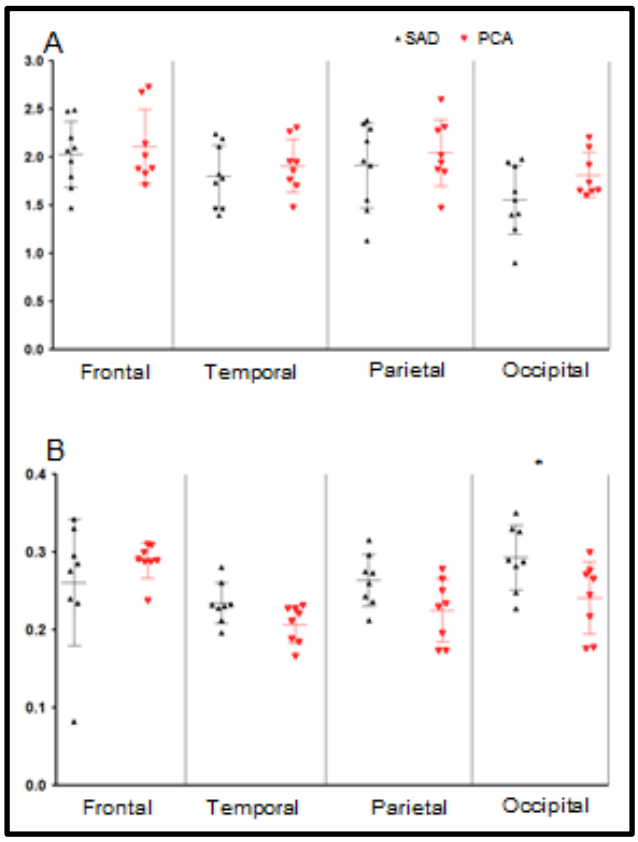


Figure 4.3. Graphic representation of [11C]-PIB (A) and [18F]-FDG (B) results in Sporadic Alzheimer's Disease (sporadic AD) and Posterior Cortical Atrophy (PCA). In both cases there is a tendency for greater posterior cerebral involvement in PCA but only occipital [18F]-FDG retention is significantly different. (* $p<0.05$).

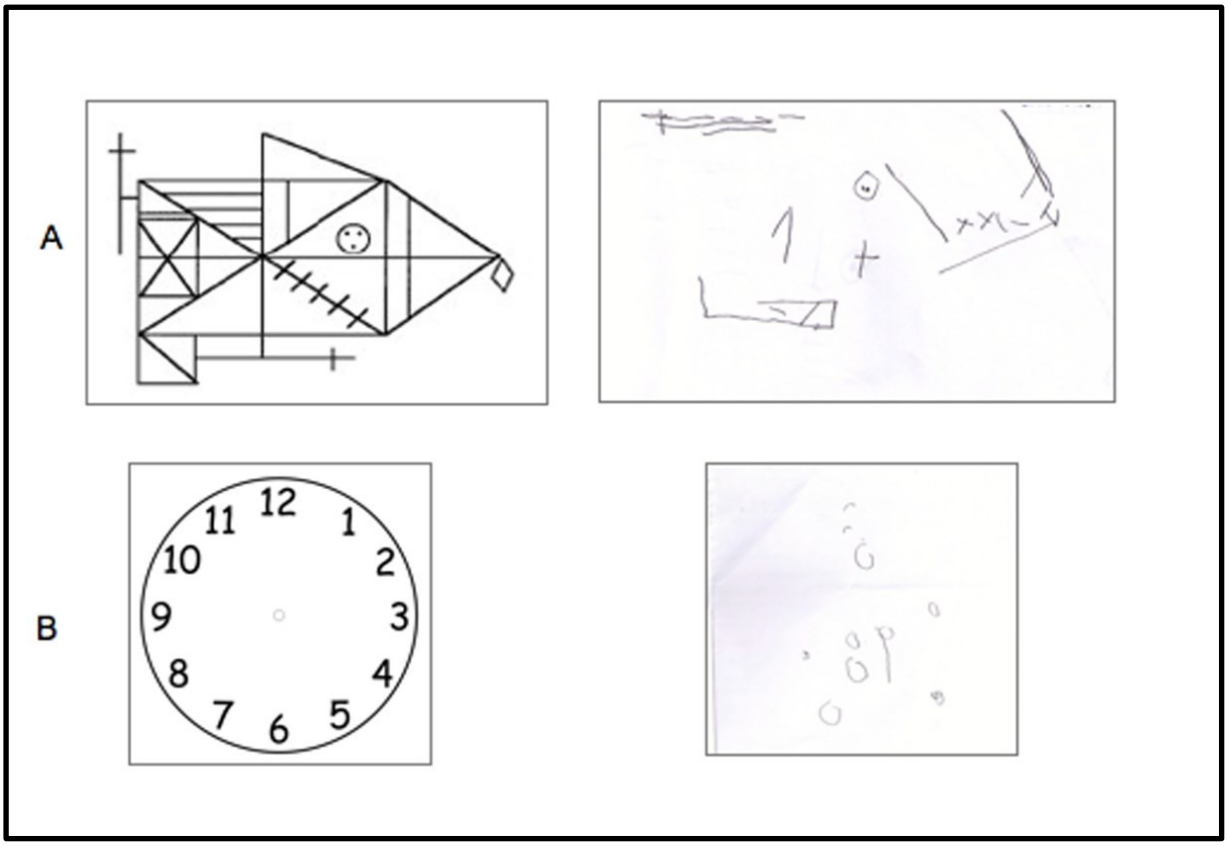


Figure 4.4**.** Profound impairment of visual spatial perception in PCA patients. **A.** Copy drawing of a Rey Osterreith complex figure of patient 3 (Pt3) **B.** Free drawing of a clock face of patient 1 (Pt1).

4.9 References

1. Tang-Wai DF, Graff-Radford NR, Boeve BF, Dickson DW, Parisi JE, Crook R, Caselli RJ, Knopman DS, Petersen RC. Clinical, genetic, and neuropathologic characteristics of posterior cortical atrophy. Neurology. 2004 Oct 12;63(7):1168-74

2. Klunk WE, Engler H, Nordberg A, Wang Y, Blomqvist G, Holt DP, et al. Imaging brain amyloid in Alzheimer's disease with Pittsburgh Compound-B. Ann Neurol. 2004 Mar;55(3):306-19.

3. Edison P, Archer HA, Hinz R, Hammers A, Pavese N, Tai YF, Hotton G, Cutler D, Fox N, Kennedy A, Rossor M, Brooks DJ. Amyloid, hypometabolism, and cognition in Alzheimer disease: an [11C]PIB and [18F]FDG PET study. Neurology. 2007 Feb 13;68(7):501-8.

4. Yu AS, Lin HD, Huang SC, Phelps ME, Wu HM. Quantification of cerebral glucose metabolic rate in mice using 18F-FDG and small-animal PET. J Nucl Med. 2009 Jun;50(6):966-73.

5. Herholz, K., Carter, S.F., Jones, M., 2007. Positron emission tomography imaging in dementia. Br J Radiol, 80, S160–7.

6. Formaglio M, Costes N, Seguin J, Tholance Y, Le Bars D, Roullet-Solignac I, Mercier B, Krolak-Salmon P, Vighetto A. In vivo demonstration of amyloid burden in posterior cortical atrophy: a case series with PET and CSF findings. J Neurol. 2011 Apr 10.

7. Bokde AL, Pietrini P, Ibáñez V, Furey ML, Alexander GE, Graff-Radford NR, Rapoport SI, Schapiro MB, Horwitz B. The effect of brain atrophy on cerebral hypometabolism in the visual variant of Alzheimer disease. Arch Neurol. 2001 Mar;58(3):480-6.

8. Rosenbloom MH, Alkalay A, Agarwal N, Baker SL, O'Neil JP, Janabi M, Yen IV, Growdon M, Jang J, Madison C, Mormino EC, Rosen HJ, Gorno-Tempini ML, Weiner MW, Miller BL, Jagust WJ, Rabinovici GD. Distinct clinical and metabolic deficits in PCA and AD are not related to amyloid distribution. Neurology. 2011 May 24;76(21):1789-96.

9. Nestor PJ, Caine D, Fryer TD, Clarke J, Hodges JR. The topography of metabolic deficits in posterior cortical atrophy (the visual variant of Alzheimer's disease) with FDG-PET. J Neurol Neurosurg Psychiatry. 2003 Nov;74(11):1521-9.

10. Schmidtke K, Hüll M, Talazko J. Posterior cortical atrophy: variant of Alzheimer's disease? A case series with PET findings. J Neurol. 2005 Jan;252(1):27-35.

11. Wahlund LO, Barkhof F, Fazekas F, Bronge L, Augustin M, Sjögren M, et al. A new rating scale for age-related white matter changes applicable to MRI and CT. Stroke. 2001 Jun;32(6):1318-22.

12. McKhann, G., Drachman, D., Folstein, M., Katzman, R., Price, D. & Stadlan, E. M., 1984. Clinical diagnosis of Alzheimer's disease: report of the NINCDS-ADRDA Work Group under the auspices of Department of Health and Human Services Task Force on Alzheimer's Disease. Neurology, 34 (7), 939-944.

13. Folstein, M.F., Folstein, S.E., McHugh, P.R., 1975. ‘‘Mini-mental state’’. A practical method for grading the mental state of patients for the clinician. J Psychiatr Res, 12, 189–98.

14. Wechsler, D., 2001. Wechsler Test of Adult Reading (WTAR) San Antonio, TX: The Psycological Corporation.

15. McKenna P, Warrington EK. Testing for nominal dysphasia. J Neurol Neurosurg Psychiatry. 1980 Sep;43(9):781-8.

16. Hammers, A., Allom, R., Koepp, M. J., Free, S. L., Myers, R., Lemieux, L., Mitchell, T. N., Brooks, D. J. & Duncan, J. S., 2003. Three-dimensional maximum probability atlas of the human brain, with particular reference to the temporal lobe. Human Brain Mapping, 19 (4), 224-247.

17. Friston KJ, Holmes AP, Worsley KJ, Poline JB, Frith CD, Frackowiak RS Statistical parametric maps in functional imaging: a general linear approach. Hum Brain Mapp. 1995;2:189–210.

18. Vana L, Kanaan NM, Ugwu IC, Wuu J, Mufson EJ, Binder LI. Progression of tau pathology in cholinergic Basal forebrain neurons in mild cognitive impairment and Alzheimer's disease. Am J Pathol. 2011 Nov;179(5):2533-50.

19. Coello C, Willoch F, Selnes P, Gjerstad L, Fladby T, Skretting A. Correction of partial volume effect in (18)F-FDG PET brain studies using coregistered MR volumes: voxel based analysis of tracer uptake in the white matter. Neuroimage. 2013 May 15;72:183-92.

20. Sakaguchi Y, Mizoguchi N, Mitsumoto T, Mitsumoto K, Himuro K, Ohya N, Kaneko K, Baba S, Abe K, Onizuka Y, Sasaki M. A simple table lookup method for PET/CT partial volume correction using a point-spread function in diagnosing lymph node metastasis. Ann Nucl Med. 2010 Oct;24(8):585-91.

Chapter 5

[11]C-PIB PET does not detect PrP-amyloid in prion disease patients

5.1 [11]C-PIB PET does not detect PrP-amyloid in prion disease patients

In this chapter I will be turning my attention to an aggressive neurodegenerative condition. Prion diseases are typified by spongiform encephalopathy and the deposition of prion protein aggregates. Thus far, there is no *in vivo* biomarker for prion protein. This chapter focuses on the usefulness of [11C]-PIB to bind to this protein aggregate.

Summary of Objectives

Although PrP-amyloid and the amyloid β plaques found in Alzheimer's disease are composed of different peptides, they share common physico-chemical properties. [11C]-PIB has a well-established role as a marker of fibrillar β amyloid plaque deposition. In this study its usefulness as a reliable biomarker for the presence of abnormal PrP-amyloid deposition in human prion diseases including a patient with variant Creutzfeldt-Jakob disease (vCJD).

Five patients at risk of, or affected by, prion disease underwent [11C]-PIB PET studies including one patient with vCJD who had a post-mortem examination 6 months following imaging. Parametric maps of [11C]-PIB retention in tissue were generated using a spectral analysis with a plasma input function using data collected 60-90 minutes after injection. Regional brain distributions were compared to those of healthy controls.

Summary of results

There was no cortical, cerebellar or subcortical [11C]-PIB retention in any of the prion subjects (including the vCJD patient, despite the high density of cortical PrP-amyloid plaques subsequently seen at post-mortem) when compared to health controls. Non-specific [11C]-

PIB binding was seen in the white matter consistent with the pattern of binding seen in healthy controls.

Despite using a sensitive analytical method for detecting amyloid *in vivo* and selecting patients likely to have PrP deposition in the form of amyloid plaques, [11C]-PIB was unable to detect PrP-amyloid *in vivo* in a series of patients with different forms of prion disease.

5.2 Introduction

Prion diseases are fatal neurodegenerative disorders associated with the misfolding of prion protein (PrP)[1]. Abnormally aggregated PrP accumulates in the brain as plaques or fibrillar deposits which may have the biophysical properties of amyloid. The neuropathology of the prion diseases is highly variable, but certain sub-types, particularly Gerstmann-Sträussler-Scheinker syndrome and variant Creutzfeldt-Jakob disease (vCJD) are associated with large PrP-amyloid plaques. Currently there are no treatments for prion disorders that slow or halt the underlying disease process [2]. The evaluation of putative therapeutics would benefit considerably from a non-invasive biomarker which directly measures the load of abnormal PrP in the brain.

Although PrP-amyloid and the amyloid β plaques found in Alzheimer's disease are composed of different peptides, they share common physico-chemical properties [3], including a high β-sheet secondary structure and the binding of thioflavins. As amyloid β load can be measured in patients with Alzheimer's disease by use of PET and the thioflavin radiotracer [11C]-PIB[4;5], it maybe that [11C]-PIB PET also proves to be an in-vivo marker of PrP-amyloid. Here I will evaluate a range of patients who are affected by, or at risk of, human prion disease to determine if [11C]-PIB PET can reliably demonstrate the presence of abnormal PrP-amyloid deposition. This would be of potential clinical importance in the early diagnosis of these diseases and in identifying asymptomatic patients who might benefit from proposed therapeutic interventions, and in monitoring treatment efficacy.

5.3 Methods

Ethical approval for the study was granted by the Research Ethics Committee of the National Hospital for Neurology and Neurosurgery and written informed consent for participation in

the study was obtained from subjects. Exclusion criteria included pregnancy, contraindication to MRI, history of cancer within the last 5 years (except skin and prostate), and patients who were unable to give valid informed consent.

5.3.1 Subjects

One patient with vCJD (PrD1, codon 129MM), 2 symptomatic patients with the P102L mutation (PrD2, codon 129MM; PrD3 codon 129MM) and 2 asymptomatic *PRNP* mutation carriers (PrD4, P102L, codon 129MM; PrD5, E200K, codon 129MM) (patient demographics in Table 5.1) were recruited into the study. Fifty per cent of mutation carriers are expected to be symptomatic by age 60 and 80% by age 80 years[6]. All subjects were referred to the National Prion Clinic, National Hospital for Neurology and Neurosurgery, London, U.K. and underwent a structured neurological assessment with mini-mental state examination at the time of the MRI study.

Ten control subjects were also investigated. Their ages ranged from 55-75 years and group consisted of 6 males and 4 females. They were recruited as part of a previous study investigating [11C]-PIB uptake in sporadic Alzheimer's disease[7].

5.3.2 MRI image acquisition

All subjects underwent MRI examination using a GE Signa LX 1.5T MRI system (GE Healthcare, Milwaukee, WI) at the National Hospital for Neurology and Neurosurgery within 1 month of the PET study. After scout images were obtained, 3-dimensional T1W image data were acquired from 124 contiguous 1.5mm thick coronal slices (inversion-recovery

prepared spoiled gradient-echo sequence; TE 5ms, TR 35ms, flip angle 35º, matrix 256x128, FOV 24x24cm).

5.3.3 PET image acquisition

PET studies were performed on an ECAT 962 EXACT HR+ scanner (Siemens, Erlangen, Germany) at the Clinical Sciences Centre, Hammersmith Hospital, Imperial College London, U.K. Following a 10 minute attenuation scan, a bolus administration of up to 370MBq of [11C]-PIB (specific activity ≥10 GBq/μmol at injection) was given intravenously over 30 seconds. Images were obtained in 32 frames over 90 minutes with dynamic acquisition frames as follows: 1 x 30 s, 1 x 15 s, 1 x 5 s, 1 x 10 s, 2 x 30 s, 9 x 60 s, 3 x 180 s, 14 x 300 s.

Arterial cannulation was performed in each patient under local anaesthetic, to allow for continuous and rapid blood sampling in order to quantitate regional cerebral [11C]-PIB uptake. Blood was initially withdrawn every 5 minutes for the first 15 minutes after injection of [11C]-PIB and then at 10 minute intervals until 90 minutes. A total of 175mls of blood was collected per scan.

5.3.4 PET image analysis

Parametric maps of [11C]-PIB retention in tissue were generated using a plasma input function and spectral analysis with data from 60-90 minutes after injection[7]. [11C]-PIB images were co-registered to each patient's MRI, which was normalized into standard stereotactic space (Montreal Neurological Institute, Quebec, Canada). A probabilistic brain atlas was used to create a standard template of regions of interest for sampling segmented

grey matter regions [8]. For analysis, six predefined cortical regions of interest were included: anterior cingulate, posterior cingulate, thalamus, striatum, frontal, temporal, parietal, occipital cortices and cerebellum.

5.3.5 Statistical analysis

Statistical analysis of ROI data was performed using SPSS for Windows version 14 (SPSS, Chicago, Illinois, USA). Student t-tests were performed to assess differences between prion disease patients and healthy controls.

5.4 Results

The vCJD patient (PrD1) demonstrated signal abnormality in the dorso-medial thalamus bilaterally (pulvinar sign) on MRI at the time of [11C]-PIB PET study. The patient died approximately 7 months later and the post-mortem revealed neuronal loss, spongiform degeneration and gliosis with extensive PrP plaque formation in the frontal and occipital cortices and in the cerebellum consistent with the diagnosis of vCJD (figure 5.1). The MRI studies from the two symptomatic patients with the P102L mutation (PrD2 and PrD3) demonstrated supratentorial volume loss, particularly in the parietal lobes but no pathological signal change. The MRI studies from the 2 asymptomatic patients (PrD4 and PrD5) were normal.

There was no cerebral cortical or subcortical [11C]-PIB retention in any prion subjects. Findings were indistinguishable from normal controls. See table 5.2 and figure 5.2. Non-specific [11C]-PIB binding was seen in the white matter consistent with the pattern of binding seen in normal controls.

5.5 Discussion

In a range of different prion disorders, [11C]-PIB PET was unable to detect PrP-amyloid *in vivo*. This is the largest reported series investigating the efficacy of [11C]-PIB PET as a biomarker in patients with prion disease and the only study to have included a patient with vCJD, where abundant "florid" PrP plaques were subsequently found. I used spectral analysis to brain time activity curves (TACs) of [11C]-PIB uptake to produce parametric images of tracer binding. This method uses a plasma input function to directly compute volumes of distribution rather than using a brain reference area to reflect non-specific binding. This approach was taken as in prion disease pathological changes can be found all brain regions including the cerebellum, the region most commonly used as the reference region in [11C]-PIB analysis. The 75 minute impulse response curve function (IRF) was used to generate the parametric map with spectral analysis. In sporadic AD this approach has previously been shown to be as sensitive for detecting amyloid deposition as Logan and Patlak graphical modelling approaches when a plasma input function is utilised[7].

The PET amyloid marker most extensively used to date is [11C]-PIB which is a neutral analogue of the histological dye thioflavin-T[9]. Although there has been controversy about non-specific tracer binding in central white matter[10], a recent study has shown that the preponderance of cortical PiB binding is to fibrillar plaques immunoreactive to both Aβ42 and Aβ40 and to vascular Aβ deposits. Binding is most robust in compact/cored plaques in the prefrontal and temporal cortices of sporadic AD subjects[5].

[11C]-PIB, also known as BTA-1, has been shown to bind PrP amyloid in tissue slices when mice are infected with prion strains[11]. Methoxy-X04, a congo-red derivative will also label PrP amyloid in human brain samples of prion subjects verified at autopsy[12]. Despite this, the first reports of [11C]-PIB PET in human prion diseases have been disappointing in that tracer

uptake was not significantly different from controls in a patient with the 6-OPRI mutation[13] and 2 patients with sporadic CJD (sCJD)[14]. It is perhaps not surprising that [11C]-PIB was not seen in sCJD where amyloid plaques are an infrequent finding and a diffuse synaptic pattern of PrP immunostaining is usually found[15]. In this study, we were careful to select patients likely to have PrP deposition in the form of amyloid plaques, such as vCJD where abnormal PrP is deposited in the form of rounded amyloid plaques with a dense eosinophilic core and patients with the P102L mutation where large multicentric PrP-amyloid deposits birefringent after congo red staining and strongly fluorescent after thioflavin S treatment are characteristically seen[15].

In the above two studies, [11C]-PIB retention was calculated by using a presumed normal region of interest (cerebellum in the 6-OPRI patient and pons in the sCJD patients) time activity curve as a reference tissue input function. Whilst a cerebellar reference region for non-specific binding may be valid for sporadic AD, in prion disease pathology is usually seen in the molecular layer of the cerebellar cortex. In this study, we ensured maximum discriminative power and reproducibility by using a plasma arterial input function and spectral analysis to generate parametric maps of [11C]-PIB binding. Statistical comparisons were performed using a bank of healthy elderly subjects as controls from a previous study. Whilst it is recognised that amyloid deposition occurs in cognitively normal elderly subjects the reported frequency of this was thought not to be sufficient to bias the control group[16]. Despite these factors, we were unable to demonstrate significant [11C]-PIB retention in patients with prion disease *in vivo*.

The lack of [11C]-PIB retention is unlikely to relate to reduced cortical blood flow in patients with prion disease as the tracer reaches equilibrium between plasma and brain[17]. It is possible that the level of [11C]-PIB binding achieved during PiB-PET studies is insufficient

for adequate detection by PET *in vivo*. 10-30mg/kg of BTA-1 has been used to demonstrate *in vivo* PrP-amyloid in prion infected mice[11] compared to 0.00006-0.0007 mg/kg used in a routine [11C]-PIB PET study in humans. Finally, as binding of [11C]-PIB to PrP-amyloid is reversible it is possible washout occurred over a 90 minute PET study so that the late acquisition scans are not a true reflection of [11C]-PIB retention in prion disease.

In conclusion, observations suggest that [11C]-PIB does not detect PrP-amyloid *in vivo*. Reports of other amyloid agents developed for Alzheimer's disease that can detect PrP-amyloid in patients *in vivo* [18] need further evaluation in larger cohorts with repeat imaging before amyloid biomarkers can be used as end-points in anti-PrP amyloid trials.

5.6 Tables

Table 5.1. Demographics of subjects and controls. MMSE – Mini Mental State Examination

	PrD1	**PrD2**	**PrD3**	**PrD4**	**PrD5**	**Controls (mean±SD)**
Age (years)	25	62	50	39	54	65.3±4.5
Gender	M	F	M	M	M	6M 4F
Codon 129	MM	MM	MM	MM	MM	-
MMSE	25	27	29	30	30	29.9±0.32
Disease duration (months)	3	25	41	-	-	-

Table 5.2. Impulse Response Function 75min [11C]-PIB PET results for patients and controls.

	PrD1	PrD2	PrD3	PrD4	PrD5	Controls (95% prediction limits)
Anterior cingulate	0.000121	0.000119	0.000147	0.000127	0.000173	0.000079–0.000203
Posterior cingulate	0.000103	0.000120	0.000139	0.000109	0.000120	0.000063-0.000211
Thalamus	0.000095	0.000085	0.000112	0.000102	0.000130	0.000065-0.000181
Striatum	0.000116	0.000118	0.000104	0.000116	0.000161	0.000088-0.000188
Frontal lobe	0.000129	0.000117	0.000151	0.000135	0.000163	0.000078-0.000206
Temporal lobe	0.0001	0.000100	0.000131	0.0001	0.000137	0.000078-0.000198
Parietal lobe	0.000114	0.000106	0.000137	0.000114	0.000126	0.000075-0.000207
Occipital lobe	0.000116	0.000112	0.000139	0.000117	0.000153	0.000076-0.000208
Cerebellum	0.000073	0.000087	0.000093	0.000073	0.000113	0.00006-0.000184

5.7 Figures

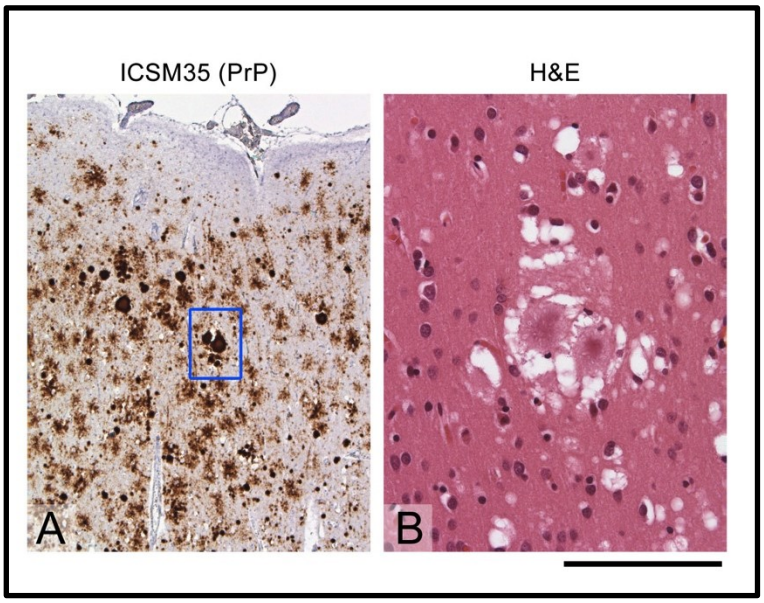


Figure 5.1. Abundant presence of prion protein plaques in the occipital cortex of the patient with vCJD (PrD1). A: A section of the cortex, immunostained for abnormal prion protein with ICSM35, an antibody that reacts with PrP. Note the frequent dense core plaques as well as abundant less compact amyloid. The blue box indicates the approximate area which is shown at higher magnification in B. B: A higher magnification image of the area delineated by the blue box in A, stained with Haematoxylin and Eosin. Note the two florid plaques with a dense core and radiating spicules, surrounded by small vacuoles. Scale bar corresponds to 480μm (A) and 120μm (B)

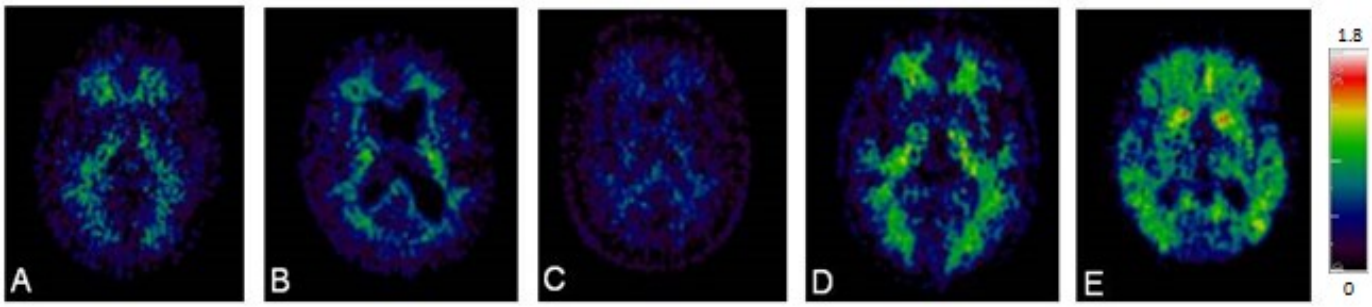


Figure 5.2. PET binding potential images at 75 minutes post-injection of [11C]-PIB. Background uptake in the white matter in is similar to that seen in controls in (A) patient with vCJD (PrD1), (B) symptomatic patient with P102L mutation (PrD2), (C) asymptomatic patient with P102L mutation and (D) normal control. [11C]-PIB retention is shown in the frontal and temporal cortex in a typical case of Alzheimer's disease (E) for comparison.

5.8 Reference

1. Tattum MH, Cohen-Krausz S, Thumanu K, Wharton CW, Khalili-Shirazi A, Jackson GS, Orlova EV, Collinge J, Clarke A, Saibil HR. Elongated oligomers assemble into mammalian PrP amyloid fibrils. Journal of Molecular Biology 2006;357:975-85.

2. Mallucci G, Collinge J. Update on Creutzfeldt-Jakob disease. Current Opinion in Neurobiology 2004;17:641-7.

3. Wroe SJ, Pal S, Siddique D, Hyare H, Macfarlane R, Joiner S, Linehan J, Brandner S, Wadsworth JD, Hewitt P, Collinge J. Clinical presentation and pre-mortem diagnosis of variant Creutzfeldt-Jakob disease associated with blood transfusion: a case report. Lancet 2006;368:2061-7.

4. Nicoll AJ, Collinge J. Preventing prion pathogenicity by targeting the cellular prion protein. Infect Disord Drug Targets 2009;9:48-57.

5. Merz PA, Somerville RA, Wisniewski HM, Manuelidis L, Manuelidis EE. Scrapie-associated fibrils in Creutzfeldt-Jakob disease. Nature 1983;306:474-6.

6. Chapman J, Ben-Israel J, Goldhammer Y, Korczyn AD. The risk of developing Creutzfeldt-Jakob disease in subjects with the PRNP gene codon 200 point mutation. Neurology. 1994 Sep;44(9):1683-6.

7. Klunk WE, Engler H, Nordberg A, Wang Y, Blomqvist G, Holt DP, Bergstrom M, Savitcheva I, Huang GF, Estrada S, Ausen B, Debnath ML, Barletta J, Price JC, Sandell J, Lopresti BJ, Wall A, Koivisto P, Antoni G, Mathis CA, Langstrom B. Imaging brain amyloid in Alzheimer's disease with Pittsburgh Compound-B. Ann.Neurol 2004;55:306-19.

8. Ikonomovic MD, Klunk WE, Abrahamson EE, Mathis CA, Price JC, Tsopelas ND, Lopresti BJ, Ziolko S, Bi W, Paljug WR, Debnath ML, Hope CE, Isanski BA, Hamilton RL, DeKosky ST. Post-mortem correlates of in vivo PiB-PET amyloid imaging in a typical case of Alzheimer's disease. Brain 2008;131:1630-45.

9. Edison P, Brooks DJ, Turkheimer FE, Archer HA, Hinz R. Strategies for the generation of parametric images of [11C]PIB with plasma input functions considering discriminations and reproducibility. Neuroimage 2009;48:329-38.

10. Hammers A, Allom R, Koepp MJ, Free SL, Myers R, Lemieux L, Mitchell TN, Brooks DJ, Duncan JS. Three-dimensional maximum probability atlas of the human brain, with particular reference to the temporal lobe. Hum.Brain Mapp. 2003;19:224-47.

11. Klunk WE, Debnath ML, Pettegrew JW. Development of small molecule probes for the beta-amyloid protein of Alzheimer's disease. Neurobiol Aging 1994;15:691-8.

12. Lockhart A, Lamb JR, Osredkar T, Sue LI, Joyce JN, Ye L, Libri V, Leppert D, Beach TG. PIB is a non-specific imaging marker of amyloid-beta (Abeta) peptide-related cerebral amyloidosis. Brain 2007;130:2607-15.

13. Ishikawa K, Doh-ura K, Kudo Y, Nishida N, Murakami-Kubo I, Ando Y, Sawada T, Iwaki T. Amyloid imaging probes are useful for detection of prion plaques and treatment of transmissible spongiform encephalopathies. J Gen.Virol 2004;85:1785-90.

14. Sadowski M, Pankiewicz J, Scholtzova H, Tsai J, Li Y, Carp RI, Meeker HC, Gambetti P, Debnath M, Mathis CA, Shao L, Gan WB, Klunk WE, Wisniewski T. Targeting prion amyloid deposits in vivo. J Neuropathol Exp Neurol 2004;63:775-84.

15. Boxer AL, Rabinovici GD, Kepe V, Goldman J, Furst AJ, Huang SC, Baker SL, O'neil JP, Chui H, Geschwind MD, Small GW, Barrio JR, Jagust W, Miller BL. Amyloid imaging in distinguishing atypical prion disease from Alzheimer disease. Neurology 2007;69:283-90.

16. Villemagne VL, McLean CA, Reardon K, Boyd A, Lewis V, Klug G, Jones G, Baxendale D, Masters CL, Rowe CC, Collins SJ. 11C-PiB PET studies in typical sporadic Creutzfeldt-Jakob disease. J Neurol Neurosurg Psychiatry. 2009;80:998-1001.

17. Collinge J, Prusiner SB. Prions and Neurodegenerative Diseases. In: Prusiner SB, Collinge J, Powell J, Anderton B, eds. Prion Diseases of Humans and Animals. London: Ellis Horwood 1992.

18. Kepe V, Ghetti B, Farlow MR, Bresjanac M, Miller K, Huang SC, Wong KP, Murrell JR, Piccardo P, Epperson F, Repovs G, Smid LM, Petric A, Siddarth P, Liu J, Satyamurthy N, Small GW, Barrio JR. PET of brain prion protein amyloid in Gerstmann-Straussler-Scheinker disease. Brain Pathol 2010;20:419-30.

Chapter 6

Adenosine2A receptor availability in dyskinetic and non-dyskinetic PD patients

6.1 Adenosine2A receptor availability in dyskinetic and non-dyskinetic PD patients

Thus far, investigations have been done in neurodegenerative conditions where cognitive decline is a major component of symptomology. In this chapter I would like to turn my attention to the second most common form of neurodegeneration worldwide, Parkinson's disease (PD). Specifically I will be looking at the biochemical changes that take place in levodopa induced dyskinesia (LID) in PD. Long held views in PD focused on dopamine and its role in motor control. Other neurotransmitter systems are invariably involved and the adenosine system will be investigated here.

Summary of objectives

To investigate striatal adenosine$_{2A}$ (A2A) receptor availability in Parkinson's disease (PD) patients with and without levodopa induced dyskinesias (LIDs). Dopamine replacement with levodopa is a mainstay of treatment in PD. While providing effective relief from the motor symptoms of PD, levodopa use is associated with development of LIDs. The A2A receptors are expressed on the bodies of indirect pathway medium spiny striatal neurons and on dopamine terminals and play a role in modulating dopamine transmission. A2A antagonists have anti-parkinsonian activity boosting levodopa efficacy. We aimed to study A2A receptor availability in PD patients with and without LIDs using positron emission tomography (PET) and [11C]-SCH442416, an A2A antagonist.

Six PD patients with and six without LIDs were studied withdrawn 12 hours from medication. Their PET findings were compared with 6 age matched healthy controls. Using spectral analysis, [11C]-SCH442416 regional volumes of distribution (V_T) were computed for the

caudate, putamen and thalamus and binding potentials (BP_{ND}) reflecting the ratio of specific:non-specific uptake were compared between groups.

Summary of results

A2A binding in the caudate and putamen of PD subjects with LIDs was significantly higher than that of PD subjects without LIDs which lay within the control range. Thalamic A2A availability was similar for all three groups.

PD patients with LIDs show increased A2A receptor availability in the striatum. This finding suggests that LIDs are associated with altered adenosine transmission and provides a rationale for the use of A2A receptor antagonists in the treatment of these motor complications.

6.2 Introduction

PD is one of the most prevalent neurodegenerative disorders worldwide[1]. The pathology of PD is characterised by the loss of dopaminergic neurons from the substantia nigra compacta in the midbrain with formation of Lewy body inclusions in surviving cells. Treatment has focused on relieving motor components of PD with emphasis placed on dopamine replacement. The pro-drug levodopa remains the most effective oral therapy and, in time, is offered to most PD patients.

Use of oral levodopa in PD, however, is not without its complications. Chronic exposure is associated with the development of involuntary movements known as dyskinesias[2]. These include choreic movements when patients are switched "on" and dystonic posturing as patients switch between "on" and "off" states with rising and falling plasma dopamine levels. The prevalence of LIDs in PD is around 50% after 5 and 90% after 10 years of exposure to levodopa treatment[2, 3]. The development of LIDs complicates the management of PD and their presence has been linked to increased mortality and weight loss[4].

The pathogenesis of LIDs remains unclear but is linked to changes in the output of the striatum to the internal pallidum via the direct and indirect pathways[5-7]. Striatal neurons of the indirect pathway express A2A receptors and project to the external pallidum, which in turn connects to the internal pallidum via the subthalamic nuclei. Striatal neurons of the direct pathway project directly to internal pallidum and do not express A2A sites. Cynomolgus monkeys lesioned with the nigral toxin MPTP that developed dyskinesia after treatment with levodopa have shown significantly higher striatal A2A mRNA levels when compared to non-dyskinetic monkeys and a normal control group[8]. In humans, post mortem studies have demonstrated increased A2A mRNA expression in PD patients with dyskinesias[5].

In this study I hypothesised that dyskinetic PD patients would have higher striatal A2A receptor availability compared to non-dyskinetic subjects resulting in underactivity of the indirect pathway. In contrast, A2A binding in the striatum of nondyskinetic PD patients would be similar or reduced compared to that of normal healthy controls.

In this study I have made use of the tracer [11C]-SCH442416. This tracer's chemical name is 5-Amino-7-(3-(4-[11C]methoxy)phenylpropyl)-2-(2-furyl)pyrazolo[4,3-e]-1,2,4-triazolo[1,5-c]pyrimidine. It is a potent antagonist to the A2A receptor[9]. It is synthesised by the methylation of the phenol precursor [11C]methyl iodide in dimethylformamide in the presence of sodium hydroxide at 90°C for 4 min[10]. It has been used previously in rat and primate studies where it has been shown to bind selectively to A2A receptors[11]. Kinetic studies confirms early and sustained concentration of [11C]SCH442416 within the striatum of primate brains. Low binding was confirmed in the cerebellum, and area of the brain with low A2A receptor expression[11,12]. The low uptake of [11C]SCH442416 in the cerebellum meant that it could be used as reference region for analysis of PET data. This is the first study involving the use of [11C]-SCH442416 in human PD subjects. It is hoped that this agent would be a useful biomarker in any future study of A2A availability.

6.3 Methods

6.3.1 Subjects

The size of the PD cohorts and control group were determined by the previously established low variance of the binding potential for [11C]-SCH442416 PET (standard deviation of BP_{ND} ~0.2 in controls). Six PD subjects with and six without dyskinesias should provide 80% power at a 5% error rate to detect an effect size of ΔBP_{ND} =0.4.

Twelve PD patients were recruited from local Movement Disorders Clinics. All patients fulfilled UK Parkinson's Disease Society Brain Bank clinical diagnostic criteria for idiopathic PD. Patients with significant co-morbidities including a previous history of another neurological condition, dementia or depression were excluded. The patient group consisted of two separate cohorts: six subjects had levodopa induced dyskinesias and a further six subjects were dyskinesia free on this medication. The effective levodopa dose for each PD subject was calculated as 100 mg levodopa = 2mg cabergoline = 1mg pramipexole or 1mg pergolide = 5mg ropinirole = 4mg rotigotine patch = 0.5mg rasagiline. The conversion factors below were used for controlled release levodopa and levodopa/carbidopa/entecapone combination: 125 mg controlled release levodopa = 65mg levodopa; 50 mg levodopa/carbidopa/entecapone combination = 65mg levodopa. Six age-matched healthy controls were also recruited. Table 6.1 summarises the clinical features of all PD patients and healthy controls.

Approval for this study was obtained from the Ethics Committee of the Hammersmith, Queen Charlotte and Chelsea and Acton Hospitals Trust. Permission to administer [11C]-SCH442416 was obtained from the Administration of Radioactive Substances Advisory Committee (ARSAC), UK.

6.3.2 Clinical assessment

All patients were assessed with the Unified Parkinson's Disease Rating Scale (UPDRS). Assessments were performed when the patients were switched "off" withdrawn from their medication.

6.3.3 PET image acquisition

PET scanning was performed at the Cyclotron Building, Hammersmith Hospital, London, UK, using a Siemens ECAT EXACT HR+ scanner. This scanner has an axial view of 15.5 cm. Sixty three transaxial image planes were acquired at 2.46mm slices with a reconstruction axial resolution of 5.4 mm and a transaxial resolution of 5.6 mm[13,14]. A 10 min. transmission scan was acquired before the emission study using a single rotating photon point source of ^{137}Cs for subsequent attenuation and scatter correction. This was followed by the injection of an average of 612 MBq of [11C]-SCH442416 over 10 seconds, 30 seconds after the start of a 90 minute dynamic emission scan (34 frames). The PET data, that were acquired in 3-dimensional mode, were corrected for attenuation, detector efficiency, random events and scatter and reconstructed into tomographic images using filtered back projection.

Prior to scanning all subjects had radial arterial cannulation under local anaesthesia. Continuous online sampling was performed for the first 15 minutes and then discrete blood samples were taken at baseline, 5, 10, 15, 20, 30, 40, 50, 60, 75 and 90 minutes. An aliquot of each discrete sample was rapidly centrifuged to obtain corresponding plasma and radioactivity concentrations that were measured in an NaI(Tl) well counter for blood and plasma separately. The continuous blood counts were corrected using the plasma/blood ratio to derive a plasma input function. The plasma was further analyzed for radiolabeled metabolites using high performance liquid chromatography (HPLC) and the plasma input function was corrected accordingly to produce a final parent radioligand input function to be used for quantification. A post hoc frame-by-frame realignment procedure was applied to compensate for head movement in the scanner. To reduce the influence of redistribution of radiotracer producing erroneous realignments[15] non-attenuation corrected images were used. Non-attenuation corrected images are considered to be more useful for the realignment algorithm because these images include a significant scalp and skull bone

marrow signal compared with attenuation corrected images. Frames were realigned to a single, 'reference' frame acquired 40 mins post-injection which had a high signal to noise ratio, using a mutual information algorithm[16] and the transformation parameters were then applied to the corresponding attenuation corrected dynamic images. The nonattenuation corrected images were denoised using a level 2, order 64 Battle Lemarie wavelet filter[17].

[11C]-SCH442416 was manufactured and supplied by Hammersmith Immanet, GE Healthcare.

6.3.4 MRI image acquisition

Each subject had a volumetric T1 weighted MRI performed with a Philips 1.5T Eclipse system for the purpose of defining the cerebellum, caudate, putamen and thalamus for sampling. The individual MR images were coregistered to the PET summed images using an automated multiresolution optimization procedure[18]. The anatomical segmentations obtained used to obtain the average time-activity curves of radioactivity concentration for the above defined regions that were then used for quantification.

6.3.5 PET quantification

Spectral analysis together with the metabolite-corrected plasma input function was used to analyse the kinetic components of the regional time-activity curves[19,20]. In brief, spectral analysis decomposes the regional time-activity course of the radioactivity concentration into separate kinetic components that are functions of the input function and of the tissue compartments with different residence times. The regional total volume of distribution (V_T) can be obtained by adding the spectral analysis components detected into a suitable kinetic

range that encompasses the free tracer in tissue plus its binding, both non-specific or specific to the A2A receptors. Finally, the measure of interest, that is the binding potential of the specifically bound radioligand relative to the non-displaceable radioligand in tissue (BP_{ND}) [21] is calculated from the volumes of distribution as:

$$BP_{ND} = V_T^{\text{target region}} / V_T^{\text{cerebellum}} - 1.$$

The cerebellum (which is devoid of A2A receptors in humans) was used as a reference region and therefore $V_T^{\text{cerebellum}}$ was used as an estimate of the free and nonspecifc binding of [11C]-SCH442416 throughout the brain. All pre-processing and quantification steps were performed using in-house routines written in Matlab 6.5 (The MathWorks Inc., Natick, MA, USA).

6.3.6 Statistical Analysis

Regional group differences in BP_{ND} were tested with the Mann-Whitney U statistic using SPSS (v.16, SPSS Inc., IBM, Chicago, IL, USA). The threshold for statistical significance was set at p=0.05.

6.4 Results

All patients and control subjects recruited had [11C]-SCH442416 PET scan and 1.5T MRI. Figure 6.1 illustrates the PET findings of the subjects scanned. The BP_{ND} of all groups are given in Table 6.2. The data, interrogated with the Mann-Whitney U statistic, revealed a 50% increase in BP_{ND} in the caudate and putamen of dyskinetic PD compared with non-dyskinetic PD and control groups ($p<0.05$). Thalamic A2A binding was equivalent in all three groups.

6.5 Discussion

In this study we have demonstrated significantly higher uptake of [11C]-SCH442416 in the caudate and putamen of the PD patients with LIDs as compared to those without LIDs or healthy controls. Additionally, no significant difference in A2A binding was found between PD patients without LIDs and healthy controls. In the human brain, the striatum contains one of the highest concentrations of A2A receptors[6,22,23]. These are found mainly on the spinous processes of the medium spiny neurones of the indirect pathway[22] and are G protein coupled. Their activation leads to inhibition of D2 receptors and an overall suppression of indirect pathway activity[6]. The increase in A2A we have identified mirrors the results of other studies where A2A receptor mRNA expression was shown to be elevated in dyskinetic patients[5] and in dyskinetic animal lesion models of PD[24].

An understanding of how increased A2A expression could result in the production of dyskinesias requires an understanding of the functioning of the indirect pathway. Reference should be made to figure 1.6 in Chapter 1, Introduction. Along with the direct pathway this system links the striatum with the globus pallidus interna (GPi)/substantia nigra pars reticulata (SNpr) complex via the external pallidal and subthalamic nuclei. The GPi projects directly to the thalamus with GABAergic output and has a final inhibitory effect on motor activity. Indirect striatal to GPe neurones are GABAergic as are neurons from the GPe to the subthalamic nucleus while the STN to GPi projections are glutametergic. The net effect of the indirect striatal output is, therefore, facilitatory on GPi and inhibitory on thalamus whereas the direct striatal pathway inhibits GPi and facilitates thalamic acitivity. The A2A receptors are found on the neurones extending from the striatum to the GPe. Activation of these receptors inhibits the activation of excitatory dopamine D2 receptors[6]. The activity of the system is however complicated by the presence of collateral interneurones also expressing A2A receptors and exerting a negative feedback on this inhibitory system. Figure

1.6 summarises this and highlights the ability of A2A activation to suppress D2 activity. The overall effect of increased A2A influence is thought to be a reduction in indirect pathway activity. Thalamic activation (and subsequent activation of the motor cortex) thus becomes increased and disorganised potentially resulting in dyskinesia.

The relationship between A2A receptor activation and dyskinesia is also influenced by other neurotransmitter systems. Preproenkephalin (PPE) is one such neuromodulator and increased PPE expression has been associated with the development of dyskinesia in MPTP monkeys[25]. PPE mRNA expression in rat striatum is facilitated by A2A activation[5]. Dyskinesia has been thought to evolve after the priming of the brain by the early use of levodopa. A2A activation may be a requirement for this early priming stage[26]. In MPTP primate models of PD, animals that did not developed dyskinesia had lower levels of A2A receptor binding and gene expression compared to those animals that developed dyskinesia. Abnormal opioid[27] and glutamate[28] transmission have also been implicated in previous investigations.

In this study, dyskinetic subjects had a longer duration of PD, higher UPDRS scores and were taking higher doses of levodopa than the non-dyskinetic cases. Thalamic [11C]-SCH442416 binding was however similar between all groups. This makes it unlikely that the differences in striatal binding observed are secondary to a pharmaceutical or pathological effect. The increase in striatal A2A availability was thus thought to be related to dyskinesia onset. This study however does not inform on the cause of dyskinesia nor were we able to make clear correlations between clinical data and [11C]-SCH442416 binding. Larger longitudinal studies would be needed for this.

The study does however demonstrate a potential pharmacological target for the management of LID. Istradylline has already been introduced clinically as an A2A blocker[25]. While it was not able to suppress dyskinesias already present, it enables lower doses of levodopa to be used earlier in the disease. It may thus have a long term benefit in delaying the onset of LID. Its early use may also have an impact on the priming of the brain and possibly delay the LID onset. Therefore, although other neurotransmitter systems are also important in the production of dyskinesia, the significant abnormalities in A2A availability identified in LIDs suggest that effective management could include the use of an A2A antagonist in addition to drugs targeting other systems.

Finally, [11C]-SCH442416 PET has been confirmed as a useful method for the *in vivo* investigations of A2A availability. This gent can thus function as a biomarker of A2A availability and would be useful when investigating dose-occupancy profiles of other A2A antagonists.

In conclusion I have been able to demonstrate higher A2A recptor levels in the putamen and caudate of PD subjects with LID.This will no doubt impact on the development of future drugs targeting this receptor in PD. Having established the binding profile of [11C]-SCH442416 such invasive procedures like arterial cannulation (to provide a blood input function) may no longer be necessary for analysis making [11C]-SCH442416 indeed.

6.6 Tables

Table 6.1. Study population

	Gender (M/F)	Age (yrs)	Disease Duration (yrs)	H&Y stage	LED (mg/day)	UPDRS
Controls N=6 Mean±SD	3/3	65 ± 6.2	NA	NA	NA	NA
PD without LID N=6 Mean±SD	4/2	67.7 ± 4.4	6.2 ± 3.4	1.9 ± 0.4	299 ± 112.2	54.7 ± 19.7
PD with LID N=6 Mean±SD	2/4	65.3 ± 11.4	13.2** ± 5.6	2.8** ± 0.3	1029** ± 477.9	64.7 ± 9.0

**p<0.05 Mann-Whitney U test

Table 6.2. [11C]-SCH442416 Binding Potential of the three groups investigated

Region	Controls	PD without LID	PD with LID	Control vs PD with LID	PD without LID vs PD with LID
Caudate Mean±SD	0.53± 0.24	0.4±0.24	0.96±0.46	p=0.041	p=0.026
Putamen Mean±SD	0.99±0.21	0.97±0.33	1.67±0.62	p=0.0087	P=0.036
Thalamus Mean±SD	0.12±0.18	0.13±0.14	0.14±0.18	NS	NS

NS – not significant

6.7 Figures

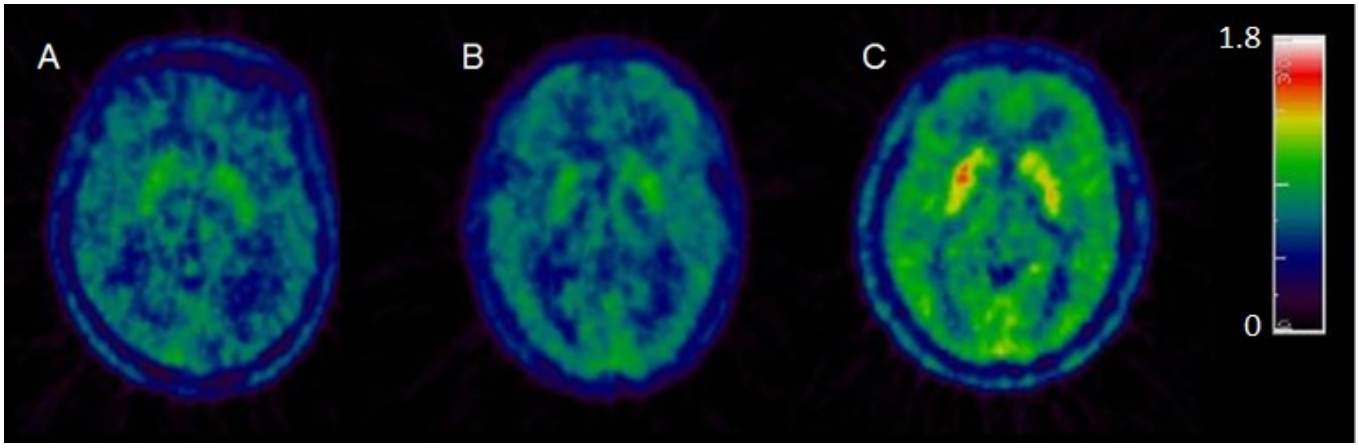


Figure 6.1. Sample PET binding potential images of [11C]-SCH442416 binding in the groups investigated. A – Normal healthy controls, B – PD subjects without dyskinesia and C – PD subjects with dyskinesia. Increased binding evident in the striatum of dyskinetic PD subjects.

6.8 References

1. Lo RY, Tanner CM, Alber KB, et al. Clinical Features in Early Parkinson Disease and Survival. *Archives of Neurology* 2009;1353-1358.

2. Ahlskog EA, Muenter MD. Frequency of Levodopa-Related Dyskinesias and Motor Fluctuations as Estimated From the Cumulative Literature. *Movement Disorders* 2001;448-458.

3. Marin C, Aguilar E, Mengod G, Cortés R, Obeso JA. Effects of early vs. late initiation of levodopa treatment in hemiparkinsonian rats. *European Journal of Neuroscience* 2009;823-832.

4. Sharma JC, Macnamara L, Hasoon M, Ross I. Cascade of levodopa dose and weight-related dyskinesia in Parkinson's disease (LD-WD-PD cascade). *Parkinsonism and Related Disorders* 2006;1075-1084.

5. Calon F, Dridi M, Hornykiewicz O, Bédard PJ, Rajput AH, DiPaolo T. Increased adenosine A2A receptors in the brain of Parkinson's disease patients with dyskinesias. *Brain* 2004;1075-1084.

6. Svenningsson P, LeMoine C, Fisone G, Fredholm BB. Distribution, Biochemistry and Function of Striatal Adensoine A2A Receptors. *Progress in Neurobiology* 1999;355-396.

7. Ding Y, Restrepo J, Won L, Hwang D-Y, Kim K-S, Kang UJ. Chronic 3,4-dihydroxyphenylalanine treatment induces dyskinesia in aphakia mice, a novel genetic model of Parkinson's disease. *Neurobiology of Disease* 2007;11-23.

8. Zeng B-Y, Pearce RKP, MacKenzie GM, Jenner P. Alterations in preproenkephain and adenosine-2a receptor mRNA, but not preprotachykinin mRNA correlate with occurance of dyskinesia in normal monkeys treated with L-DOPA. *European Journal of Neuroscience* 2000;12:1096-1104.

9. Leung K. 5-Amino-7-(3-(4-[11C]methoxy)phenylpropyl)-2-(2-furyl)pyrazolo[4,3-e]-1,2,4-triazolo[1,5-c]pyrimidine. Molecular Imaging and Contrast Agent Database (MICAD) [Internet]. Bethesda (MD): National Center for Biotechnology Information (US); 2004-2013. 2007 Jul 07.

10. Shinkre BA, Kumar TS, Gao ZG, Deflorian F, Jacobson KA, Trenkle WC. Synthesis and evaluation of 1,2,4-triazolo[1,5-c]pyrimidine derivatives as A2A receptor-selective antagonists. Bioorg Med Chem Lett. 2010 Oct 1;20(19):5690-4

11. Moresco RM, Todde S, Belloli S, Simonelli P, Panzacchi A, Rigamonti M, et al. In vivo imaging of adenosine A2A receptors in rat and primate brain using [11C]SCH442416. Eur J Nucl Med Mol Imaging. 2005 Apr;32(4):405-13.

12. Svenningsson P, Le Moine C, Fisone G, Fredholm BB. Distribution, biochemistry and function of striatal adenosine A2A receptors. Prog Neurobiol. 1999 Nov;59(4):355-96.

13. Brix G, Zaers J, Adam LE, et al. Performance evaluation of a whole-body PET scanner using the NEMA protocol. National Electrical Manufacturers Association. Journal of Nuclear Medicine 1997;38:1614-1623.

14. Dagher A, Gunn R, Lockwood G, Cunningham V, Grasby P, Brooks DJ. Measuring neurotransmitter release with PET: methodological issues. In: Carson P, Daube-

Witherspoon M, eds. Quantitative functional brain imaging with positron emission tomography. San Diego: 1998:449-454.

15. Studholme C, Hill DL, Hawkes DJ. Automated three-dimensional registration of magnetic resonance and positron emission tomography brain images by multiresolution optimization of voxel similarity measures. *Medical Physics* 1997;25-35.

16. Turkheimer FE, Brett M, Visvikis D, Cunningham VJ. Multiresolution analysis of emission tomography images in the wavelet domain. *Journal of Cerebral Blood Flow Metabolism* 1999;1189-1208.

17. Heckemann RA, Hajnal JV, Aljabar P, Rueckert D, Hammers A. Automatic anatomical brain MRI segmentation combining label propagation and decision fusion. *Neuroimage* 2006;33:115-126.

18. Cunningham VJ, Jones T. Spectral Analysis of dynamic PETstudies. *Journal of Cerebral Blood Flow and Metabolism* 1993;13:15-23.

19. Turkheimer FE, Moresco RM, Lucignani G, Sokoloff L, Fazio F, Schmidt K. The use of spectral analysis to determine regional cerebral glucose utilization with positron emission tomography and [18F]fluorodeoxyglucose: theory, implementation, and optimization procedures. *Journal of Cerebral Blood Flow Metabolism* 1994;406-433.

20. Innis RB, Cunningham V, Delforge J, et al. Consensus nomenclature for in vivo imaging of reversibly binding radioligands. *Journal of Cerebral Blood Flow and Metabolism* 2007;27:533-539.

21. Jenner P, Mori A, Hauser R, Morelli M, Fredholm BB, Chen JF. Adenosine, adenosine A2A antagonists, and Parkinson's disease. *Parkinsonism and Related Disorders* 2009;406-413.

22. Svenningsson P, Hall H, Sedvall G, Fredholm BB. Distribution of Adenosine Receptors in the Post Mortem Human Brain: An extended Autoradiographic Study. *Synapse* 1997;322-335.

23. Kaein-Lang A, Liniger P, Probst A, Lauterburg T, Burgunder J-M. Adenosine A2A receptor gene expression in the normal striatum and after 6-OH-dopamine lesion. *Journal of Neurotransmission* 2000;851-859.

24. Calon F, Birdi S, Rajput AH, Hornykiewicz O, Bedard PJ, DiPaolo T. Increase of preproenkephalin mRNA levels in the putamen of Parkinson disease patients with levo-dopa induced dyskinesia. *Journal of Neuropathology and Experimental Neurology* 2002;61:186-196.

25. Brotchie JM. Nondopaminergic Mechanisms in Levodopa-Induced Dyskinesia. *Movement Disorders* 2005;20:931.

26. Piccini P, Weeks RA, Brooks DJ. Alterations in Opioid Receptor Binding in Parkinson's Disease Patients with Levodopa-Induced Dyskineisas. *Annals of Neurology* 1997;720-726.

27. Thanvi B, Lo N, Robinson T. Levodopa-induced dyskinesia in Parkinson's disease: clinical features, pathogenesis, prevention and treatment. *Postgraduate Medical Journal* 2007;384-388.

28. LeWitt PA, Guttman M, Tetrud JW, et al. Adenosine A2A Receptor Antagonist Istradefylline (KW-6002) Reduces "Off" Time in Parkinson's Disease: A Double-Bind, Randomized, Multicenter Clinical Trial (6002-US-005). *Annuals of Neurology* 2008;295-302.

Chapter 7

Conclusion

7.1 Conclusion

As the population ages it is clear that dementia and neuro-degeneration will play an increasingly important role. In this thesis I have been able to investigate potential causes underlying cognitive failure. Not surprisingly much of dementia work has focused on fibrillar amyloid plaques. However this thesis supports the concept of neuro-degeneration being multifactorial with many different proteins playing a role.

Investigations into TBI have raised interesting questions into the importance of the amyloid plaque in cognitive impairment. Results were indeed surprising with on-going microglial activation without evidence of plaque deposition. Unexpected also was the disassociation between plaque deposition and reduced cerebral metabolism found in PCA. Results of these investigations have supported the notion that cerebral damage occurs even without plaque deposition. Although in PCA, subjects may have an increased posterior cerebral susceptibility, it is very likely that other proteins, e.g. tau, are more neuro-toxic and are driving inflammation and cognitive decline. This concept is still to be proven and such studies would benefit from *in vivo* biomarkers for tau. The establishment of a spacio-temporal relationship between tau and inflammation may indeed impact the development of new treatment options against tau.

TBI investigations also fuel the debate of whether the microglial cell is a friend and foe. Regardless of the guilty protein (amyloid, tau, α-synuclein etc.) the result is the ignition of a cascade of events that keep microglial cells activated. By its phagocytic activities, it helps clear any cellular debris and deal with any aberrant protein products but is its chronic activation linked to actual protein deposition and neuronal death? Should treatment thus be targeted to the switch off these microglia and keep them switched off? The potential here is the developments of disease modifying treatments. Obviously caution is necessary as

deactivation of microglial cells can potentially increase the infection risk or worsen the speed of cognitive decline with reduce protein phagocytosis. Further investigations are clearly warranted.

My investigation into A2A and LID has strengthened arguments into the use of A2A antagonist in the management of motor complications of PD. Thus far no effective treatment of LID has been identified. With further evidence of the *in vivo* pathogenesis in humans, the usefulness of the A2A receptor as a target for the development of pharmaceutical agents is established. SCH442416 may also prove to be a useful as a biomarker in PD and LID and further investigations utilising this ligand are warranted.

This thesis strengthens the argument that a larger amourment of *in vivo*, minimally invasive biomarkers for the diagnosis, and follow up of dementia patients is needed. The usefulness of agents like PIB lies partially in their sensitivity and specificity for fibrillar amyloid. The prion disease study however illustrated that it cannot be relied on as a marker of other proteins that also form βsheet plaques. Currently a reliable in vivo marker of prion protein has not been established. PET however has a proven track record for being a useful tool for the serial investigation of protein deposition and the development of such a tracer will prove invaluable.

This thesis has generated far more questions than answers. Results were far from expected and bring into question the importance of the amyloid plaque as the driving force in dementia. Results demonstrate a clear role for chronic microglia activation and suggest that imaging of other proteins e.g. tau would also be of importance. The future may thus lie in pursuing these concepts and they should be considered with any future drug development.

The use of minimally invasive biomarkers is important in the investigation of any treatment piloted and development must be continued to further our knowledge on especially for rare conditions.